Universitat Autònoma de Barcelona

Terahertz Displacement Current in Resonant Tunnelling Diodes including Coherent Electron-Photon interaction

Matteo Villani

Universitat Autònoma de Barcelona

Department Of Electronic Engineering

Doctoral thesis in
Electronic Engineering and Telecommunication

Terahertz Displacement Current in Resonant Tunnelling Diodes including Coherent Electron-Photon interaction

Author:
Matteo Villani

Thesis Director:
Prof. Xavier Oriols

2021/2022

TeraApps

MARIE CURIE ACTIONS

Departament d'Enginyeria Electrònica
Edifici Q 08193 Bellaterra (Cerdanyola del Vallès)
TEL +34 93 581 31 83
d.eng.electronica@uab.es

The undersigned, **Dr. Xavier Oriols Pladevall**, full professor of the Department of Electronic Engineering (Engineering School) of the Universitat Autònoma de Barcelona,

CERTIFY:

That the thesis entitled **"Terahertz Displacement Current in Resonant Tunnelling Diodes including Coherent Electron-Photon interaction"** has been written by the **Ph. D. candidate Matteo Villani** under his supervision, in fulfillment of the requirements for the PhD degree of Electrical Engineering and Telecommunication.

And hereby to acknowledge the above, sign the present.

Xavier Oriols

Matteo Villani

Bellaterra (Cerdanyola Del Vallés) 4 March 2022

Abstract

There is a great interest in developing portable low-power devices working at room temperature in the so-called Terahertz (THz) Gap, defined as the frequency domain between 100 GHz and 30 THz. Below this frequency domain, when the working frequencies are smaller than the inverse of the electron transit time of the active region, the current can be predicted from the amount of charge crossing the electron device and modelled through an electrostatic approximation of the electromagnetic fields.

However when the working frequencies are inside the THz domain, the proper prediction of the current needs the inclusion of the displacement current. I show in this thesis that there is plenty of room for engineering new THz electron nanoscale devices for a wide range of applications, when a proper quantum time-dependent treatment of the displacement current is taken into account. To include the displacement current component I propose a tool called the Displacement Current Coefficient. The models developed in this thesis are used to study Resonant Tunnelling Diodes (RTDs) in the THz gap. With the inclusion of the displacement current component, for example, one can predict the behaviour of RTD and other devices even beyond the transit time limit, and engineer non-linearities at such high frequencies to develop THz sources and detectors. I underline that high frequency non-linearities are independent of the ones typical of the characteristics of an RTD device, so that they present an additional opportunity for engineers to control the non-linear response of the device in high frequency.

The electrostatic approximation mentioned above does only involve the longitudinal component of the electric field. For a complete description of the effects of the interaction between electrons and electromagnetic fields on the displacement current, it is necessary to introduce also the effect of the transversal electric and magnetic fields on the dynamics of the electron. This requires new degrees of freedom to describe the electromagnetic field. In this thesis I will use a general approach to include coherently the interaction of the electron with the transversal electric field. This approach can then be applied to a classical transversal electromagnetic field or a quantized one with the inclusion of

photons.

The introduction of this quantization of electromagnetic fields is usually treated as a collision in the computational nanoelectronics community. However this thesis goes beyond this typical approach by discussing the effect of coherent electron-photon interaction on the displacement current, by using a wavefunction for the joined description for the electron and for the electromagnetic field.

The coherent electron-photon interaction leads to phenomena which, despite being well-known in the quantum optics community, remain mainly ignored in the electronic community. In this thesis, a special effort is devoted to discuss how these exotic effects are seen in the total (particle plus displacement) current. In particular, I observe a splitting of the energy eigenstates of the quantum well of the RTD device, when the coherent electron-photon interaction is included.

Another message of this thesis is the advantage of modelling electrons as particles with well-defined positions, and electromagnetic fields with well-defined properties, in the quantum regime. This description is widely favoured by the electronic engineering community and finds conceptual rigour in the Bohmian explanation of quantum phenomena used throughout this thesis. In addition, the Bohmian theory is known to provide a tool, namely the Bohmian Conditional Wavefunction, to give rigorous justification for the description of open systems in terms of pure states. I show the advantages of this alternative tool to describe collisions in open systems, in comparison with the Density Matrix and the Wigner function representation.

"It's a victory when the weapons fall silent and people speak up."

- Volodymyr Zelensky

Acknowledgements

I would like to thank everyone that helped during these years, or by supporting me or just by their presence.
I thank my supervisor Prof. Xavier Oriols for his patience, and for being the most caring supervisor. I thank all my colleagues in UAB, Devashish, thank you for the many advices and for being an inspiration, Laura, for a very nice 6 months in Cerdanyola, Carlos, for being an adventurer and a teacher at the same time, I thank Enrique, Guillermo and Prof. Xavier Cartoixà for their most useful opinion and help on my work.
I am thankful for my fellow UAB students Jonathan, Marti, Ana, Alvaro, Emili, Joan for all the time spent together, and for making me laugh all these years. And I thank Ertugrul, and wish him all the best for his future.
Thank you to all my office mates Eiglys, Ivan and Gerard, for their power of sharing and of listening.
I am grateful to Dr. Werner Prost and Prof. Nils Weimann for hosting me in Duisburg and for the very proficient period where I learned a lot. And I thank all my colleagues and friends in Duisburg: Simone and Ada, Nazli, Alexander, Christian and Robin, for making me feel at home. I thank all my colleagues from TeraApps, professors and fellow students.

And I thank my friends in Barcelona: Eleonora, Jessica, Alejandro, Casper, Dessy, Riccardo, Paula, Michaela, Victoria, Fabri and Martina, Fabiola, Gabriele, Andrea, Stefania and all the others for teaching me so much and for being there in the moment of need, even when we are far apart.

I am most grateful to Elena for her sweetness and pride.

I thank my parents, and all my family, and Alfredo, Annamaria, Pippo and Maril, which will always be with me.

Funding

This thesis has received funding from the European Union's Horizon 2020 research and innovation programme under the Marie Skłodowska-Curie grant agreement No 765426 (TeraApps). Other funding that has supported this thesis are Spain's Ministerio de Ciencia, Innovación y Universidades under Grant No. RTI2018-097876-B-C21 (MCIU/AEI/FEDER, UE), the "Generalitat de Catalunya" and FEDER for the project 001-P-001644 (QUANTUMCAT) and the European Union's Horizon 2020 research and innovation programme under Grant No. 881603 (GrapheneCore3).

Contents

Publications related to this thesis

Publications

- M. Villani, X. Oriols, "Can Wigner distribution functions with collisions satisfy complete positivity and energy conservation?", *Journal of Computational Electronics*, Nov. 2021 DOI 10.1007/s10825-021-01798-1

- M. Villani, G. Albareda, C. Destefani, X. Cartoixà, X. Oriols, "Scattering in Terms of Bohmian Conditional Wave Functions for Scenarios with Non-Commuting Energy and Momentum Operators", *Entropy*, vol. 23, no. 4, Mar. 2021 DOI 10.3390/e23040408

- M. Villani, S. Clochiatti, W. Prost, N. Weimann, X. Oriols, "There is Plenty of Room for THz Tunneling Electron Devices Beyond the Transit Time Limit", *Electron Device Letters*, pp. 1-4, Feb 2021 DOI 10.1109/LED.2021.3049229

- D. Pandey, L. Bellentani, M. Villani, G. Albareda, P. Bordone, A. Bertoni, and X. Oriols, "A Proposal for Evading the Measurement Uncertainty in Classical and Quantum Computing: Application to a Resonant Tunneling Diode and a Mach-Zehnder Interferometer", *Applied Science*, vol. 9, no. 11, 2300, 2019 DOI 10.3390/app9112300

- D. Pandey, M. Villani, E. Colomés, Z. Zhan, X. Oriols, "Implications of the Klein tunneling times on high frequency graphene devices using Bohmian trajectories", *Sem. Sci. and Tech.*, vol. 34, no. 3, 2019 DOI 10.3390/app9112300

Conferences

- M. Villani, X. Oriols, "Scattering implementation in the quantum transport BITLLES simulator", *International Workshop on Comp. Nanotechnology*, Daejeong, South Korea, June 2021 (conference paper) ISBN 978-89-89453-30-7, pg. 55

- M. Villani, X. Oriols, "On the Wigner-Boltzmann equation of motion for scenarios with non-commuting energy momentum operators", *International Wigner Workshop*, Wien, Austria, 2021 (conference paper). ISBN 978-3-9504738-2-7, pg. 48

- M. Villani, S. Clochiatti, W. Prost, N. Weimann, X. Oriols, "The accurate predictions of THz quantum currents requires a new displacement current coefficient instead of the traditional transmission one", *3rd International Workshop on Microwaves Technologies*, Essen, Germany, pp. 1-5, July 2020 (conference paper). DOI 10.1109/IWMTS49292.2020.9166410

- D. Pandey, L. Bellentani, M. Villani, G. Albareda, P. Bordone, A. Bertoni, X. Oriols, "Eliminating Quantum Uncertainty in Quantum Electron Devices: Leveraging Classical and Quantum Computing" *International Workshop on Computational Nanotechnology*, Chicago, Illinois, USA, pp. 9-10, May 2019, pp. 9 ISBN 978-3-9504738-0-3

- M. Villani, D. Pandey, E. Colomés, X. Oriols, Z. Zhan, "Tunneling Times in Graphene FET: From Fundamental Physics to Practical Engineering", *2018 Spanish Conference on Electronic Devices*, Salamanca, Spain, pp. 1-4, Oct. 2018. DOI 10.1109/CDE.2018.8597054

- D. Pandey, Z. Zhan, E. Colomés, M. Villani and X. Oriols, "Electron Injection Model for Linear and Parabolic 2D Materials: Noise as a Parabolic or Linear Band Detector", *2018 Spanish Conference on Electronic Devices*, Salamanca, Spain, Oct. 2018, pp. 1-4. DOI 10.1109/CDE.2018.8596808

Introduction

The so called THz gap is defined in the frequency range between 300 GHz and 10 THz. The electronic industry faces important challenges in building reliable electron devices for developing sources and detectors at such frequencies. Other non-electronic technologies working at this THz gap are bulky and expensive, so that they are unattractive for the telecom industry. As a consequence, the use of sources of radiation in the THz gap is for now mainly relegated to the development of prototypes in scientific and research entities.

Let us mention that the closure of this THz gap, with devices working at room temperature, would enable a large body of applications with significant societal impacts [1], such as non-ionizing imaging of human tissues [2–4] including cancer screening [5,6], non-destructive materials testing, security imaging [1], and higher data rates associated to the use of higher carrier frequencies for wireless information transmission [7–10].

In fact, the THz gap is quite atypical in the sense that its position in the frequency spectrum is located between two domains that are technologically and theoretically very different. At the lower end of the THz spectrum, I find the electronic technology, whose main interest is describing electrons dynamics inside semiconductor devices and, at most, engineering the electromagnetic fields outside these devices. The relevant figure of merit here is the total current for a given external voltage. On the other end of the THz spectrum, there is the world of photonics, where the relevant "particle" is no longer the electron, but the photon defined as a quantum of energy of the electromagnetic fields. The relevant engineering in photonics is done basically inside the device, looking for improvements of parameters such as the quantum efficiency related to electromagnetic radiation power, while the dynamics of the electron alone is less relevant here.

It seems reasonable to expect that a proper exploitation of the whole THz spectrum requires moving the previous technologies from their actual "comfort zone" at both borders of the THz spectrum. Either, the electronic industry has to approach the photonic technology, or vice-versa. This thesis is an attempt to extend the typical electronic technology towards higher frequencies by including the displacement current with a quantum

treatment of the electron and electromagnetic fields.

The attempt of approximating electronic and photonics technologies in this thesis will be studied in a device named Resonant Tunnelling Diodes (RTD), which in its simplest definition is a device built from 3 layers of materials creating a quantum well between two potential barriers. This structure of the active region of an RTD is short enough so that electrons undergo ballistic transport through the barrier region and tunnelling can be observed in the macroscopic current. This quantum transport phenomenon, in proper conditions, leads to negative differential conductance that can be properly engineered to produced power gain at frequencies up to a few THz [11, 12].

We explain below the structure of this thesis. It is divided into five big parts: (i) THz Technology, (ii) Theoretical introduction, (iii) Models, (iv) Results and (v) Conclusions. In Part I in Chapter 1 I will present an overview of technologies enabling THz radiation sources, and in Chapter 2 I discuss the actual development of RTDs as sources and detectors of THz radiation.

In Part II, in Chapter 3 I will present the Bohmian formalism, which is the theory used to develop the computational models in this thesis. In Chapter 4 I will briefly mention the different treatments done in the literature for open quantum systems. In particular, I will focus on three models for open systems: the Density Matrix, the Wigner distribution function (derived from the first one) and the Bohmian conditional wave function.

In Part III I will present different models developed in this thesis to study the THz behaviour of RTDs. First, in Chapter 5 I explain the decomposition of the Maxwell equations into parallel and transversal fields and some approximations assumed in this thesis to estimate the total current at THz frequencies. In Chapter 6 I show how light-matter interaction can be treated in RTDs, while treating the electromagnetic fields in a classical or quantum way. Finally in the Model part, in Chapter 7 a non-coherent approach for the light-matter interaction will be built to reduce the computational burden by implementing an electron-photon collision model in large many-body systems, through the mentioned Bohmian conditional wave function. Then, in Chapter 8 I explain what I have named the *Displacement current coefficient*, which is a tool similar to the transmission coefficient to estimate the response of a ballistic device at high-frequency, where the displacement current component becomes relevant. This chapter can be understood as an attempt to introduce the displacement current component into a Landauer-like model to estimate the total current of a device. The mentioned modelling of light-matter interaction in Chapter 6 will be re-written to study the *Displacement current coefficient*, in the

case of coherent interaction of the electron with the quantized electromagnetic field.

In Part IV I present the numerical results based on the theory of the previous part. In particular, in Chapter 9 I show results of the light-matter interaction with coherent evolution. The results of the non-coherent models explained in Chapter 7 will be shown in Chapter 10, where I also show the limitations of the Wigner Function description (or the density matrix) to properly describe electron-photon collisions and how such limitations are overcame when dealing with the Bohnmian conditional wave function. Then in Chapter 11, I compute the *Displacement current coefficient* in a typical RTD to study the high-frequency behaviour of this device beyond the transit time limit. I show that it is possible to accurately predict the small-signal non-linearities of this device at THz frequencies, and engineer them to build novel THz devices. In this chapter, only the parallel electromagnetic field (Poisson law) is considered to influence the evolution of electrons inside the active region. Finally, in Chapter 12, I provide numerical simulations unifying the models of Chapters 6 and 8, computing the total (particle and displacement) current of the RTD with the inclusion of light-matter interaction in a coherent way (including the quantization of the transversal electromagnetic fields), with the final goal of looking into a theory of electron transport that can better approach electronics and photonics.

Part I

THz technology

Chapter 1

The THz gap

The main difficulties of state-of-the-art technologies in the THz frequency domain is to reach applications with high enough power (above 1 mW), at high enough frequencies (at 1 THz and above), with compact devices that can work at room temperature [8, 9]. In this chapter I overview some of the main technologies that enable THz radiation, dividing them between photonic and electronic technologies.

Photonic sources Currently if only power and frequency are taken into consideration (and not compactness), the best THz sources are factory-sized structures like synchrotrons, reaching high power levels at any frequency range within the THz domain [13]. The goal of these big structures is to make electrons oscillate in a vacuum, with the use of high-intensity magnetic fields, and, sometimes with a resonant cavity. Then, they use the dipole radiation generated by such electron oscillations [14]. The obvious drawback is that the industry is looking for compact (not factory-sized) devices. Other optical sources for THz radiations [15] are, for example, the THz radiation from gas lasers, where the rotational resonance of given molecules produce dipole oscillation. This resonance and the cavity of the laser amplify only the proper frequency. The main limitation is the availability of the given molecule [16]. Another type of THz laser is the p-Germanium (p-Ge) laser, which is a waveguide-shaped device where holes are accelerated in a $\mathbf{E} \perp \mathbf{B}$ field [17,18]. The p-Ge laser offers tunable broadband emission in the terahertz frequency range but has the drawback of the strong heating of the crystal, which must be maintained at temperatures below 20K.

A further family of sources in the optical range that can be scaled down to the THz regime is based on non-linear optics. One type of such sources uses materials with non-linear electric susceptibility, which convert two photons of optical frequencies into one THz-frequency photon. This down-conversion is inherently inefficient, since a large

amount of energy is lost through thermalization. These materials are usually crystalline structures that need a relatively large propagation length of the photons inside the lattice, limiting miniaturization. Non-linear optical sources however can also work as photomixers, where through the creation of an electron-hole pair, with the absorption of an optical photon, many THz photons can be emitted. This second type of down-conversion is more efficient than the previous one as ideally there is no loss of energy [14].

Another interesting photonic source of THz radiation is the Quantum Cascade Laser, which is a special kind of semiconductor laser not based on transitions between different electronic bands, but on intersubband transitions of a semiconductor structure. Quantum Cascade Lasers usually emit mid-infrared light.

Electronic sources Next, I discuss THz devices based on electronic sources [19, 20]. As briefly indicated above, one way of producing THz radiation is the use of a Negative Differential Resistance (NDR) as a power source in a resonant circuit. If the device can, at a given bias, maintain a negative conductivity at frequencies in the THz domain, then radiation will be induced in the circuit in such domain. One of the most well-known electron devices capable of achieving NDR is the mentioned RTD [21]. This device will be introduced in Chapter 2. In fact, the RTD is the electron device used all along this thesis in the result in Chapters 9, 10, 11 and 12. The key element to have THz output frequencies in this and other electron devices is related to the miniaturization of the device, to reach ballistic transport, while reducing geometric and quantum capacities. Besides the RTD technology, electron NDR-based THz sources can be achieved using Esaki diodes [22, 23] or Gunn diodes [24–26]. The Esaki diodes in particular produce NDR in their current-voltage characteristics through a transition between the conduction and valence bands in a heavily doped p-n junctions.

Another electron source of THz radiation is the High Electron Mobility Transistor. This technology uses a hetero-junction structure that creates an excess electron concentration along the junction, with 2D geometry [27].

Chapter 2

RTD-based THz technology

In this chapter I provide a brief overview of RTD-based THz technology. The RTD will be the device where I will implement, through numerical simulation, all transport models developed in this thesis.

As indicated in the introduction, the essential structure of an RTD device is composed of a material with a low energy gap, the quantum well, sandwiched between two high-energy gap materials, the barriers. The low energy-gap material is then used to build the contacts. See the potential profile schematically shown in Fig. 2.1(a). The transport of electrons inside this double barrier structure, with a typical length L usually under 20 nm, is defined as ballistic meaning that electrons do not suffer any collision during the time spent in the barrier (phonon scattering can be ignored as a reasonable approximation) so that its initial total energy remains constant. Electrons interacting with this structure will undergo tunnelling through the barriers. At some specific energies, which depends on the geometry of the structure, the electrons will not only suffer tunnelling, but resonant tunnelling, meaning that their transmission coefficient can be close to one. At these resonant energies, the electrons traverse the double barrier more easily than just one barrier. This apparent paradox is just a consequence of the quantum wholeness.

The resonant energies of the whole structure in Fig. 2.1(a) are shown in Fig. 2.1(b). These resonant energies roughly coincide with the quantized energies allowed in an (infinite) quantum well with the same dimensions. These energy levels, working similar to an artificial atom, can host determined densities of carriers, and can be easily occupied when the energy level of the contacts are in energetic resonance with them. This is the main message of the so-called Landauer model [28, 29] applied to RTD devices [30]. The fact that electron transport occurs when the energy of the injected electrons coincides with the energies allowed in the quantum well can lead to highly non-linear I-V charac-

teristics. The most innovative feature is the presence of a bias region called NDR as in Fig. 2.1(c). This NDR is characterized by peak voltage V_P, as the voltage where I observe the maximum value of the current (peak current) I_P, and valley voltage V_V, where the end of the NDR is reached, where I observe the relative minimum of the current (valley current) I_V. The NDR was first predicted theoretically in [30] back in 1973, and then demonstrated experimentally in [31]. The small dimensions of the RTD in the transport direction lead to a small transit time τ of electrons inside the active region of the device, on the order of 1 ps or less. As indicated in the introduction, the NDR finds applications in THz radiation source, proven, in the latest results, to reach frequencies up to 2THz [11] when coupled with an external resonant circuit.

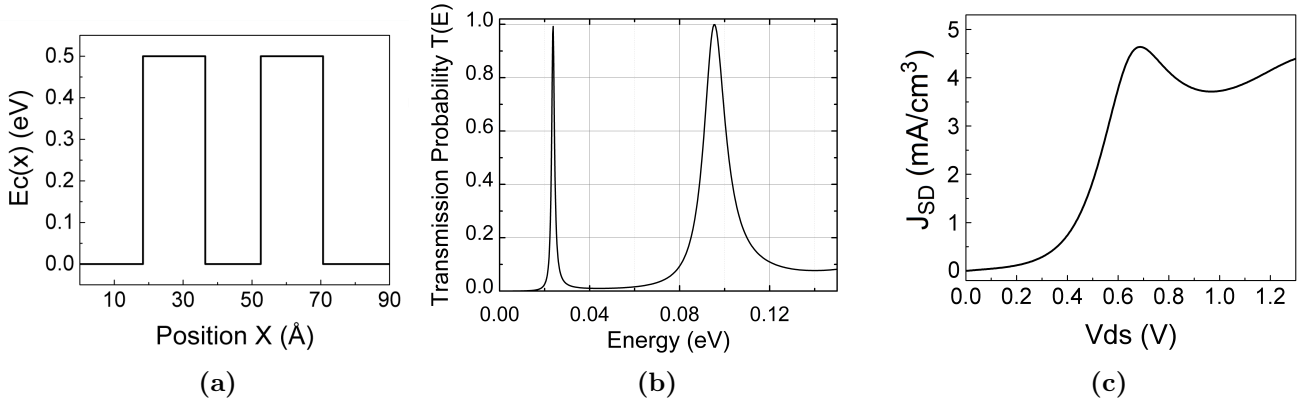

Figure 2.1: (a) Conduction band in function of position of a simple Double Barrier RTD device, (d) typical DC transmission coefficient in function of the injection energy (c) typical DC I-V curve of the RTD device, showing the NDR at bias from $V_P = 0.65\,\mathrm{V}$ to $V_V = 0.95\,\mathrm{V}$, and showing broadening of the peak voltage.

In a real device, taking into account thermal effects such as electron-phonon scattering and fabrication defects, the NDR region tends to be not very sharp, however, experimental results of good quality RTD devices show that the NDR can have sometimes almost vertical slope [32].

The above explanation of the RTD is known as the coherent-tunnelling model in the literature. An alternative explanation has been presented to understand the working mechanism of carrier tunnelling in the RTD device. This is the so-called sequential-tunnelling model. This has been first proposed in [33–35]. The main idea is that firstly electrons tunnel from the emitter to the quantum well, and then they can undergo scattering or thermalization inside the well. Secondly, electrons can be transmitted to the collector. At the end of the day, both models are just simplified explanations of what happens inside the RTD. At the fundamental level, electron transport inside an RTD has

to be explained from a proper many-body quantum transport equation (i.e. a proper modelling of a quantum open systems).

Finally, I also mention the possibility of using a triple barrier RTD (instead of a double barrier) as a tool to have additional room for the engineering of the RTD I-V curve [36, 37].

RTD technology as THz source The main applications of the RTD device are related to the use of the strong non-linearities of the I-V curve [21, 38, 39]. The NDR can be used to build a power amplifier element inside a resonant circuit at frequency f. As long as the resonant circuit induces on the RTD bias and frequency or operation where the differential conductivity of the device is still negative, this amplification will be possible at the frequency of the resonant circuit. If such frequency is selected in the THz range, radiation at such frequencies with an acceptable power is possible. The first relevant result of THz range emission with the use of an RTD-based oscillator (source application) appeared in 1991 when the NDR of the RTD was shown to maintain negative differential conductivity at frequencies of $\approx 700\,\mathrm{GHz}$ [40, 41].

Another important step appeared in the early 2010s with frequencies above the 1THz [12, 32, 42], and as already said recent results suggest the possibility of reaching frequencies around 2THz [11]. Additional examples of RTD devices as THz sources are [43, 44].

In general, RTD designs that minimize the length L_x of the active region are needed to reach higher working frequencies of the oscillator. However, fabrication limits, in particular in the growth of high quality contacts, will increase the contact resistance and capacity, adding additional complexity to the engineering of the device.

RTD as intrinsics oscillator at THz frequency The RTD THz oscillators mentioned above can be also called extrinsic oscillators because the condition to reach oscillations is the resonant circuit at frequency f, which is external to the RTD. The role of the RTD is to provide a negative resistance around the bias point, producing gain. A second, more exotic, category of RTD-based THz oscillators can be defined as intrinsic oscillators. Here the only component needed for the oscillation is the RTD itself. The intrinsic oscillator consisting exclusively of a double barrier RTD has been predicted in various theoretical works. In the following simulation works [45–48], a bistable state of the output current is observed in the region of negative resistance. However, the intrinsic oscillation has not been experimentally proven yet, even for rather simple geometries of the RTD device, and with the expected frequencies in the THz range. These approaches

are based on the Wigner function description [49]. I will talk in Section 4.2 about this description and its criticism when treating collisions inside the well, which can create unphysical oscillations in the numerical results. I give some numerical proof of these criticisms in Chapter 9, and for additional reads, I recall [50, 51].

RTD for detection of THz radiation Another application of RTD devices can be in THz detection. In this application, the decrease of the noise-to-signal ratio is the key element to detect low-power high-frequency THz signals. Some RTD devices can be used outside of the NDR for this kind of application. In this case, devices need to have non-symmetrical geometry to have strongly non-linear behaviour around zero bias. Then, an external THz source oscillating around zero can be converted into a non-zero DC signal of the RTD. See for example the RTD as THz detectors [37, 52, 53], with the advantage of having off-state power. Additionally in [43] the same geometry could be used, for a different bias, as a THz source.

2.1 Fundamental versus phenomenological modelling

The final goal of a simulation of an RTD is determining which is the output current given some particular bias conditions. Important decisions are needed to be taken when deciding a strategy to provide such output current. One can choose between a more phenomenological or a more fundamental approach. Both options have pros and cons. In this section, I will make an example of a simple phenomenological approach used to model RTDs, and I will explain the strengths and limitations of such a phenomenological approach compared with a more fundamental one.

In principle, one would say that a more fundamental approach is better suited for improving RTD-based technology because it does not need to anticipate or presuppose any behaviour for the RTD. Then, I can elaborate a model where the output macroscopic current is predicted from the microscopic dynamics of the electrons. I underline that, from a microscopic physical point of view, an RTD device is a many-body open quantum system outside of thermodynamic equilibrium. As such, it is one of the most complicated physical systems to be simulated and important approximations are needed if one wants to reach numerical predictions from a fundamental simulation. The typical approximation is based on treating the electron inside an RTD from a single-particle quantum picture (ballistic transport) where the rest of electrons (or other relevant degrees of freedom) are re-introduced from a type of mean-field effect. Let us notice that a fundamental approach

of RTD at THz frequencies has an extra source of complication because of the quantum measurement of the total electrical current at such high frequencies.

Another possibility to predict the performance of an RTD is directly ignoring the microscopic description of the electrons and looking for some macroscopic equations for the output current itself. Typically, a modelling of the output current as a function of the input voltage can be conducted by using circuit theory and modelling the RTD as a circuit with basic elements like resistors and capacitors. Certainly, such a type of phenomenological model is more manageable than a fundamental one, but the key question here is how can I be sure that the microscopic complexity of an RTD can be simplified as a simple combination of circuit elements? Which circuits elements have to be chosen? Which values for such elements? Typically the answer to these questions is based on checking if a given circuit model reproduce or not experimental results in a given range of bias or frequencies. The clear advantage of this strategy is that, if the selected values fit the experimental results, then I have a very simple model that summarizes the complexity of an RTD. Such phenomenological selection of the values of the elements of the circuit is a hard handicap to be able to predict novel behaviours or applications of the RTDs.

In this thesis, I will conduct a fundamental analysis of an RTD, to look for novel applications of RTD at THz frequencies. However, before doing this, I would like to give an example of one simple possible phenomenological approach used to model the RDT device in the THz community. I will focus on the application of the RTD as a THz source. The first relevant parameters are usually linked to the transit time τ, since it is assumed that as the working frequency approaches the inverse of this parameter $f \to 1/\tau$, the conductance in the NDR will lose its negativity. The maximum power available for by these sources is usually assumed to be equal to the current and voltage spacing between the peak and valley values of the NDR device: $P_{max} \approx |(V_P - V_V) * (I_P - I_V)|$. Additionally, the real part of the admittance $Y_{11}^f(V)$ is the differential conductance, which I call $G_{11}(V, f) = Re\{Y_{11}^f(V)\}$, which is bias and frequency dependent [54,55]. When these devices parameters are included in a small-signal circuit model, the delay created by the transit time τ and other physical phenomena is included inside a total capacitance of the RTD C_{tot}. Finally from these parameters, the goal is to have a negative $G_{11}(V, f)$ and a negative inductance $L_{RTD} \approx \tau/G_{11}(V, f)$, so that the RTD can provide gain. From these conditions, the maximum operating frequency, defined as the maximum frequency where

the inductance $G_{11}(V, f)$ stays negative, was obtained as [21, 56, 57]:

$$f_{max} \approx -\frac{G_{11}(V,f)}{2\pi C_{tot}} \sqrt{\frac{1}{G_{11}(V,f)\, R_s} + 1}, \tag{2.1}$$

where the total capacitance C_{tot} is considered the sum of two main terms, the quantum and geometrical capacitances: $C_{tot} = C_q + C_g$. Of these, C_q is related to the quantum dynamics of electrons inside the well by: $C_q \approx \tau\, G_{11}(V, f)$, and C_g is the geometric capacity, given by the charging of the RTD-contacts interface. Additionally R_s is the series resistance included to take into account the contact resistance, in the circuit shown in Fig. 2.2. All of these term are bias and frequency dependent, and usually these are estimated with a fitting from experimental data, with the first practical limitations that state-of-the-art measurement apparatuses do not usually characterize devices beyond 200 GHz, so that an extrapolation to estimate the behaviour at higher frequencies is always needed. We will deal with the estimation of τ in quantum mechanics in expression (5.1), but I note that sometimes this value is estimated in RTD devices in a more practical way with

$$\tau = \tau_e \tau_c / (\tau_e + \tau_c), \tag{2.2}$$

where τ_e and τ_c are usually estimated from the energy broadening of the emitted and collector transmission probabilities.

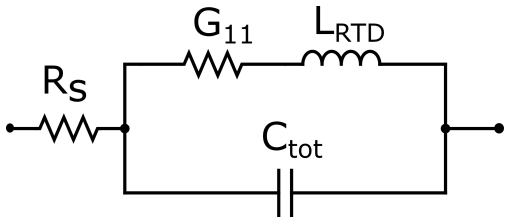

Figure 2.2: Example of small-signal equivalent model of a RTD, from [54].

The conceptual limitations of using this kind of description are:(i) the need for an educated guess about the tunnelling times, (ii) the fact that all of these parameters are bias and frequency dependent, (iii) the high-frequency response of ballistic devices is never linear, and new components rise in the spectrum of the output signal of the device, so that the use of $Y_{11}(V, f)$ is not accurate in a domain where the device is approaching $f \approx 1/\tau$, (iv) the definition of τ as in (2.2) lacks the idea of quantum wholeness so that in part ignores the quantum nature of the RTD.

All these problems are well known in the engineering community and in fact approximations that try to neglect such issues are included with caution and in very small frequency domains of operation. The literature about the determination of these and

other small-signal parameters is beyond the scope of this thesis, but I recall [58, 59] for additional reading on the theory behind this phenomenological approach. In this thesis, I will work on a more fundamental time-dependent quantum approach that deals with the microscopic behaviour of electrons to directly estimate the output signal of the device in the time and frequency domain.

Part II

Theory introduction

Chapter 3

Bohmian theory

All the models developed in this thesis for the RTD are inspired by, or find their rigorous justification in, the Bohmian quantum mechanics. In this chapter, I will provide a brief explanation of such theory. The Bohmian theory is in agreement with all experimental quantum phenomena known today, as happens with the so-called orthodox (or Copenhagen) theory, but the Bohmian theory has the conceptual advantage in front the Copenhagen theory that electrons have microscopic properties (like position and velocities) even when such properties are not measured. And this is exactly how most engineers and chemists imagine the behaviour of microscopic particles.

3.1 Bohmian mechanics in electronics

The introduction of the quantum theory at the beginning of the 20^{th} century was induced by the observation of several physical phenomena (like the photoelectric effect, the light pressure or the black-body radiation) that had no explanation from the classical laws of physics. When the quantum theory was introduced, it was fast understood that quantum phenomena were open to multiple interpretations, like the orthodox (Copenhagen) theory [60] or the Many-worlds interpretation [61]. The birthplace of another one of these interpretations can be found as early as 1927, when de Broglie built a description of quantum mechanics based on (non-classical) trajectories for particles. This was the base for what is now called the pilot-wave formulation of quantum mechanics [62].

David Bohm in 1952 in his work [63, 64] rediscovered De Broglie's work on the pilot-wave theory and underlined the main advantages included in such interpretation, like the elimination of deep conceptual difficulties in the orthodox description of quantum measurement. Such interpretation is now called the De Broglie-Bohm theory or the Bohmian theory. This is based on describing a quantum system, not only with the use of

a wavefunction, but also with deterministic trajectories. Such deterministic trajectories guided by the wavefunction, in the case of the RTD mentioned here, define the position of unobserved electrons. I will also mention that in 1964 inspired by Bohm's work, John Bell developed the famous Bell inequalities [65]. Bell's theorem showed that quantum phenomena are not local. In fact, Bohmian theory is non-local because the velocity of one electron depends not only on the local position of the electron itself, but on the position of all other electrons (or particles) to tackle the non-local quantum wholeness.

On the other hand, simultaneously with the work of de Broglie, some researchers working in Copenhagen developed an explanation of the quantum phenomena where the wavefunction is the only tool needed to describe an unmeasured quantum electron. This explanation is what is now known as the orthodox explanation of Quantum Mechanics, and also known as the Copenhagen interpretation. This is the standard explanation of the Quantum domain found in many books. In the case of an RTD, it says that electrons have no position, only a wave function. The only case when electrons have positions is when I explicitly measure their position with a measuring apparatus. This effect of the action of measuring on the *reality* of the electron is called the collapse law because the initial extended wave function of the electron collapse into a delta function when the position is measured. But, there is no way of having position measurements inside the active region of a device. Then, according to the orthodox theory electrons have no position in the active region. Notice that the orthodox theory is not saying that the electrons are somewhere inside the active region, but I do not know it. No. The orthodox theory says that electrons are ontologically nowhere. They have no position. But, then, where are the electrons? Such type of questions is usually ignored in the electronic modelling community under the philosophy of "shut up and calculate" [66].

Strictly speaking, the wave function of an electron does not provide a type of charge distribution, but a probability distribution of *finding* an electron at one position when it is measured (not the probability of *being* there when it is not measured). However, for the DC current, an ergodic argumentation can be used to establish that an electron measured many times gives similar results to many electrons measured a single time each. Then, if I assume a large number of electrons in an RTD described by the same single-particle wave function, I can really interpret the square root of the wave function as a type of current distribution, without worrying about the collapse of the wave function due to the measurement. For example, this is the point of view raised by Esaki's works [30] in 1973 on RTD devices. Consequently, the Copenhagen interpretation of quantum mechanics,

by far the most used one in the physics community, was introduced in the electronics community. For additional reading about the adoption of the Copenhagen interpretation, inserted in a historical context, I drive the reader to [67]. However, before the inclusion of quantum phenomena in the description of electrons, the modelling of devices was done by treating electrons as particles with determined positions. Nowadays, rather curiously, despite the more and more widespread use of orthodox quantum mechanics in electronics, the deep understanding of electron transport inside the engineering community remains linked to a trajectory description of electrons.

The author of this thesis argues that, even if the complexities of the Copenhagen interpretation were accepted but not deeply understood by the engineering community, such understanding of quantum phenomena forbidding the use of trajectories is not needed, and would be even detrimental, in the state-of-the-art high-frequency electronics. In fact, as I have explained above, a good and intuitive alternative explanation of quantum phenomena in THz RTDs can be given according to the proposal of de Broglie and Bohm.

As an example, while Esaki was successful in using the Copenhagen interpretation in the 1970s in its analysis [30, 31] for DC applications, let us mention unnecessary problems that appear in the modelling of high-frequency RTDs when I eliminate the use of trajectories. The estimation of the cutoff frequency in the RTD as THz source [33–35] is, in fact, linked to the so-called tunnelling time. However, the orthodox theory has many difficulties in properly defining a tunnelling time. The orthodox theory has renounced to define the position of an electron but, then, how can I model the time needed for one electron to pass from one position to another (from the begging of the barrier to the end of the barrier) if the electron, indeed, has no position at all? For an explanation on how electronic engineering, and its view of electron transport, can be related to Bohmian mechanics, to avoid the unnecessary complications of the Copenhagen interpretation, I recall the work "Why engineers are right to avoid the quantum reality offered by the orthodox theory?" [68].

In this chapter, the fundamentals of Bohmian mechanics will be introduced. These will then be used within this thesis to explain a tool called the Bohmian Conditional Wavefunction, used all along this thesis for the modelling of open systems and the electron-photon coherent interaction. Finally I suggest some literature for a deeper look into theory [69, 70], implications [71] and applications [72, 73] of Bohmian mechanics.

3.2 Bohmian mechanics for many-particle systems

In this section, I will explain the mathematical base of the Bohmian theory, as introduced by De Broglie in [62]. In the case of typical two-contacts nanodevice, where the lateral area is much larger than the length of the active region L in the transport direction x, it is common to assume that the degrees of freedom x, y and z of the electron evolve independently and that only the degree of freedom x, evolving in a 1D space, are needed to be explicitly simulated to compute transport properties. With this 1D simplification, in the Bohmian theory, a system composed of N particles is described by a many-particle wavefunction $\Psi = \Psi(\vec{x},t) = \psi(x_1, x_2, x_3, ..., x_N, t)$ evolving in the configuration space, and by N trajectories $\{x_1[t], x_2[t], x_3[t], ..., x_N[t]\} = \vec{x}[t]$, each one evolving in the physical space. So that $\vec{x}[t]$ can also be seen as the single trajectory of the many-body system in the configuration space with N degrees of freedom. Notice that the vector is not in the 3D real space, but on the N-dimensional configuration space.

In principle, the evolution of this many-body wavefunction $\psi(\vec{x},t)$ should also include the degrees of freedom of the atoms, or other "external" perturbations, that can be the origin of scattering as photons, phonons, crystalline defects etc..., however, to provide a first simple explanation of the Bohmian approach, in this chapter, only electrons and the electron-electron Coulomb interaction among each other will be taken into account in the discussion. The wavefunction $\Psi(\vec{x},t)$ is guided by the many-body Schrödinger equation:

$$i\hbar\frac{\partial\Psi(\vec{x},t)}{\partial t} = \left(-\sum_{i=1}^{N}\frac{\hbar^2}{2m}\frac{\partial}{\partial x_i^2} + U(\vec{x},t)\right)\Psi(\vec{x},t), \tag{3.1}$$

where m is the electron mass, inside the simulation box (to take into account the different electron masses in the structure a modification of this expression can be also considered), $\hbar$ is Planck's constant, and $U(\vec{x},t)$ is the electron-electron Coulomb interaction. The evolution of the probability presence, defined as $\rho(\vec{x},t) = |\psi(\vec{x},t)|^2$ guided by this N-electron Hamiltonian can be found by rearranging (3.1) and its complex conjugate as follows $\Psi^* \cdot \frac{\partial\Psi}{\partial t} + \Psi \cdot \frac{\partial\Psi^*}{\partial t}$, so that a continuity equation is formed:

$$\frac{\partial|\Psi(\vec{x},t)|^2}{\partial t} = -\sum_{i=1}^{N}\left(\frac{\partial}{\partial x_i}\frac{i\hbar}{2m}\left(\Psi(\vec{x},t)\frac{\partial\Psi^*(\vec{x},t)}{\partial x_i} - \Psi^*(\vec{x},t)\frac{\partial\Psi(\vec{x},t)}{\partial x_i}\right)\right), \tag{3.2}$$

which tells us that the current related to each i-th electron is:

$$J_i(\vec{x},t) = \frac{i\hbar}{2m}\left(\Psi(\vec{x},t)\frac{\partial\Psi^*(\vec{x},t)}{\partial x_i} - \Psi^*(\vec{x},t)\frac{\partial\Psi(\vec{x},t)}{\partial x_i}\right). \tag{3.3}$$

Then, it is natural to define a velocity $v_i(\vec{x},t)$ of the i-th trajectory liked to $\rho(\vec{x},t) = |\Psi(\vec{x},t)|^2$ as $J_i(\vec{x},t) = \rho(\vec{x},t)v_i(\vec{x},t)$, so that the definition of Bohmian velocity is:

$$v_i(\vec{x},t) = \frac{J_i(\vec{x},t)}{|\Psi(\vec{x},t)|^2}. \tag{3.4}$$

I insist that $\vec{x}$ is a vector in the configuration space showing the non-local character of quantum phenomena. The Bohmian velocity is used, then, to evolve each trajectory in a deterministic way, simply following:

$$x_i[t] = x_i[t_0] + \int_{t_0}^{t} v_i(\vec{x}[t'],t')dt'. \tag{3.5}$$

The relevance of this definition of velocity, given by the continuity equation (3.2), is that if a set of trajectories are distributed according to $|\Psi(\vec{x},0)|^2$ at time $t = 0$. Then, if such trajectories move according to the velocity in (3.4), they will reproduce the distribution $|\Psi(\vec{x},t)|^2$ at any other time t. As such, the trajectories can be understood as a microscopic description beneath the orthodox probability distribution. In other words, the orthodox theory plays the role in the quantum regime that statistical mechanics plays in the classical mechanics, while the Bohmian trajectories plays the role in the quantum regime of Newton classical trajectories.

Quantum equilibrium The condition that each initial position $x_i[0]$ of each trajectory $x_i[t]$ in the physical space is chosen by the following probability density $\rho(\vec{x},0) = |\Psi(\vec{x},0)|^2$ given by the many-body wavefunction can be written mathematically as:

$$|\Psi(\vec{x},0)|^2 = \lim_{M\to\infty} \frac{1}{M} \sum_{j=1}^{M} \prod_{i=1}^{N} \delta(x_i - x_i^j[0]). \tag{3.6}$$

Equation (3.6) argues that for a $M \to \infty$ number of simulated trajectories (experiments) the probability distribution will be perfectly reproduced at the initial time. Additionally, the continuity equation of the charge $\rho(\vec{x},t)$, in (3.2), can now be written in a simpler way by substituting (3.3), as:

$$\frac{\partial \rho(\vec{x},t)}{\partial t} + \sum_{i=1}^{N} \frac{\partial}{\partial x_i} J_i(\vec{x},t) = \frac{\partial \rho(\vec{x},t)}{\partial t} + \sum_{i=1}^{N} \frac{\partial}{\partial x_i} \left(\rho(\vec{x},t)v_i(\vec{x},t)\right) = 0. \tag{3.7}$$

This tells us that since trajectories are evolved using Eq. (3.5) with (3.4), at any time t we will get:

$$|\Psi(\vec{x},t)|^2 = \lim_{M\to\infty}\frac{1}{M}\sum_{j=1}^{M}\prod_{i=1}^{N}\delta(x_i - x_i^j[t]). \tag{3.8}$$

Now, I gave reason to why the Bohmian theory is able to exactly reproduce the same results as the orthodox one. Both formulations satisfy the Born law. The condition (3.8) is named quantum equilibrium, and the reader should realize that (3.8) is just a mathematical consequence of (3.6). Now, the question is what is the physical justification of (3.6) at the initial time? This topic is far from the scope of this thesis, but there are several justifications for the use of such distribution [69–72].

Notice also that, even when I know the initial state, I have no technological control to prepare or determine what is the initial position $x_i^j[0]$. Thus, I do not have the technological means to know which will be the output. This is how the quantum randomness is explained in Bohmian mechanics. I emphasize that there is a big difference between saying that the position of the electron is well-defined but unknown experimentally (as said in Bohmian mechanics) and that the electron position is unknown because the electron has no position (as said by the orthodox theory).

A different presentation of the Bohmian velocity can be done by a reformulation of the guiding wavefunction in polar form, as it was originally formulated by Bohm in 1952 in [63], by writing the wavefunction as $\Psi(\vec{x},t) = R(\vec{x},t)e^{iS(\vec{x},t)/\hbar}$, where if $\Psi(\vec{x},t)$ is complex, $R(\vec{x},t)$ and $S(\vec{x},t)$ are real values. See Appendix B for this formulation.

Chapter 4

Physics of open systems

In this chapter, I will explain some of the main techniques used to treat open systems in the quantum domain. This explanation will be divided between orthodox and Bohmian techniques. In particular, for the orthodox case, I will present the Density Matrix, and its deriving description that is the Wigner Function, while for the Bohmian approach I will explain the so-called Bohmian Conditional Wavefunction. I anticipate that the use of a wavefunction to describe an open system is not natural nor rigorous in the orthodox theory, but it is accurate and well justified in the Bohmian approach. The discussions in this chapter will be later relevant to discuss electron quantum transport with the inclusion of electron-photon and electron-phonon interactions.

4.1 To be or not to be Markovian

An electron device involves many electrons, atoms, inside and outside of the active region. The explicit simulation of all these particles is impossible. Thus, only some particles (the electrons inside the active region) are explicitly simulated. In other words, the simulation of an electron device is an example of the simulation of an open system [74]. In this section I explain when an open system can be considered as a Markovian or non-Markovian one. This is interesting because, for the simulation of open systems, a Markovian transition can be described with a simpler algorithm, reducing the computational cost but also losing information about the qualitative evolution of the system.

By definition, a closed system is a Markovian system because what happens in the future *does* only depends on the values of all degrees of freedom at the present. On the other hand, in principle, an open system is a non-Markovian system because what happens in the future *does not* only depend on the values of the degrees of freedom of the open system (explicitly simulated) at the present. There is always the possibility

that a non-simulated degree of freedom has a large influence on the behaviour of the open system. Even though this is not the scope of this thesis, let us provide a more mathematical description of what is a Markovian system.

The analysis of a classical Markovian system can be helpful. Suppose I am considering a stochastic process taking values in a numerable set of positions $\{x_i\}$ with $i = 1, .., N$. For simplicity, let us assume that I want to describe the probability that the system is in different x_i at different numerable times $t_n > t_{n-1} > ... > t_1 > t_0$. The process is said to be Markovian if the probability that the system is defined by x_n at time t_n (that in principle depends on all the previous history) can be written as:

$$p(x_n, t_n|x_{n-1}, t_{n-1}; x_{n-2}, t_{n-2}; .....; x_0, t_0) = p((x_n, t_n|x_{n-1}, t_{n-1}), \tag{4.1}$$

so that the probability only depends on the last assumed value, and not on previous ones x_{n-1} at t_{n-1}. In this sense the process is said to lack memory.

The quantum definition of Markovianity also relies on the lack of memory, but the conditional probability in orthodox quantum mechanics needs to be linked to a measurement process. The mentioned probabilities have to be linked to a measurement or observation time t_s. To have a more intuitive understanding of what is a quantum Markovian system, let us assume that the perturbation is acting on the system at every time interval t_s (for example, I am measuring an electron device every picosecond or the environment is perturbing the system once every picosecond). Let us define the duration of such perturbation as τ_s. During the time interval τ_s, the open system is entangled with the measuring apparatus or with the environment and what happens to the system cannot only be understood from the degrees of freedom of the open system. After such time τ_s, the open system loses its interaction with the measurement apparatus and it evolves basically only according to the degrees of freedom of the open system. Then, if I have a scenario with $t_s > \tau_s$ I can consider that the open system is still Markovian. What I see at every time t_s is basically dictated by the open system alone. On the contrary, if $t_s < \tau_s$, then the system is non-Markovian because the external measuring apparatus is affecting the behaviour of the open system. Now, the reason why the system's evolution during the perturbation time τ_s is not described by the open system alone is due to the fact that the environment or the measuring apparatus is not a degree of freedom of the evolution, so that how the open system affects the environment, or the environment's state, are not accessible informations [75].

The conclusion is that a quantum system that wants to be described at very short times t_s tends to be non-Markovian, while the same system in large times t_s can be

considered Markovian. In a language closer to engineers, the DC performance of an electron device can be modelled with a Markovian approach, without memory, while a non-Markovian approach, which includes memory, will be needed for the same electron device in high-frequency conditions.

4.2 Orthodox tools for open systems

In this section, I briefly present the literature about the description of open systems within orthodox quantum mechanics. In particular, first, I will discuss the Density Matrix and the Liouville equation used to evolve it [74, 76–78]. Then, I will give a description of the Wigner function and its equation of motion [47, 79–82]. An additional description for modelling open systems in orthodox quantum mechanics is the use of a wavefunction evolved with a Stochastic Schrödinger Equation under some limitations [83–88].

Every description will be presented in the present section, while in Section 4.4 I will explain some criticisms for each of these descriptions on how collisions are implemented. Additional description of an open system found in the literature are the Green's function [89–92], Kubo-Bastin Formalism [93–95], Pauli Master Equations [96–98], etc. The analysis of these last orthodox descriptions for open systems is beyond the scope of this thesis.

4.2.1 The Density Matrix

For a system described by a total wavefunction $\Psi(x, y, t)$, where x is the degree of freedom of the open system and y is the one of the environment, the density matrix operator $\rho(x, x', t)$ (in the position representation) is defined as:

$$\rho(x, x', t) = \int dy\, \Psi^*(x', y, t)\Psi(x, y, t). \tag{4.2}$$

The $\rho(x, x', t)$ is referred to as the reduced density matrix because the y degree of freedom has been eliminated. The observable $\langle O(t)\rangle$, related to the operator $O(x)$ of the system is also described by the density matrix operator $\hat{\rho}(t)$, and it is estimated by applying what is called the trace of the operator on $\hat{\rho}\hat{O}$:

$$\begin{aligned}
\langle O(t)\rangle &= \int dx \int dy\, \Psi^*(x', y, t)O(x)\Psi(x, y, t) \\
&= \int dx\, O(x) \left(\int dy\, \Psi^*(x', y, t)\Psi(x, y, t) \right) \\
&= \int dx\, O(x)\, \rho(x, x', t) = Tr(\hat{\rho}\hat{O}),
\end{aligned} \tag{4.3}$$

where Tr is the trace defined as the integral of the x degree of freedom when the operator $\hat{\rho}\hat{O}$ in the position representation is evaluated only on the diagonal elements ($x' = x$). As an example if I take an open system described by $\hat{\rho}_0(t)$, which absorbs a photon with energy E_γ at time t_s, the mean energy before the absorption is $\langle E(t_s)\rangle = Tr(\hat{\rho}_0(t)\hat{H}_0)$ where $\hat{H}_0$ is the operator linked to the total energy of the electron. After the absorption I will have $Tr(\hat{\rho}^s(t)\hat{H}_0) = Tr(\hat{\rho}_0(t)\hat{H}_0) + E_\gamma$. Where $\hat{\rho}^s(t)$ is the generic scattered Density Matrix. The typical equation of motion of the density operator is the Liouville-Von Neumann equation:

$$\frac{d\hat{\rho}(t)}{dt} = -i\frac{1}{h}\left[\hat{H}\hat{\rho}(t)\right] = -i\frac{1}{h}\left[\hat{H}_0\hat{\rho}(t)\right] + \hat{C}\hat{\rho}(t). \tag{4.4}$$

Where the first term on the right-hand side of (4.4) gives the unperturbed unitary evolution of the open system alone. On the other hand, the second term is the interaction term [99], which models the perturbation acting on the open system due to external effects (the environment of the measurement). Here $\hat{H}_0$ is the Hamiltonian of the free electron

$$H_0 = \frac{\mathbf{p}^2}{2m} + U_{ext}(\mathbf{r}, t). \tag{4.5}$$

the term $U_{ext}(\mathbf{r}, t)$ is an "external" arbitrary potential which may contain many contributions. The explicit discussion about $U_{ext}(\mathbf{r}, t)$ will be done in the following chapter. The Hamiltonian $\hat{H}_0$ can be understood as the free Hamiltonian of the open system composed of kinetic energy plus a potential energy $\hat{V}$ that in our case will be a double barrier profile.

For example, let us analyze a scattering process due to the operator $\hat{C}$ in (4.4). I define $\hat{\rho}(t_s)$ as the density matrix before the scattering and $\hat{\rho}(t_s + \tau_s)$ the density matrix when the scattering process has finished, where I dropped the apex s for simplicity. With a finite difference approximation of $\frac{d\hat{\rho}(t)}{dt} \approx \frac{\hat{\rho}(t_s+\tau_s)-\hat{\rho}(t_s)}{\Delta t}$ with $\Delta t = \tau_s$ I get:

$$\hat{\rho}(t_s + \tau_s) = \hat{\rho}(t_s) + \frac{\tau_s}{i\hbar}\left[\hat{H}_0\hat{\rho}(t_s)\right] + \tau_s\hat{C}[\hat{\rho}(t_s)]. \tag{4.6}$$

This last expression will be relevant later when discussing collision with orthodox tools. In principle, the density matrix description has no limitations for what concerns the representation of Markovian or non-Markovian open systems. The Markovianity of the approach used to evolve the density matrix depends on which is the definition of the interaction operator $\hat{C}$. As we will see, the problem in practical scenarios will be to find the proper operator $\hat{C}$ to build realistic collisions.

4.2.2 Wigner function

The Wigner function is a tool to represent the density matrix of a given system in a phase space, with momentum k and position x as degrees of freedom (instead of x and x' as happens in the density matrix). The Wigner-Weyl transform is applied on the density matrix $\hat{\rho}(t)$ to reach the Wigner function $f_W(x,k,t)$ defined as:

$$f_W(x,k,t) = \frac{1}{2\pi}\int dx' \langle x + \frac{x'}{2}|\hat{\rho}(t)|x - \frac{x'}{2}\rangle e^{-ikx'}. \tag{4.7}$$

The equation of motion for the Wigner function is also obtained from the Wigner-Weyl transformation of the previous Liouville equation in (4.4) given the Wigner equation [81, 99].

$$\frac{\partial f_W(x,k,t)}{\partial t} + \frac{\hbar}{m}k\frac{\partial f_W(x,k,t)}{\partial x} + \frac{1}{\hbar}\frac{\partial U_{ext}(x,t)}{\partial x}\frac{\partial f_W(x,k,t)}{\partial k} = \hat{C}_W f_W(x,k,t) + \hat{Q}_W f_W(x,k,t). \tag{4.8}$$

Where $\hat{Q}_W$ is an additional term related to the potential energy $U_{ext}(x,t)$ of the free electron Hamiltonian H_0, and:

$$Q_W f_W(x,k,t) = \int dk' U_q(x,k-k') f_W(x,k',t). \tag{4.9}$$

with U_p the Wigner-Weyl transformation of the potential $U_{ext}(x,t)$. In addition, I have $\hat{C}_W$ which is the Wigner-Weyl transform of the typical Collision operator in the Liouville equation (4.4). As it happens with the density matrix, such collision operator can either be described by a Markovian or by a non-Markovian approach. The most widely used approach for treating collisions is the so-called Boltzmann-like collision operator, which consists in the use of the scattering rate s_{k,k_s} which, as in the classical Boltzmann equation, gives the transition rate from the wavevector k to k_s due to a collision, or vice versa [80, 100, 101],

$$C_W f_W(x,k,t) = \frac{1}{2\pi}\int \left[s_{k,k_s} f_W(x,k_s,t) - s_{k_s,k} f_W(x,k,t)\right] dk_s. \tag{4.10}$$

I will show in Chapter 6 how this collision term conserves the energy only in very particular conditions.

4.2.3 Stochastic Schrödinger equation

The Stochastic Schrödinger equation is a technique based on using a decomposition of the reduced density matrix in (4.2) in terms of pure states $\Psi_j(x,t)$ of the open system

alone

$$\rho(x,x',t)=\sum_j P_j(t)\Psi_j^*(x',t)\Psi_j(x,t). \tag{4.11}$$

With $P_j(t)$ the probability of the different pure states. Pseudo-Schrödinger equations can be found for the dynamic evolution of $\Psi_j(x,t)$. The evolution is mostly independent on the environment, which is simulated as a type of stochastic noise in the pseudo-Schroedinger equation [83–87, 102, 103].

For Markovian condition, when the observation time is larger than the time interval while the open system is entangled with the environment, $t_s > \tau_s$, the pure states $\Psi_j(x,t)$ in (4.11) can be understood as the real states of the open system. As described in Sec. 4.1, after a time τ_s, the open system is disentangled from the environment and it can be considered for a while as a closed system described by the pure state $\Psi_j(x,t)$. After a measurement or collision with the environment, the system can be considered to be described by another pure state $\Psi'_j(x,t)$. However, for general non-Markovian conditions, the state $\Psi_j(x,t)$ can only be considered as a mathematical tool (not a physical state of the system) within the orthodox theory.

It has been recently shown that systems under non-Markovian condition can still be studied with pure states with the use of the Bohmian theory, where the additional information about the environment described by the degree of freedom y can be invoked as the Bohmian trajectory $y[t]$, while keeping a wavefunction description for the open system. See the recent works [88, 104–106] for an enlarged explanation. In conclusion, within a strictly orthodox quantum description, the wavefunction is *not* enough to describe the system under non-Markovian condition. A better description for such a goal is the Bohmian quantum theory applied to open systems, which provides a tool that I will explain in the following section.

4.3 Bohmian tools for open systems

In this section I will present a formal description of the Conditional Wavefunction for a system with N-particles. I will see that the wavefunction with a N-dimensional description can be substituted by N one-dimensional wavefunctions. For each one-dimensional wavefunction, only one degree of freedom remains, while all other $N-1$ degrees of freedom, related to the other trajectories, are treated as time-dependent parameters (i.e. as deterministic Bohmian trajectories). This description will be used later in Chapter 6 to treat electron-photon collisions with the use of pure states. The Bohmian Conditional

wavefunction has an important role in the results reported in this thesis in Part IV.

4.3.1 Bohmian conditional wavefunction

The direct solution of the N particle Schrödingher equation in (3.1) is practically not feasible, as it needs the solution of the equation along all N of its degrees of freedom simultaneously, to find the evolution of the N-dimensional many-body wavefunction. This is called the many-body problem.

One solution to this many-body problem is to use the so called Bohmian Conditional wavefunction. The Bohmian Conditional wavefunction approach was first proposed in [107, 108]. As I said, a N particle systems is described in the Bohmian theory by N-dimensional wave function $\Psi(x_1, x_2, ..., x_N, t)$ plus N trajectories $\{x_1[t], x_2[t], ..., x_N[t]\}$. I will substitute some of the degrees of freedom inside the N-dimensional many-body wavefunction with the instantaneous value of $N-1$ trajectories. To simplify the notation, I define $\vec{x_b} = \{x_1[t], x_2[t], ..., x_{a-1}[t], x_{a+1}[t], ..., x_N[t]\}$. Then, the Bohmian Conditional wavefunction will only include one degree of freedom x_a as.

$$\psi(x_a, t) \equiv \Psi(x_a, \vec{x_b}[t], t). \tag{4.12}$$

This Bohmian Conditional wavefunction will useful to compute the a-th trajectory, $x_a[t]$. Notice that the trajectory $x_i[t] = x_i[t_0] + \int_{t_0}^{t} v_i(\vec{x}[t'], t')dt'$ in (3.5) requires the knowledge of the Bohmian velocity at the position $\vec{x}[t']$. From (3.3), I see that the Bohmian velocity does only require a partial derivative in the x_a direction thus

$$\begin{aligned} J_a(\vec{x}, t)|_{\vec{x}=\vec{x}[t']} &= \frac{i\hbar}{2m}\left(\Psi(\vec{x}, t)\frac{\partial\Psi^*(\vec{x}, t)}{\partial x_a} - \Psi^*(\vec{x}, t)\frac{\partial\Psi(\vec{x}, t)}{\partial x_a}\right)|_{\vec{x}=\vec{x}[t']} \\ &= \frac{i\hbar}{2m}\left(\Psi(x_a, \vec{x}_b[t], t)\frac{\partial\Psi^*(x_a, \vec{x}_b[t], t)}{\partial x_a} - \Psi^*(x_a, \vec{x}_b[t], t)\frac{\partial\Psi(x_a, \vec{x}_b[t], t)}{\partial x_a}\right)|_{x_a=x_a[t']} \\ &= \frac{i\hbar}{2m}\left(\psi(x_a, t)\frac{\partial\psi^*(x_a, t)}{\partial x_a} - \psi^*(x_a, t)\frac{\partial\psi(x_a, t)}{\partial x_a}\right)|_{x_a=x_a[t']}. \end{aligned} \tag{4.13}$$

In conclusion, the Bohmian velocity in (3.4) can be computed from $\Psi(\vec{x}, t)$ evaluated at $\vec{x} = \vec{x}[t']$ or from $\psi(x_a, t)$ evaluated at $x_a = x_a[t']$. This Bohmian Conditional wavefunction can be also understood as a projection of the many-body wave function $\Psi(x_1, x_2, ..., x_N, t)$ on the x_a degrees of freedom [109]. The Bohmian Conditional wavefunction tool is implemented in the home-made BITLLES simulator [110] used in some results of this thesis.

The next question is what is the equation of motion of such conditional wave function. It can be shown that the Bohmian Conditional wavefunction can be guided by an equation

of motion where again all the $N-1$ degrees of freedom are taken as parameters for the evolution of the a-th trajectory $x_a[t]$, guided by $\psi_a(x_a,t)$. The equation of motion reads [109]:

$$i\hbar\frac{\partial\psi_a(x_a,t)}{\partial t} = \left(-\frac{\hbar}{2m}\frac{\partial^2}{\partial x^2} + U_a(x_a,\vec{x}_b[t],t) + G_a(\vec{x}[t],t) + iJ_a(\vec{x}[t],t)\right)\psi_a(x_a,t). \quad (4.14)$$

Where I defined the total Coulomb potential as:

$$U(x_a,\vec{x}_b[t],t) = U_a(x_a,\vec{x}_b[t],t) + U_b(\vec{x}_b[t],t), \quad (4.15)$$

where $U_a(x_a,\vec{x}_b[t],t)$ is the interaction with a potential external to the electron system, like the conduction band, and $U_b(\vec{x}_b[t],t)$ is the electron-electron Coulomb interaction, acting on the a-th particles, taking all the other trajectories as parameters ($\vec{x}_b = \vec{x}_b[t]$). The explicit definition of G_a and J_a can be found in Appendix C

The Bohmian conditional wave function can describe either the Markovian or non-Markovian evolutions of a system. Notice that in the above development I have not specify any particular (Markovian or non-Markovian) condition to reach the Bohmian Conditional wavefunction in (4.12). The proper definition of interacting potentials $U_a(x_a,\vec{x}_b[t],t)$, $G_a(x_a,\vec{x}_b[t],t)$ and $J_a(x_a,\vec{x}_b[t],t)$ can be re-written to describe the effect that the environment has on the electron. In Chapter 6 I will give an example of this re-definition, while some numerical results will be given in Chapter 9.

4.4 Implementation of orthodox and Bohmian tools

In this section I will comment on the advantages and limitations of the descriptions explained in the previous Sections 4.2 and 4.3. First, I report two conditions needed to implement the environment perturbation (collisions) in a physically accurate way. Then I talk about how and if these conditions are verified in those orthodox and Bohmian tools. When modelling electron devices through open system theories explained in the previous Sections 4.2 and 4.3, a key element to build a physically realistic simulation is the inclusion of the proper term for the external perturbation in the dynamics of simulated electrons.

4.4.1 Complete positivity and energy conservation

Obviously, collisions are difficult to be treated in an exact way because the external degrees of freedom (atoms for phonons and electromagnetic fields for photons) are not

explicitly simulated in the theories of open systems. The most I can do is an approximate model. Typically, the approach used to model collisions is changing from one initial state to a final one. The question now is how I can certify if the perturbation algorithm that has been implemented is correct or not. Certifying is not trivial because it would require solving the whole system, open system plus environment, as a closed system, and comparing it with the result. A simpler way to certify that the implemented method is correct, is by checking some properties of the model. I explain below two conditions:

Complete Positivity: The density matrix $\rho(x', x, t)$, the Wigner function and the wavefunction $\psi(x, t)$ encode probabilistic information of the open system. As such I require them to provide always (before and after the collisions) positive value of the probability. For the wavefunction, it means $|\psi(x, t)|^2 > 0$ at every position of the simulation box x and at every time t of the evolution. Identically, for the density matrix, it requires $\rho(x', x, t)|_{x'=x} > 0$ at every value of x and t. A similar condition for the Wigner function. I will see that the accomplishment of the Complete Positivity is not always evident in the Wigner and density description of an open system.

Energy Conservation: The total energy of the global system (including the open system plus the environment) satisfies the conservation of energy for any type of interaction between the parts of the system. In principle, the amount of energy added/eliminated to the open system by a collision of an electron with a phonon or a photon is well defined. Provided by that the energy of the interacting particles is known, this is a quite straightforward condition. So that, one can intuitively check if the implemented collision model is acceptable or not by checking this condition.

These conditions need to be satisfied by any model of collisions in open systems, either Markovian or non-Markovian.

4.4.2 Checking orthodox tools

In this section, I will explain how the previous checks (Complete positivity and Energy conservations) are difficult to be fully satisfied when implementing collisions from an orthodox quantum description of open systems, either with the Density Matrix or the Wigner Function representation.

For a general system, the Density Matrix is the tool needed by orthodox quantum mechanics to treat open systems, as explained in 4.2.1. The density matrix by its nature eliminates the information about which individual states $\psi_i(x,t)$ is used to build it. Let us imagine that the density matrix $\hat{\rho}(t)$ operator provides a description of our system as follows:

$$\rho(x,x't) = \frac{1}{M}\sum_{i=1}^{N} M_i \psi_i^*(x',t)\psi_i(x,t), \tag{4.16}$$

where M_i is the number of states $\psi_i(x,t)$ present in the system with $M = \sum_{i=1}^{N} M_i$ the total number of components used to build the N-particle density matrix representing the open system. In any practical model we will work with the right hand side of (4.16), and evolve $\hat{\rho}(t)$ following the Liouville equation (4.4), then I will have no access to the information about each state $|\psi\rangle$. In fact, the orthodox theory says that such information does not exist in a general (non-Markovian) system. This means losing the information about the single-particle state of each electron in the system.

The density matrix after a scattering process, $\rho(x,x',t_s+\tau_s)$, can be written as:

$$\rho(x,x',t_s+\tau_s) = \rho(x,x',t_s) - \frac{1}{M}\psi_-^*(x',t)\psi_-(x,t) + \frac{1}{M}\psi_+^*(x',t)\psi_+(x,t), \tag{4.17}$$

where $\psi_-(x,t)$ is the eliminated state and $\psi_+(x,t)$ is the added states. This is nothing else than the typical description of the creation and annihilation of quantum states in an open system after the effect of an external perturbation. This evolution due to collisions, in the case that not every state in $\rho(t_s)$ are known, could lead to the elimination of states that were not present. Notice that the right hand side of (4.16) is not a physical information in the orthodox theory (there are no orthodox pure states able to describe a open system). In fact, the new evaluation of the density matrix after the scattering will be computed from (4.6) that I rewrite here

$$\hat{\rho}(t_s+\tau_s) \approx \hat{\rho}(t_s) + \tau_s \hat{C}[\hat{\rho}(t_s)]. \tag{4.18}$$

Notice that, for simplifying the discussion, I have eliminated the free evolution due to $\hat{H}_0$ under the assumption that the scattering is fast. Since I do not know what I am really

doing on the states when implementing the scattering process in terms of $\tau_s \hat{C}[\hat{\rho}(t_s)]$, I will have problems in satisfying complete positivity after the scattering process. In other words, (4.17) can give negative values when $\rho(x, x', t_s + \tau_s)$ is evaluated at $x = x'$, which means the nonphysical result of a negative probability of finding an electron at x.

As similar problem appears in the conservation of the energy. Let us consider an open system that has an energy $\langle E(t_s)\rangle$ before the scattering, and an energy $\langle E(t_s + \tau_s)\rangle$ after it. Let us assume, for example, that I am dealing with an absorption of the energy E_γ of a photon so that the proper conservation of energy condition would read $\langle E(t_s + \tau_s)\rangle = \langle E(t_s)\rangle + E_\gamma$. From (4.3) and (4.17), I can write the energy of the density matrix $\rho(x, x', t_s + \tau_s)$ after the scattering as:

$$\langle E(t_s + \tau_s)\rangle = Tr(\hat{\rho}(t_s + \tau_s)H_0) = \sum_{i=1}^{N} \frac{M_i}{M}\langle E_i(t_s)\rangle - \frac{1}{M}\langle E_-(t)\rangle + \frac{1}{M}\langle E_+(t)\rangle, \quad (4.19)$$

where M_i is the number of the components building the single-particle state of each i-th electron, and M is the total number of components used to build the N-particle density matrix. In fact, we have $M = \Sigma_{i=1}^{N} M_i$. Where $\langle E_-(t)\rangle$ is the energy of the removed state $|\psi_-(t)\rangle$ using (4.3), and $\langle E_-(t)\rangle$ is the energy of the added state $|\psi_+(t)\rangle$. However, exactly as it is not guaranteed that the state $|\psi_-(t)\rangle$ removed from the density matrix in (4.17) is present in the density matrix, also its associated energy $\langle E_-(t)\rangle$ may not be present, and the elimination of this energy value does not always respect the conservation of energy $-\frac{1}{M}\langle E_-(t)\rangle + \frac{1}{M}\langle E_+(t)\rangle = E_\gamma$ where, by construction, I define $\langle E(t_s)\rangle + E_\gamma = \sum_{i=1}^{N} \frac{M_i}{M}\langle E_i(t_s)\rangle$.

The Wigner function suffers from similar drawbacks mentioned above. The reason is that the Wigner function is just a simple metamathematical transformation of the density matrix. The Wigner-Weyl transformation of the Density Matrix is also *hiding* information about the $i-$th particle inside a $N-$particle Wigner Function $f_W(x, k, t)$. Some works underlining issues about guaranteeing complete positivity in the Wigner description are the following [51,111,112]. Additional problems will be underlined in Section 6, following results from [113], which reveal problems about respecting energy conservation in this description.

4.4.3 Checking Bohmian tools

The Bohmian mechanics representation of an open system, which uses the tool of the Bohmian Conditional Wavefunction, can treat both Markovian and non-Markovian sys-

tems. Once I deal with a conditional wave function for each j-electron $\Psi_j(\vec{x},t)$, it is obvious that it satisfies Complete Positivity because $\sum_j |\Psi_j(\vec{x},t)|^2 > 0$ by construction. I will show numerically in Chapter 9 that it also satisfies energy conservation when proper modelling of the effect of the perturbation is provided. Examples of implementation of non-Markovian systems using the Bohmian Conditional wavefunction are: [104, 114, 115].

The reason why these conditions can be more easily respected in the Bohmian view, in comparison with the orthodox one is that the Bohmian Conditional Wavefunction allows for a microscopic description of each electron and its single-particle wve function and properties such as energy, position, velocity, etc. Without the need for a measurement process. Then, the knowledge of which properties are needed to be changed because of the collision event is quite simple, because many variables are well defined at the time of the collision. On the contrary, the orthodox view does only provide a global information of the whole system through the density matrix $\rho(x',x,t)$ (or the Wigner function $f_W(x,k,t)$) for all electrons. Then, it is not possible to know which are the microscopic properties of each electron that need to be changed.

In simple words, as said when I presented in the Bohmian theory in Chapter 3, the orthodox theory plays, within the quantum domain, the same role that statistical mechanics plays in the classical domain. On the other hand, the Bohmian theory plays, within the quantum domain, the same role that Newtown classical trajectories. The former approach has very little information about the single states of each element of the system, while the latter has a huge amount of information about them. Certainly, in the classical regime, it is much easier to implement collisions from Newton law, than from a statistical formulation. The same happens in the quantum regime. It is simpler to understand and implement collisions from the (microscopic) Bohmian mechanics than from a (macroscopic) orthodox formulations.

The reader can argue that the Stochastic Schrödinger equation, which also works with states, can be understood also as a microscopic description in the orthodox theory. This is false. Or, only partially true. In a system under Markovian condition, one can accept that the individual states of the Stochastic Schrödinger equation describe the physical system, but in a general system with a general non-Markovian condition this is not true because the states of the Stochastic Schrödinger equation are only mathematical tools, not physical elements that describe the open system. At the end of the day, one of the postulates of the orthodox theory is negating the existence of microscopic properties of a quantum system, as long as such properties are not measured. This is the key element that

makes the implementation of collisions with the orthodox view much more complicated than with the Bohmian one.

Part III

Models

Chapter 5

Maxwell equations and displacement current

In electron devices, the typical output is the electrical current. In this chapter, I will discuss how such electrical current is evaluated in the frequency range of the THz gap. Starting from Maxwell's equations, I will define the total current including the particle and displacement components. The role of the second term in high-frequency scenarios will be emphasized. The results of this chapter will be used in the next Chapter 8 to build the *Displacement Current Coefficient*. Additionally, the effect of the electromagnetic field on the dynamics of the electron will be treated in Chapter 6.

Please notice that now I use the notation $\mathbf{W}$ to refer to an arbitrary vector W in the three-dimensional real space. All the vectors shown in Chapter 3 and 4.12 use the notation $\vec{W}$, to represent an array of deterministic values of a given observable (position, velocity, etc.), representing a N-particle system in a Bohmian description.

5.1 Maxwell equations

In this section, I will describe Maxwell's equations to introduce some notation used all along the thesis. In particular, I will divide the electromagnetic fields between transversal (with divergence equal to zero) and longitudinal (with curl equal to zero) ones.

For the electric field, the Helmholtz decomposition allows us to write the electric field $\mathbf{E}(\mathbf{r}, t)$:

$$\mathbf{E}(\mathbf{r}, t) = \mathbf{E}_{\perp}(\mathbf{r}, t) + \mathbf{E}_{\parallel}(\mathbf{r}, t). \tag{5.1}$$

These two components will satisfy Maxwell equations [116, 117]:

$$\nabla \cdot \mathbf{E}_{\perp}(\mathbf{r},t) = 0, \tag{5.2}$$

$$\nabla \times \mathbf{E}_{\perp}(\mathbf{r},t) = -\frac{\partial \mathbf{B}(\mathbf{r},t)}{\partial t}, \tag{5.3}$$

$$\nabla \times \mathbf{E}_{\parallel}(\mathbf{r},t) = 0, \tag{5.4}$$

$$\nabla \cdot \mathbf{E}_{\parallel}(\mathbf{r},t) = \frac{\rho(\mathbf{r},t)}{\epsilon_0}, \tag{5.5}$$

$$\tag{5.6}$$

where $\rho(\mathbf{r},t)$ is the charge density. For simplicity, I use the ϵ_0 is the electric permittivity in vacuum but, if needed, ϵ_0 can be substituted to the corresponding value in a specific material. I then call the vector potential $\mathbf{A}(\mathbf{r},t)$ which satisfy $\mathbf{E}(\mathbf{r},t) = \nabla \times \mathbf{A}(\mathbf{r},t)$. Along this thesis, I will use the Coulomb Gauge $\nabla \cdot \mathbf{A}(\mathbf{r},t) = 0$ so that the vector potential is also a transversal field. Then, I can write the two components of the electric field as:

$$\mathbf{E}_{\perp}(\mathbf{r},t) = \frac{\partial \mathbf{A}(r,t)}{\partial t}, \tag{5.7}$$

$$\mathbf{E}_{\parallel}(\mathbf{r},t) = -\nabla U(\mathbf{r},t). \tag{5.8}$$

This will also let us rewrite (5.6) as the Poisson equation:

$$\nabla^2 U(\mathbf{r},t) = -\frac{\rho(r,t)}{\epsilon_0}. \tag{5.9}$$

From Maxwell's laws, I know that the magnetic field $\mathbf{B}(\mathbf{r},t)$ has only a transversal component, so that:

$$\nabla \cdot \mathbf{B}(\mathbf{r},t) = 0. \tag{5.10}$$

and

$$\nabla \times \mathbf{B}(\mathbf{r},t) = \epsilon_0 \mu_0 \frac{\partial \mathbf{E}_{\parallel}(\mathbf{r},t)}{\partial t} + \mu_0 \mathbf{J}_c(\mathbf{r},t), \tag{5.11}$$

where $\mathbf{J}_c(\mathbf{r},t)$ is the particle current and μ_0 is the magnetic permeability in vacuum. The above parameters give the well-known relationship $c = \frac{1}{\sqrt{\epsilon_0 \mu_0}}$ as the speed of light in vacuum.

5.1.1 Bohmian sources of Maxwell's equation

An important note appears now, about how I define the sources of Maxwell's equation in a quantum scenario. Defining the charge $\rho(\mathbf{r},t)$ and the current and $\mathbf{J}_c(\mathbf{r},t)$ with the orthodox quantum theory is not easy at all because, unless I have some measured

properties, the wave function is all the information that I have about the electron. In other words, the wave function does not explain to us which is the position of the electron or its velocity, it only provides probabilistic information on what would happen if one property is measured. But, what happens if I want to know such properties when no measurement is done? The orthodox theory cannot help us. On the contrary, the Bohmian mechanics, describing the system with both wave function and deterministic trajectories $\mathbf{r}_i[t]$ for each electron, does provide such type of unmeasured information. Then, I can write the charge density as:

$$\rho(\mathbf{r},t) = \sum_{i=1}^{N} e\mathbf{v}_i(\mathbf{r},t)\delta(\mathbf{r}-\mathbf{r}_i[t]), \tag{5.12}$$

and the current density as

$$\mathbf{J}_c(\mathbf{r},t) = \sum_{i=1}^{N} e\mathbf{v}_i(\mathbf{r},t)\delta(\mathbf{r}-\mathbf{r}_i[t]). \tag{5.13}$$

In summary, I identify three components of the electromagnetic field: two related to the decomposition of the electric field $\mathbf{E}(\mathbf{r},t) = \mathbf{E}_\perp(\mathbf{r},t) + \mathbf{E}_\parallel(\mathbf{r},t)$, and $\mathbf{B}(\mathbf{r},t)$. These three components respect equations (5.3)(5.4)(5.6)(5.10), and (5.11) which couple them together. The sources of such components are the current defined in (5.13), which acts on the components of the electric field through (5.11), and the charge density (5.12), which is inserted in (5.6).

5.2 The displacement current

In this section I will show that the definition of the displacement current is hidden in Maxwell's equations. Applying a divergence on (5.11), and substituting (5.6) I have

$$\begin{aligned}\nabla\cdot(\nabla\times\mathbf{B}(\mathbf{r},t)) &= \epsilon_0\mu_0\frac{\partial\nabla\cdot\mathbf{E}_\parallel(\mathbf{r},t)}{\partial t} + \mu_0\nabla\cdot\mathbf{J}_c(\mathbf{r},t)\\ &= \mu_0\left(\frac{\partial\rho(\mathbf{r},t)}{\partial t} + \nabla\cdot\mathbf{J}_c(\mathbf{r},t)\right) = 0,\end{aligned} \tag{5.14}$$

which provides a continuity equation, and a definition of a the total current $\mathbf{J}(\mathbf{r},t)$ with the condition $\nabla\cdot\mathbf{J}(\mathbf{r},t) = 0$ as:

$$\mathbf{J}(\mathbf{r},t) = \mathbf{J}_c(\mathbf{r},t) + \frac{\partial\mathbf{E}_\perp(\mathbf{r},t)}{\partial t} + \frac{\partial\mathbf{E}_\parallel(\mathbf{r},t)}{\partial t}. \tag{5.15}$$

Notice the inclusion of the term $\frac{\partial\mathbf{E}_\perp(\mathbf{r},t)}{\partial t}$ in the definition of the total current because $\nabla\cdot\mathbf{E}_\perp(\mathbf{r},t) = 0$. From the above definitions, the components of (5.15) can also be

written as

$$\mathbf{J}(\mathbf{r},t) = \mathbf{J}_c(\mathbf{r},t) + \frac{\partial^2 \mathbf{A}(\mathbf{r},t)}{\partial t^2} + \frac{\partial \nabla U(\mathbf{r},t)}{\partial t}. \tag{5.16}$$

Notice that the property $\nabla \cdot \mathbf{J}(\mathbf{r},t) = 0$ implies that in a two-terminal device, as the RTD, the instantaneous current entering in one contact is the same that is leaving the other. This equivalence does not need to be true for the particle current alone $\mathbf{J}_c(\mathbf{r},t)$. As a well-known example, the particle current entering in a capacitor can be different from the particle current in the middle of the capacitor, but the total current in both points is the same at any time. It is in this sense that what I have to predict in high frequency electron devices is the total current in the active region, not the particle current.

5.2.1 The Ramo-Shockley-Pellegrini theorem

We now explain a practical way of computing the total current of (5.15). This result was found by Ramo, Shockley and later extended by Pellegrini [118–123].

We define an arbitrary mathematical volume Ω enclosed by a closed surfaces S that can be subdivided into different surfaces $S = \{S_1, S_2, ...\}$. I define the total observable current $I_j(t)$ as the current estimated on one of these surfaces, $I_j = \int_{S_j} \mathbf{J}(x,t) d\mathbf{s}$. I define a function G_j related to surface S_j using Dirichlet conditions, so that $G_j(\mathbf{r}) = 1$ in any point of the j-th surface, while $G_j(\mathbf{r}) = 0$ on any other surface. We also define the vector function $\mathbf{F}_j(\mathbf{r})$ as follows

$$\mathbf{F}_j(\mathbf{r}) = -\nabla \mathbf{G}_j(\mathbf{r}), \tag{5.17}$$

so that I will have:

$$\nabla \cdot [\epsilon_0(\mathbf{r}) \mathbf{F}_j(\mathbf{r})] = -\nabla \cdot [\epsilon_0(\mathbf{r}) \nabla \mathbf{G}_j(\mathbf{r})] = 0. \tag{5.18}$$

Finally, thanks to the definition of $G_j(\mathbf{r})$, I can go from the integral on the surface S to the one within the volume Ω, which gives

$$I_j(t) = \int_S \mathbf{G}_j(\mathbf{r},t) \mathbf{J}(\mathbf{r},t) \cdot ds = -\int_\Omega \mathbf{F}_j(\mathbf{r},t) \cdot \mathbf{J}(\mathbf{r},t)\, dv, \tag{5.19}$$

and, by substituting (5.15), I find [118, 119]:

$$I_j(t) = -\int_\Omega \mathbf{F}_j(\mathbf{r},t) \cdot \mathbf{J}_c(\mathbf{r},t)\, dv + \Gamma_e + \Gamma_m, \tag{5.20}$$

where the two components related to the transversal and longitudinal electric field terms are:

$$\Gamma_e = \int_\Omega \mathbf{F}_j(\mathbf{r},t)\cdot\frac{\partial \mathbf{E}_\parallel(\mathbf{r},t)}{\partial t}\,dv = \int_\Omega \mathbf{F}_j(\mathbf{r},t)\cdot\frac{\partial \nabla U(\mathbf{r},t)}{\partial t}\,dv, \tag{5.21}$$

$$\Gamma_m = \int_\Omega \mathbf{F}_j(\mathbf{r},t)\cdot\frac{\partial \mathbf{E}_\perp(\mathbf{r},t)}{\partial t}\,dv = \int_\Omega \mathbf{F}_j(\mathbf{r},t)\cdot\frac{\partial^2 A(\mathbf{r},t)}{\partial t^2}\,dv. \tag{5.22}$$

Now I can use the so-called the Darwin approximation where $E_\perp(\mathbf{r},t)$ is considered non negligible with respect to $E_\parallel(\mathbf{r},t)$, while its derivative is negligible in comparison with the derivative of $E_\parallel(\mathbf{r},t)$ so that, (5.15) with the use of (5.13), will be

$$\mathbf{J}(\mathbf{r},t) \approx \mathbf{J}_c(\mathbf{r},t) - \frac{\partial \mathbf{E}_\parallel(\mathbf{r},t)}{\partial t}. \tag{5.23}$$

Notice that the Darwin approximation keeps the vector potential $\mathbf{A}(\mathbf{r},t)$ as a relevant element, and also its time dependent derivative $\frac{\partial \mathbf{A}(\mathbf{r},t)}{\partial t} \neq 0$. I will use later $\mathbf{A}(\mathbf{r},t)$ to see the effect of the transversal fields on the description of the interaction of the electron with the electromagnetic field. I now substitute Γ_e from (5.22) into (5.23) with $\Gamma_m \approx 0$ because $\frac{\partial^2 \mathbf{A}(\mathbf{r},t)}{\partial t^2} \ll \frac{\partial \mathbf{A}(\mathbf{r},t)}{\partial t}$ due to the Darwin approximation. Then using (5.17), I write Γ_e as an integral on the surface of the simulation box S containing the simulated volume Ω as

$$\int_\Omega \epsilon_0 \mathbf{F}_j(\mathbf{r},t)\cdot\frac{\partial \nabla U(\mathbf{r},t)}{\partial t}\,dv = \int_S \epsilon_0(\mathbf{r})\mathbf{F}_j(\mathbf{r},t)\cdot\frac{\partial U(\mathbf{r},t)}{\partial t}\cdot ds. \tag{5.24}$$

We assume that the surfaces of the arbitrary volume Ω parallel to the transport direction are in the contact regions (reservoirs). If I assume then the contact regions (reservoirs) to be made of ideal metal, I can assume that no electric field is present in the mentioned parallel surfaces S of volume Ω so that $\frac{\partial U(\mathbf{r},t)}{\partial t} \approx 0$. This means that the electrons outside the active region (inside the contacts) have a screening time equal to zero, so that electrons outside the active region do not contribute to the electrical current. I also assume that the other surfaces of the volume Ω are far from the active region where there are electrons so that I get $\frac{\partial U(\mathbf{r},t)}{\partial t} \approx 0$ at such other surfaces. Then, Γ_e in the shape (5.24) can be also neglected. I then only need to take into account the first term of in (5.20) and, finally, the total current on the surface S_j can be computed from

$$I_j(t) = \int_\Omega \mathbf{F}_j(\mathbf{r},t)\cdot\mathbf{J}_c(\mathbf{r},t)dv, \tag{5.25}$$

If then I substitute (5.13), I have the expression in function of the (Bohmian) velocity of the particles inside the volume Ω:

$$I_j(t) = -\sum_{i=1}^{N(t)} e\mathbf{v}_i(\mathbf{r}_i(t),t)\mathbf{F}_j(\mathbf{r}_i(t),t). \tag{5.26}$$

We remember that both particle and displacement current components are included in (5.26). In fact, the i-th electron in the sum of (5.26) contributes to the total current $I_j(t)$ detected at the j-th surface, even if it is far away from the surface S_j. The reasons why such electron contributes to the (total) current without crossing the j-th surface is because its movement provides displacement current on such surface.

For a 2 terminal device with lateral areas much larger than the distance between the transport direction of the active region, one can assume that $\mathbf{F}_j(r_i(t),t) \approx \frac{1}{L}\,\hat{u}_x$, with $\hat{u}_x$ indicating the unitary vector along the x direction (assumed as the transport direction). This gives the total current through the surface S_j as [115, 118, 119]:

$$I_j(t) = \sum_{i=1}^{N(t)} \frac{e v_i(x)}{L}. \tag{5.27}$$

Where L is the length device, e is the fundamental charge, and $N(t)$ is the number of electrons that at time t are inside the volume Ω. This last expression will be used in all the rest of the thesis to compute the current in RTD at high frequencies.

5.2.2 Interaction of the active region with the contacts

The Ramo-Shockley-Pellegrini theorem gives us a practical way to estimate the current in the case of a device 1D device, with very large lateral contacts. To build such model, however, I used the approximation that (5.24) can be neglected in (5.23), because of the very small screening time of electrons inside the metallic contacts. This approximation assumes that the active region of the device is not affecting the state of the contacts. However, in a real device, the active region acts on the contacts, and produces processes that propagate energy throughout the contacts that can also reflect some of this energy. To build a model that enables this kind of self-consistent phenomenon between the system and the contact, I propose in Appendix A, an algorithm that uses (5.27) from a time-dependent system, as an input for an external circuit that mimics the contacts (or some antenna placed next to the RTD active region). Such algorithm was implemented in the BITLLES simulator [110].

Chapter 6

Coherent interaction of electrons with transversal field

The typical way of treating the effects of the electromagnetic fields on the dynamics of electrons is by assuming the electromagnetic fields as something "external" to the electrons. In this chapter, however, I will first propose a model for the coherent explanation of the electrons and electromagnetic fields. From the Coulomb gauge, the longitudinal electric field is perfectly well-defined when I know the positions of all electrons, on the contrary, the transversal electric and magnetic fields are not defined only by the position of the electrons. New degrees of freedom are needed for the transversal electromagnetic fields. When these new degrees of freedom are treated quantum-mechanically I reach the quantization of the energy of the electromagnetic fields (the so-called photons).

6.1 Hamiltonian for electrons and electromagnetic fields

The computation of the total current $I(t)$ of a device, as introduced in Chapter 5, requires the knowledge of the dynamics of a set of N electrons, in the Bohmian description each electron is also described by its determined position $r_i[t]$ and velocity $v_i[t]$. Additionally, I know that the dynamics of the electrons are coupled to Maxwell's equations. What I am still missing is a motion equation that takes into account everything together, electrons and the electromagnetic fields, in a general way. In this section I will look for such general (or classical or quantum) equation of motion. For this goal, I will start using the Helmholtz decomposition (5.1), and Maxwell equations (5.3)(5.4)(5.5)(5.6)(5.10) and (5.11).

In this section, I will consider one electron interacting with one mode of the electro-

magnetic field. In electron device computations, such approximation is usually accepted when ballistic electron transport is assumed. This ballistic assumption implies that there is no Coulomb interaction in the Hamiltonian that I will develop (because there is only one electron). This is not a strong assumption as I will re-introduce the many-body Coulomb interaction through an external potential profile within a mean-field approximation. The single-particle Hamiltonian will then be:

$$H = \frac{[\mathbf{p} - e\mathbf{A}(\mathbf{r},t)]^2}{2m} + U(\mathbf{r},t) + U_{ext}(\mathbf{r},t) + H_\gamma, \tag{6.1}$$

with e is the signed fundamental electron charge, $\mathbf{p}$ is the canonical momentum. $\mathbf{A}$ is the vector potential, that introduces the effect of an external longitudinal electric field on the electron, as will be explained in the following paragraph. On the other hand, $U_{ext}(\mathbf{r},t)$ is the mentioned external potential energy that accounts for the spatial variation of the conduction band inside the active region of the device. I write also $U(r,t)$, which is the Coulomb electron-electron interaction, to insist that $U(r,t) = 0$ which implies that $\mathbf{E}_\parallel(\mathbf{r},t) = 0$ in our simple single-particle example. I insist that I have assumed $\mathbf{E}_\parallel(\mathbf{r},t) = 0$ only to find the single-electron Hamiltonian, but I have considered many electrons inside the active region, and $\mathbf{E}_\parallel(\mathbf{r},t) \neq 0$, in the computation of the displacement current. Additionally, in our development of the single-electron Hamiltonian, the energy of the electromagnetic field is defined through the two components $\mathbf{E}_\perp(\mathbf{r},t)$ and $\mathbf{B}(\mathbf{r},t)$, and this will define $\hat{H}_\gamma$ as [124]:

$$\hat{H}_\gamma = \frac{\epsilon_0}{2}\int d\mathbf{r}\left[\mathbf{E}_\perp^2(\mathbf{r},t) + c^2\mathbf{B}^2(\mathbf{r},t)\right]. \tag{6.2}$$

To better specify which terms of the Hamiltonian introduce interaction between electrons and electromagnetic fields, I now include the dipole approximation, which is verified if the vector potential (and the electric field) is space-independent inside the active region of the device, or $\mathbf{A}(\mathbf{r},t) \approx \mathbf{A}(\mathbf{r}_0,t)$. Clearly, this can be justified by the frequency domain that is treated by this model. In fact, if I define L as the space of the simulation box, where a reasonable value can be $L \approx 50\,\text{nm}$, then I can define a maximum frequency $f_{max} = c/L \approx 100\,\text{THz}$. Any working frequency much smaller than f_{max}, for example an operating frequency around 20 THz used in our numerical examples, justify the approximation $\mathbf{A}(\mathbf{r},t) \approx \mathbf{A}(\mathbf{r}_0,t)$. As I have said, in our single electron Hamiltonian the Coulomb potential is $U(\mathbf{r},t) = 0$, so that from (5.1) and (5.8), I get $\mathbf{E}(\mathbf{r},t) = \mathbf{E}_\perp(\mathbf{r},t) = -\frac{\partial\mathbf{A}(\mathbf{r},t)}{\partial t}$. Then in the Coulomb Gauge $\nabla\cdot\mathbf{A} = 0$, I can use a gauge transformation $\mathbf{A}' = \mathbf{A} + \nabla\Sigma$ and $U' = U + \frac{\partial\Sigma}{\partial t}$ which is satisfied by $\Sigma = -e\mathbf{A}(\mathbf{r}_0,t)\cdot\mathbf{r}/\hbar = -e\mathbf{E}_\perp(\mathbf{r},t)\cdot\mathbf{r}/\hbar$, I re-write

the Hamiltonian (6.1) in a way that separates the electron part from the electromagnetic field part:

$$H = \frac{\mathbf{p}^2}{2m} + U_{ext}(\mathbf{r}, t) - e\mathbf{r} \cdot \mathbf{E}_{\perp}(\mathbf{r_0}, t)/\hbar + H_{\gamma}. \tag{6.3}$$

In this way it is clear that a big part of the energy is determined by two variables, $\mathbf{E}_{\perp}(\mathbf{r}, t)$ and $\mathbf{B}(\mathbf{r}, t)$ which are not only dependent on the electron dynamics but are new degrees of freedom needed to define the whole electron-electromagnetic system. Here I see the reason for using the Darwin approximation in our description of the displacement current, in doing so, I can use (6.3) as the equation of motion of the matter-light system, because the Darwin approximation states that $\mathbf{E}_{\perp}(\mathbf{r}_0, t) \neq 0$, while I can still compute the displacement current with a simplified expression (5.23).

Canonical conjugate variables It will be very interesting to arrive at a general expression of (6.3) in terms of the so-called canonical variables. When I write a Hamiltonian with canonical variables it is very easy to pass from a classical scenario to a quantum one. Thus, our goal now is to find such canonical variables. The first two terms of the Hamiltonian (6.3) represent the electron part of the energy as a function of canonical conjugate variables, $\mathbf{r}$ and $\mathbf{p}$. This is because such variables respect the following relationships:

$$\begin{aligned} \frac{\partial H}{\partial \mathbf{p}} &= \frac{d\mathbf{r}}{dt}, \\ \frac{\partial H}{\partial \mathbf{r}} &= -\frac{d\mathbf{p}}{dt}, \end{aligned} \tag{6.4}$$

for the electron Hamiltonian, that we report from (4.5)

$$H_0 = \frac{\mathbf{p}^2}{2m} + U_{ext}(\mathbf{r}, t). \tag{6.5}$$

In [125] it is shown how Eq. (6.2) (when only one mode, one frequency, of the electromagnetic field is considered) can be represented in terms of two Canonical Conjugate variables Q and P in the following way:

$$H_{\gamma} = \frac{\epsilon_0}{2} \int d\mathbf{r} \left[\mathbf{E}_{\perp}^2(\mathbf{r}, t) + \mathbf{B}^2(\mathbf{r}, t)\right] = \frac{\omega}{2}(\hat{Q}^2 + \hat{P}^2), \tag{6.6}$$

where ω is the frequency of the one mode electromagnetic field. In fact, it is easy to show that (6.4) is also valid for Q and P related to the new operator $\hat{H}_{\gamma}$:

$$\frac{\partial H}{\partial Q} = -\frac{dP}{dt}, \tag{6.7}$$

$$\frac{\partial H}{\partial P} = \frac{dQ}{dt}. \tag{6.8}$$

And a general Hamiltonian for the coupled dynamics of electrons and electromagnetic fields can be written using the four canonical conjugate variables, $\mathbf{p}$ and $\mathbf{r}$ for the electron, and Q and P for the electromagnetic field as.

$$H = \frac{\mathbf{p}^2}{2m} + U_{ext}(\mathbf{r}, t) - e\mathbf{r} \cdot Q + \frac{\omega}{2}\left(Q^2 + P^2\right). \tag{6.9}$$

Equation (6.9) is general in the sense that it can be used either for classical or quantum systems. When $\{\vec{r}, \vec{p}\}$ and $\{Q, P\}$ are treated as ordinary variables I have a classical scenario, while when each pair of the canonical variables are treated as non-commuting operators I reach a quantum scenario. In the result of this thesis, I will always deal with quantum electrons, however, sometimes I will discuss classical electromagnetic fields and some other quantum electromagnetic fields. Below, I describe these two possible scenarios used in this thesis. In the latter case, I will see that the energy of the electromagnetic fields is quantized in terms of photons.

6.2 Classical electromagnetic field

In the quantum optics literature, the quantum treatment of electrons and the classical treatment of the electromagnetic field in (6.9) is named semi-classical approximation. In this section, I build a semiclassical version of the general Hamiltonian (6.9). To do so, need the definition of degrees of freedom of the electron as operators $\hat{r}$ and $\hat{p}$, while the electromagnetic field's degrees of freedom are substituted by time-dependent variables $Q \to Q(t)$ and $P \to P(t)$. For simplicity, I now assume a 1D electron system (as is typical in RTDs modelling), and the electron operators in the position representation are x and $p = i\hbar\partial/\partial x$, which it is well-known to have non-commuting properties. Then, the semi-classical approach to the Hamiltonian in (6.9), for a 1D system, is

$$H_S = \frac{\hat{p}^2}{2m} + U_{ext}(x, t) - ex \cdot Q(t) + \frac{\omega}{2}\left(Q(t)^2 + P(t)^2\right), \tag{6.10}$$

where the last two terms (giving the electromagnetic energy) are time dependent potentials without spatial dependence so that they do not affect the evolution of the electron wave function and can be neglected. The third term is the interaction term H_I between the electrons and the electromagnetic fields in the semi-classical approximation. Finally, since the position and momentum of the electron are not well-defined simultaneously, the electron is defined by a wave function $\psi(x, t)$ that satisfies the following Schroedinger equation

$$i\hbar\frac{\partial\psi(x,t)}{\partial t} = -\frac{\hbar}{2m}\frac{\partial^2\psi(x,t)}{\partial x} + U_{ext}(x,t)\psi(x,t) - exQ(t)\psi(x,t). \tag{6.11}$$

the variable $Q(t)$ models the oscillating electromagnetic field acting on the conduction band of the device $U_{ext}(x,t)$. From [124], if I do not assume a perfect monochromatic electromagnetic field, but a superposition of components with small frequency dispersion δf, then the interaction term $\hat{H}_I$ can be written as:

$$H_I = -exQ(t) = -ex\frac{\gamma_s}{\sqrt{\omega}}q(t), \tag{6.12}$$

where $\gamma_s = \omega e\sqrt{\delta k \epsilon_0 (2\pi)^3}$ is the coupling strength, and $q(t)$ is the oscillating electromagnetic field with frequency ω_γ, so that $q(t) \propto cos(\omega_\gamma t)$.

So that the general Hamiltonian $\hat{H}_S$ taking into account the interaction of the electron with the transversal components of the electromagnetic field in the semi-classical approximation will be

$$H_S = -\frac{\hbar}{2m}\frac{\partial^2}{\partial x^2} + U_{ext}(x,t) - ex\frac{\gamma_s}{\sqrt{\omega}}q(t). \tag{6.13}$$

In the next section, I develop the full quantum Hamiltonian, where the degrees of freedom of electrons and electromagnetic fields are both treated quantum-mechanically.

6.3 Orthodox Quantum electromagnetic field

Let us now look for a fully quantum form of the general Hamiltonian (6.9), within the orthodox theory. The canonical variables Q and P are associated with time independent Hermitian Operators $\hat{Q}$ and $\hat{P}$. Being operator associated with canonical variables, exactly as $\hat{r}$ and $\hat{p}$ for the electron's position and momentum, the commutation between these operators yields:

$$\left[\hat{Q}, \hat{P}\right] = i\hbar\mathbb{I}. \tag{6.14}$$

Two operators that satisfy such non-commuting property are $Q = \sqrt{\omega}q$ and $P = (-i\hbar/\sqrt{\omega})\partial/\partial q$. The interaction term of the Hamiltonian in the q and x space can be written as:

$$H_I = -e\vec{r}\cdot Q = \gamma_q x q, \tag{6.15}$$

where $\gamma_q = e\epsilon_0\sqrt{2\omega/\hbar}$ [124], indicates the coupling strength between electron and photon open systems. Additionally, knowing (6.8), $\hat{H}_\gamma$ in the q space becomes:

$$H_\gamma = -\frac{\hbar^2}{2}\frac{\partial^2}{\partial q^2} + \frac{\omega^2}{2}q^2, \tag{6.16}$$

Finally, the wave function $\Psi(x,q,t)$ in the $\{x,q\}$ describing the quantum nature of the electrons and electromagnetic field is the solution of the following two-dimensional Schrödinger equation:

$$\begin{aligned} i\hbar\frac{\partial\Psi(x,q,t)}{\partial t} = & -\frac{\hbar^2}{2m}\frac{\partial^2\Psi(x,q,t)}{\partial x^2} + U_{ext}(x)\Psi(x,q,t) \\ & -\frac{\hbar^2}{2}\frac{\partial^2\Psi(x,q,t)}{\partial q^2} + \frac{\omega^2}{2}q^2\Psi(x,q,t) \\ & +\gamma_q\, x\, q\, \Psi(x,q,t), \end{aligned} \tag{6.17}$$

where both the photon and electron systems evolve each one in one dimension, respectively q and x, and the interaction term couples these two dynamics in a coherent way. I call $\hat{H}_Q$ the coherent (or fully-quantum) Hamiltonian.

6.3.1 The electron-photon state

We now develop a bit the wave function $\Psi(x,q,t)$ to get a better understanding of its meaning. I define $\phi_m(x)$ as the eigenstates of the electron Hamiltonian $\hat{H}_0$ in (6.5), and $\phi_n^{(\gamma)}(q)$ the eigenstate related to the electromagnetic energy operator $\hat{H}_\gamma$ in (6.16). The components $\phi_n^{(\gamma)}(q)$ are eigenstates of the Harmonic Oscillator. The energy of each of these eigenstates is quantized so that I can talk about the quantization of the electromagnetic energy in terms of photons. The optical cavity is assumed to host a single mode with frequency ω. In a general way, the whole electron-photon $\Psi(x,q,t)$ wave function can be written as a combination of electron and photon eigenstates in the following way:

$$\Psi(x,q,t) = \sum_m^{N_e(t)}\sum_n^{N_\gamma(t)} c_{n,m}(t)\phi_m(x)\phi_n^{(\gamma)}(q), \tag{6.18}$$

where $N_e(t)$ is the number of electron eigenstates and $N_\gamma(t)$ the number of photons eigenstates. I can re-write as a superposition of photon eigenstates and electron wavepacket

$$\Psi(x,q,t) = \sum_n^{N_\gamma(t)} \psi_n(x,t)\phi_n^{(\gamma)}(q), \tag{6.19}$$

where

$$\psi_n(x,t) = \sum_m^{N_e(t)} c_{n,m}(t)\phi_m(x), \tag{6.20}$$

in (6.19) and (6.20) I create a one-to-one correspondence between the n-th photon eigenstate and its own associated n-th electron wavepacket (composed of many m-th

electron eigenstates). Thus, the presence of the n-th electron wavepacket in the simulation will also indicate the existence of the n-th photon.

If I substitute (6.19) into the Schrödingher equation (6.17), and then integrating on the degree of freedom of the photon, I can go to a general equation of motion to evolve the electron wave functions $\psi_n(x,t)$, related to the n-th photon states in the optical cavity $\phi_n^{(\gamma)}(q)$. This would be:

$$\begin{aligned} i\hbar\frac{\partial\psi_n(x,t)}{\partial t} &= -\frac{1}{2m}\frac{\partial^2\psi_n(x,t)}{\partial x^2} + U_{ext}(x)\,\psi_n(x,t) \\ &+ \hbar\,\omega_\gamma\left(n+\frac{1}{2}\right)\psi_n(x,t) \\ &+ \gamma_q\,x\left(\sqrt{n+1}\,\psi_{n+1}(x,t) + \sqrt{n}\,\psi_{n-1}(x,t)\right). \end{aligned} \tag{6.21}$$

6.3.2 Practical computation

To simplify our discussion of emission and absorption of a photon by an electron in an RTD, let us assume that only the zero photon state, $\phi_0^{(\gamma)}(q)$, and the one-photon state, $\phi_1^{(\gamma)}(q)$, are relevant inside the active region of the device. The eigenstate $\phi_0^{(\gamma)}(q)$ is related to the absence of a photon (ground state of the Harmonic oscillator), $\phi_1^{(\gamma)}(q)$ is the state of the optical cavity where only one photon is present. Then, I can rewrite the wave function $\Psi(x,q,t)$ solution of (6.17) as:

$$\Psi(x,q,t) = \psi_A(x,t)\phi_0^{(\gamma)}(q) + \psi_B(x,t)\phi_1^{(\gamma)}(q), \tag{6.22}$$

with

$$\psi_A(x,t) = \int \phi_0^{(\gamma)*}(q)\Psi(x,q,t)dq, \tag{6.23}$$

$$\psi_B(x,t) = \int \phi_1^{(\gamma)*}(q)\Psi(x,q,t)dq. \tag{6.24}$$

In other words, $\psi_A(x,t)$ and $\psi_B(x,t)$ are the projection of the electron wave function respectively on the eigenstates $\phi_1^{(\gamma)}(q)$ (with zero photons) and $\phi_0^{(\gamma)}(q)$ (with one photon). From a practical point of view, this means that it is possible to observe the whole two-dimensional light-matter system $\Psi(x,q,t)$ from one-dimensional computations involving the solution of $\psi_A(x,t)$ and $\psi_B(x,t)$ [50]. The equation of motion of $\psi_A(x,t)$ and $\psi_B(x,t)$ can be obtained by introducing the definition (6.22) into (6.17) and by integrating in the

degree of freedom q:

$$i\hbar\frac{\partial\psi_A(x,t)}{\partial t} = -\frac{\hbar^2}{2m}\frac{\partial^2\psi_A(x,t)}{\partial x^2} + \left(V(x)+\frac{1}{2}\hbar\omega_\gamma\right)\psi_A(x,t) + \gamma_q' x\psi_B(x,t),$$

$$i\hbar\frac{\partial\psi_B(x,t)}{\partial t} = -\frac{\hbar^2}{2m}\frac{\partial^2\psi_B(x,t)}{\partial x^2} + \left(V(x)+\frac{3}{2}\hbar\omega_\gamma\right)\psi_B(x,t) + \gamma_q' x\psi_A(x,t), \tag{6.25}$$

where I have defined $\gamma_q' = \gamma_q \int \phi_0^{(\gamma)}(q)\ q\ \phi_1^{(\gamma)}(q)\ dq$ and I have used $\int \phi_0^{(\gamma)*}(q)\ q\ \phi_0^{(\gamma)}(q)\ dq = \int \phi_1^{(\gamma)*}(q)\ q\ \phi_1^{(\gamma)}(q)\ dq = 0$.

Equations (6.25) will be used to evolve coherently the total wave function $\Psi(x,q,t)$ with a practical approach that only requires solving two coupled one-dimensional equations (under the assumption that only the $n=0$ and $n=1$ photon states are relevant). This type of computation will be done in Chapter 9 and 12. A generalization where two other photon states n and $n+1$ (with n arbitrary) can be done straightforwardly, showing that the numerical results presented later can properly capture the emission and absorption of light due to the interaction of the electron with the transversal electromagnetic field.

6.4 Bohmian Quantum electromagnetic field

In this section, I am interested in building a Bohmian framework to complete the description of the quantum equation of motion (6.17). This is done to avoid the unnecessary complications deriving from the need for measurement, typical of the orthodox view. The Bohmian theory uses the same wave function $\Psi(x,q,t)$ that I have mentioned in the orthodox case, while including additional variables in the description of the quantum state so that I get more information on how is the quantum system behaving. For example, from the wave function $\Psi(x,q,t)$ I cannot know which is the position of the electron or which is the amplitude of the electromagnetic field. On the contrary, from the Bohmian trajectories $q[t]$ and $x[t]$ in the $\{x,q\}$ space I can know such properties. So that, the Bohmian electron has the well-defined position $x[t]$ and the electromagnetic field (with one mode at frequency ω) has the well-defined amplitude $q[t]$. This additional microscopic information is very valuable in several topics in this thesis. Similarly as done in Chapter 3, from the definition of the Bohmian velocity (3.4), I can define the "velocity" v_q for the $q[t]$ particle (degree of freedom of the electromagnetic field) as:

$$v_q \equiv v_q(x,q,t) = \frac{J_q(x,q,t)}{|\Psi(x,q,t)|^2}, \tag{6.26}$$

and for the the $x[t]$ particle:

$$v_x \equiv v_x(x,q,t) = \frac{J_x(x,q,t)}{|\Psi(x,q,t)|^2}. \tag{6.27}$$

where $J_q(x,q,t)$ is the single-mode current in the q space, which has the typical quantum mechanics definition

$$J_q(x,q,t) = \frac{i\hbar}{2}\left(\Psi(x,q,t)\frac{\partial\Psi^*(x,q,t)}{\partial q} - \Psi^*(x,q,t)\frac{\partial\Psi(x,q,t)}{\partial q}\right). \tag{6.28}$$

The single-particle current $J_x(x,q,t)$ in the x space will be analogous to (6.28) but with the derivative in x. The Bohmian velocity is used to evolve each trajectory similarly to (3.5), both in the q space and in the physical x space in a deterministic way, simply following:

$$q[t] = q[t_0] + \int_{t_0}^{t} v_q(x[t'], q[t'], t')dt', \tag{6.29}$$

$$x[t] = x[t_0] + \int_{t_0}^{t} v_x(x[t'], q[t'], t')dt'. \tag{6.30}$$

Notice that $x[t]$ is really a trajectory in the physical space, while $q[t]$ is a trajectory in the abstract space of the electromagnetic field. For many trajectory $M \to \infty$, the quantum equilibrium condition in (3.8) reads, in the $\{x,q\}$ space summing on each i-th trajectory (each i-th trajectory is in fact a i experiment with the same preparation of the wave function):

$$|\Psi(x,q,t)|^2 = \lim_{M\to\infty}\frac{1}{M}\sum_{i=1}^{M}\delta(x-x^i[t])\delta(q-q^i[t]), \tag{6.31}$$

similarly to what was done in (3.6) for a 1D system. Then the particle current density in the x space can be also written as

$$J_c(x,q,t) = \lim_{M\to\infty}\frac{1}{M}\sum_{i=1}^{M}v_x\delta(x-x^i[t])\delta(q-q^i[t]). \tag{6.32}$$

This discussion will be relevant in the next section about non-coherent electron-photon interaction, where the Bohmian Conditional wave function approach will be used in the following Chapter 7, and also for the definition of the Displacement Current Coefficient in Chapter 8.

Now I would like to give an example of the trajectories evolved with (6.29) and (6.29) in the $\{x, q\}$ space. To do so, I imagine a 2D wavepacket $\Psi(x, q, t)$ in an simplified model for the quantum well of the RTD device. I will assume that only two states of the quantum well are available to the electron. This electron interact with a quantum electromagnetic field where only two states are available: zero photon and one photon. In other words, I rebuild the conditions of Subsection 6.3.2, where I can describe the system using the wavefunction (6.22), where the two electron components $\psi_A(x, t)$ and $\psi_B(x, t)$ are evolved with the two equation of motion (6.25). Now I would like to show qualitatively what the particles evolved using (6.29),(6.30) where the velocities are given by (6.26),(6.27) and (6.28). In this way I define as $\vec{\chi}(t) = \{x(t), q(t)\}$ the instantaneous position of the electron-photon system in the $\{x, q\}$ space, the evolution of these trajectories in the case of initial injection of a wavepacket at the second level of the quantum well, initially in absence of a photon, is shown in Fig. 6.1:

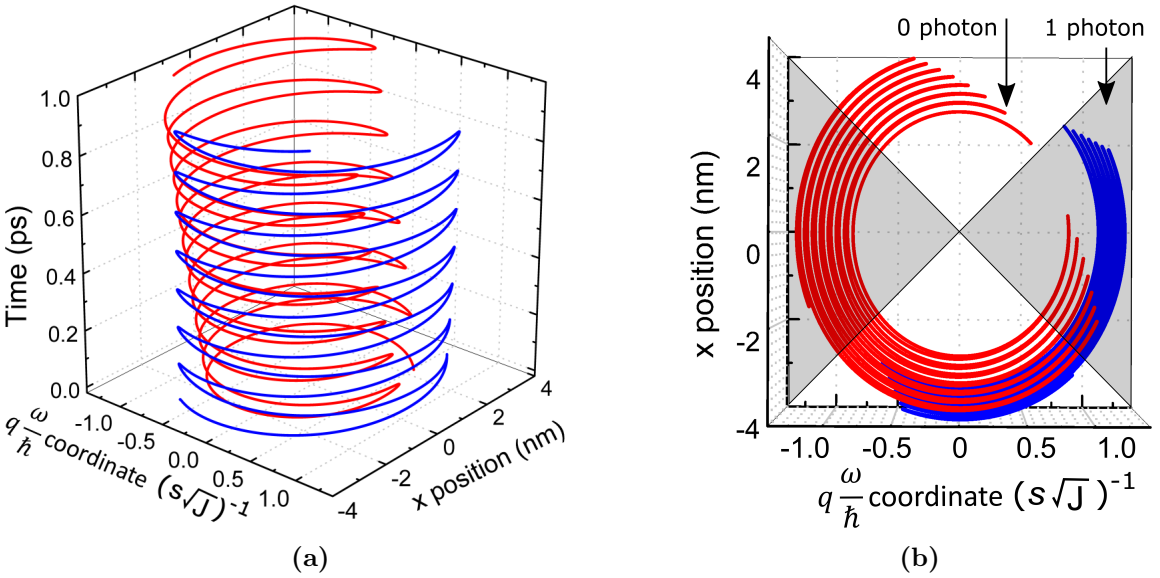

Figure 6.1: Two trajectories $\chi(t) = \{x(t), q(t)\}$ evolving in function of time, chosen at arbitrary initial positions $\{x(t_0), q(t_0)\}$ (a) with a side view of the evolution (b) with a top view showing an oscillation between two quadrants.

Notice that if for example I take the blue trajectory in Fig. 6.1 I see that it will follow a circular path, which means that it oscillates between two electron-photon states. First excited state in the harmonic oscillator (sides of axis q), and bottom state in the quantum well (center of axis x), which are the grey quadrants, corresponding to a higher probability presence of a photon. The bottom state in the harmonic oscillator (center of axis q), and second state in the quantum well (sides of axis x), which are the white quadrants,

corresponding to higher probability of absence of a photon. There is continuous transition between these two states, which means that the system keeps emitting and absorbing a photon, creating this circular periodic behaviour, which is another way of observing the Rabi oscillation.

Chapter 7

Non-coherent interaction of electrons with transversal field

In the previous Chapters 5 and 6 I provide a coherent description of the interaction of electrons with the transversal electric and the magnetic fields. The topics explained in those chapters are quite common in the quantum optic community but are not so common in the electronic community. To the best of my knowledge, it is the first time that such coherent evolution of light and matter are studied for electrons devices. Such a type of simulation requires a large computational effort. Let us mention that the electromagnetic energy is quantized can be included in the simulation of electron devices without having to solve such complicated equations. In fact, in most simulators, the interaction of electrons with light is considered in terms of collisions (scattering mechanism). In the language of the physics of open systems used in previous chapters, the electron is simulated explicitly, while the role of the photons is considered as an external effect that provokes the modification of the electron properties. I named this approach electron-photon scattering in a non-coherent description. In addition, I provided an explanation of such collisions models in terms of wave functions.

7.1 Collisions in terms of Bohmian conditional wave functions

In this chapter, the treatment of photon-electron interaction will be introduced in the single-particle description of a wave function. The properties of an initial wave function of an electron $\psi(x, t_s)$ at time t_s will be modified during the collision that takes a time τ_s. Then, at time $t_s + \tau_s$ I will get a new $\psi(x, t_s + \tau_s)$ with new properties. From the point of view of Orthodox quantum physics, this procedure for collision in terms of wave

functions is not be justified, since the orthodox element that describes an open system is the Density Matrix (not a pure state) for general Non-Markovian scenarios needed in high-frequency devices. On the contrary, in this thesis, the use of the Bohmian Conditional wave function explained in Section 4.3 is the key element that justifies the choice of using a wave function to describe such open system. Let us consider an electron interacting with an electromagnetic field described by the wave function $\Psi(x, q, t)$ developed in the previous chapter with full coherence between both degrees of freedom. Then, the electron wave function alone used in this chapter can be defined in the Bohmian language as:

$$\psi(x, t) \equiv \Psi(x, q^i[t], t), \tag{7.1}$$

where $q^i[t]$ is one Bohmian trajectory specifying the properties of the electromagnetic field in the i-th experiment. In principle, I will have to keep the parametric dependence of the conditional wave function on $q^i[t]$. But, to simplify the notation, hereafter I will omit such dependence.

The equation of motion of this Bohmian Conditional wave function will not be derived in an exact way (which requires the knowledge of the whole electron-photon wave function whose explicit computation I want to avoid), but I will study two different scenarios to provide a reasonable equation of motion for the conditional wave function, $\psi(x, t_s) \rightarrow \psi(x, t_s + \tau_s)$, when the scattering with light occurs. In particular, to find such simplified equation of motion, I will check a model $\psi(x, t_s) \rightarrow \psi(x, t_s+\tau_s)$ that satisfies conservation of energy during the electron-photon interaction (with either absorption or emission) and a model which satisfies conservation of momentum during the interactions. The numerical results of these two algorithms will be compared with the coherent model and between each other in Chapter 9. In any case, I anticipate that the model with conservation of energy is the one that best fits the coherent evolution of $\psi(x, t) \equiv \Psi(x, q^i[t], t)$ in most (not all) conditions.

7.2 Momentum exchange model

In this section, I consider an electron defined by a single-particle (Bohmian conditional) wave function that at time t_s undergoes a scattering event, during the time interval τ_s. I defined t_s as the time just before and $t_s + \tau_s$ as the time just after the scattering event. This model was first presented in [106], with an algorithm that can be understood as a selection of the initial electron wave function, $\psi(x, t_s)$, with expectation value of the momentum $\langle p(t_s)\rangle$ and of the final one, $\psi(x, t_s + \tau_s)$, with expectation value of the mo-

mentum $\langle p(t_s+\tau_s)\rangle$. I consider that an external particle with momentum p_f is interacting with the electron, during the time interval t_s, so that $p_f = \langle p(t_s+\tau_s)\rangle - \langle p(t_s)\rangle$. In this momentum-based model, the expected evolution of the electron wave function can be easily understood by written it as superposition of momentum eigenstates $\phi_p(x)$ as:

$$\psi(x,t_s) = \int dp\; b(p,t_s)\; \phi_p(x), \tag{7.2}$$

with $b(p,t_s) = \int dx\; \psi(x,t_s)\; \phi_p^*(x)$.

And the expectation value of the momentum before the scattering $\langle p(t_s)\rangle$ is

$$\langle p(t_s)\rangle = \int dp\; p\; |b(p,t_s)|^2, \tag{7.3}$$

that can be increased to get the new expectation value of the momentum $\langle p(t_s+\tau_s)\rangle = \langle p(t_s)\rangle + p_\gamma$ at $t_s+\tau_s$ as:

$$\begin{aligned}\langle p(t_s+\tau_s)\rangle &= \langle p(t_s)\rangle + p_\gamma = \int dp\; (p+p_\gamma)\; |b(p,t_s)|^2 = \int dp'\; p'\; |b(p'-p_\gamma,t_s)|^2 \\ &= \int dp'\; p'\; |b(p',t_s+\tau_s)|^2,\end{aligned} \tag{7.4}$$

where $b(p,t_s+\tau_s) = b(p-p_\gamma,t_s)$.

In this particular model, I know the explicit shape of the momentum eigenstates, $\phi_p(x) = 1/\sqrt{2\pi}e^{(ip_\gamma x/\hbar)}$, so that

$$\begin{aligned}\psi(x,t_s+\tau_s) &= \int dp\; b(p,t_s+\tau_s)\; \phi_p(x) = \int dp\; b(p-p_\gamma,t_s)\; \phi_p(x) \\ &= \int dp \int dx'\psi(x,t_s)\; \phi^*_{p-p_\gamma}(x')\phi_p(x) \\ &= \int dp \int dx'\; \psi(x,t_s)\; \frac{1}{2\pi} e^{ip(x-x')/\hbar} e^{ip_\gamma x'/\hbar} = e^{ip_\gamma x/\hbar}\psi(x,t_s).\end{aligned} \tag{7.5}$$

The increase of the global phase, in a flat potential scenario, means an increase of the speed of the electron (for positive p_γ). In fact, if I estimate the Bohmian velocity after the collision (at $t_s+\tau_s$), I have that:

$$v_x^i[t_s+\tau_s] = \frac{1}{m}\frac{\partial s(x,t_s+\tau_s)}{\partial x}|_{q=q^i[t]} = \frac{1}{m}\frac{\partial s(x,t_s)}{\partial x}|_{q=q^i[t]} + p_\gamma/m. \tag{7.6}$$

we keep the notation $q = q^i[t]$ to emphasize that p_γ/m is the perturbation of the electron by the "external" photon of a particular experiment i. This is exactly what was done for the solution of the many-body problem in (C.2) in Appendix C. Eq.(7.6) says that the new velocity $v_x^i[t_s+\tau_s]$ is just the old velocity $v_x^i[t_s]$ plus the momentum given by the interaction with the scattering photon p_γ/m.

The implementation of the non-coherent evolution of the momentum exchange needs a finite time step to happen. In fact, in the results shown in [50, 113], the time interval dedicated to the collision is divided into several steps, each one must last a time δt_s divided by the number of steps. In the results of Chapter 9 I will discuss if this type of scattering satisfies complete positivity and energy conservation. In [106] it is explained how a change of momentum p_γ in a wave packet in free space can be performed with a unitary Schrödinger equation, I report this explanation in Section 7.4.

7.3 Energy exchange model

As done in the previous section, now I consider an electron defined by a single-particle Bohmian conditional wave function that at time t_s undergoes a scattering event. Again t_s is the time just before and $t_s + \tau_s$ is the time just after the scattering event. Also here, as I have seen in Section 7.2 such transition between initial and final Bohmian Conditional wave functions takes a finite time because, from a conceptual point of view, it has to guarantee the continuity of the Bohmian Conditional wave function in space and time. The initial and final Bohmian Conditional wave functions are $\psi(x, t_s)$ and $\psi(x, t_s + \tau_s)$, which satisfy $\langle E(t_s + \tau_s)\rangle = \langle E(t_s)\rangle + E_\gamma$, with E_γ the energy of a photon. Within the energy representation, the wave packet can be decomposed into a superposition of Hamiltonian eigenstates $\phi_E(x)$ of the electron Hamiltonian H_0 as:

$$\psi(x, t_s) = \int dE\ a(E, t_s)\ \phi_E(x), \tag{7.7}$$

with $a(E, t) = \int dx\ \psi(x, t)\ \phi^*_E(x)$. The central energy $\langle E(t_s)\rangle$ is then:

$$\langle E(t_s)\rangle = \int dE\ E\ |a(E, t_s)|^2, \tag{7.8}$$

which can be increased to get the new central energy at $t_s + \tau_s$ as

$$\begin{aligned}\langle E(t_s + \tau_s)\rangle &= \langle E(t_s)\rangle + E_\gamma = \int dE\ (E + E_\gamma)\ |a(E, t_s)|^2 = \int dE'\ E'\ |a(E' - E_\gamma, t_s)|^2 \\ &= \int dE'\ E'\ |a'(E', t_s + \tau_s)|^2,\end{aligned} \tag{7.9}$$

where I have defined $a'(E, t_s + \tau_s) = a(E - E_\gamma, t_s)$. Thus, the new wavepacket after the collision is

$$\psi(x, t_s + \tau_s) = \int dE\ a'(E, t_s + \tau_s)\ \phi_E(x) = \int dE\ a(E' - E_\gamma, t_s)\ \phi_E(x). \tag{7.10}$$

This transition corresponds to absorption of energy by the electron. Emission of energy can be identically modelled by using $\langle E(t_s + \tau_s)\rangle = \langle E(t_s)\rangle - E_\gamma$. If required, the *technical*

discontinuity between $\psi(x, t_s)$ and $\psi(x, t_s + \tau_s)$ can be solved by just assuming that the change of energy is produced in N_{t_s} smaller time interval. Then, at each time step of the simulation, the change in the wave packet central energy will be E_γ / N_{t_s}.

7.4 Coherent or non-coherent models?

In these models, I do not include explicitly the phonon degree of freedom. Thus, I am treating the electron-photon closed system with the techniques of open systems where only the degree of freedom of the electron is simulated explicitly. However, in principle, the fact that I am using an equation of motion (in our case, an equation of motion for the conditional wave function) to deal with the electron interacting with a photon does not mean that I am losing the coherence (quantum wholeness). At the practical level, the development of an equation of motion for the open system with proper treatment of the quantum wholeness is, most of the time, a very complicated task (if not impossible). So, the best I can offer is a reasonable equation of motion. In this particular case of the electron-photon interaction, I will see that I am able to capture most of the physics of such interaction (but not all) with the model of exchange of energy. I will see in the results section that there are some scenarios, with resonances between electrons and photons eigenenergies, where the model cannot capture all the physical phenomena. It is in this sense that the title of the present chapter is "Non-coherent interaction of electrons with transversal fields", to differentiate from other exact models of the interaction with the direct solution of $\Psi(x, q, t)$ in the closed system with the $\{x, q\}$ space.

Chapter 8

Displacement Current Coefficient

In this chapter I use the definition of the total current given in Chapter 5 and I build a new tool named Displacement Current Coefficient $D^{(f)}(E,t)$, with the goal of including the displacement current present in (5.27) inside a Landauer-like formula that can be applicable at THz. The use of this Displacement Current Coefficient $D^{(f)}(E,t)$ extends the possibility of estimating the current of a ballistic device (RTD) well inside the THz gap, overcoming the transit time limit. In the result section, I will discuss this scenarios with (in Chapter 11) and without (in Chapter 12) the presence of quantized transversal electromagnetic fields.

8.1 The Landauer model

We consider here a two-terminal device with an active region of length $L = b - a$ defined as the space between the source and drain contacts ($a < x < b$), where the source contact is at $-\infty < x < a$ and the drain is at $b < x < \infty$. For DC computations, the Landauer model condensates all informations about the nature of the active region inside a *transmission coefficient* $T(E)$, which interacts with the contacts only based on the energy levels. The DC current I_{DC} for the electrons injected from left to right contact can be defined as

$$I_{DC} = \int_0^\infty dE f(E) g(E) T(E), \tag{8.1}$$

where $f(E)$ is the Fermi distribution function of the electron in the left contact [126] with total energy E, and $g(E)$ is the density of states of the system. A similar expression can be computed for the DC current of the electrons from the right to left, with a new Fermi distribution function depending on the applied bias.

The *transmission coefficient* $T(E)$ of the $i-$th electron injected from the left or source contact ($x < a$), at time t_i, is expressed by:

$$T(E) = \int_b^{\infty} |\psi_i(x, t_i + \tau')|^2 \, dx = \int_{t_i}^{t_i+\tau'} J_i(b, t) dt, \tag{8.2}$$

where $|\psi_i(x,t)|^2$ is the quantum probability distribution of the single-electron wavepacket, $J_i(b,t)$ is the associated current density as defined in (3.3) calculated at the right or drain contact ($x > b$). Finally τ' is a time interval large enough to ensure that the i-th electron has completely crossed the active region, ideally $\tau' \to \infty$. I define the time τ as the tunnelling or dwell time. For an accurate estimation of $T(E)$ the main condition is that the time τ' in the above expression (8.2) is larger than the tunnelling (dwell) time τ [127, 128]. This is simply to be sure that all of the wave function $\psi_i(x,t)$ has been fully transmitted or fully reflected when estimating the transmission probability.

The Landauer model assumes the device to be in static condition. The electron sees the same potential profile while traversing the active region during the time τ. However, this assumption is no longer true at high frequencies. In fact, it is well-known that the Landauer model ignores the displacement current.

8.2 Electronics beyond the transit time limit

We have seen above that in the discussion of high-frequency electronics I need to know which is the tunnelling or dwell time τ of the electron inside the active region. However, the definition and estimation of τ is a controversial and complicated topic following the orthodox rules [129, 130]. If electrons have no well-defined position, then, it is not possible to know at what time the electron has entered the active region. According to the orthodox theory, the only way to now, with certainty, when the electron has entered into the active region ($a < x < b$) is placing a position detector at $x = a$. But, then, such position measuring apparatus inside the active region will destroy our original electron device performance because the position measurement will collapse the electron into something like a delta function and completely modify the transmission coefficient.

On the contrary, the Bohmian theory is much more helpful since the knowledge of trajectory can directly provide the electron transit time. The (average) transit time can be estimated by building a set of Bohmian trajectories associated with the same wave function. With the use of such trajectories, it will be easy to understand the approximate ensemble time needed to move from the source to the drain. In fact, with a given single-electron wave function $\psi_i(x,t)$ in the Bohmian description, guiding a deterministic trajectory $x_i[t]$, with velocity $v_i = J_i/|\psi_i(x,t)|^2$ (from Eq. (3.4)), the (average) transit

time of the electron in an active region defined as $a < x < b$, will be:

$$\tau_{Di} = \int_0^\infty dt\Theta[x_i(t) - a]\Theta[b - x_i(t)], \tag{8.3}$$

where $\Theta[x_i - l]$ is the Heaviside function. And for N particles system, the transit time will be the ensemble value: $\tau_D = \sum_i^N \tau_{Di}/N$. This was used for example in works in graphene in [131–135]. This is a very intuitive and natural way of estimating times needed for electrons to cross the active region. Such final expression can be rewritten in a more compact way as:

$$\tau_D = \int_0^\infty dt \int_a^b dx|\psi(x,t)|^2. \tag{8.4}$$

Many researchers argue that the Orthodox quantum mechanics can provide (8.4) as the definition of the dwell time. This can be true from a mathematical point of view, but it cannot be true from a physical point of view. The orthodox theory has given up in providing information on what happens in the active region (if such information is not measured). Since the present thesis is based on Bohmian mechanics, I assume that I can get the information of the dwell time of our RTD without any conceptual problem and use it to evaluate our high-frequency current where the transit time is a very relevant Figure of Merit to understand if the device can be considerer in static conditions or not. Some numerical estimations of the transit time for the typical RTD structures used in this thesis are on the order of 0.1 ps. Thus, clearly at frequencies of few THz, even hundreds of GHz, the static assumption of the Landauer model is no longer valid.

8.3 The Displacement Current Coefficient without transversal field

In this and the next section, I will use the final expression of the total current (5.27) developed in Chapter 5 to build a new parameter named Displacement Current Coefficient $D^{(f)}(E,t)$, with the goal of including the displacement current in an approach for quantum transport similar to the Landauer model of (8.2). The use of this Displacement Current Coefficient $D^{(f)}(E,t)$ extends the possibility of estimating the current of a ballistic device (RTD) well inside the THz gap, overcoming the transit time limit. I will discuss in this section a scenario without the presence of quantized transversal electromagnetic fields. In the next section within the present chapter, the quantization of the transversal field will be considered.

We consider a single-electron wave function $\psi_i(x,t)$, used through (3.3) and (3.4) to determine the velocity of the electron, used in (5.27). This wave function is solution of

the electron Hamiltonian $H_0 = \frac{p^2}{2m} + eU_{ext}(x,t)$, where I repeat that the potential energy $U_{ext}(x,t)$ can include many "external" interactions (as the conduction band of the device or the Coulomb interaction) in a type of mean-field approximation. In particular, the external potential (in Volts) $V_{ext}(x,t) = U_{ext}/e$ is described as:

$$V_{ext}(x,t) = V_{in}(x,t) + E_c(x)/e. \tag{8.5}$$

Where V_{in} is the input signal applied at the external contacts of the device:

$$V_{in}(x,t) = V_0\, cos(2\pi f t + \theta) \cdot \frac{x - L/2}{L}, \tag{8.6}$$

Where in the input signal $V_{in}(x,t)$, f is the frequency of an input external signal applied on the device, θ as the phase of the signal, whose use will be explained in Chapter 5.1. Notice that this type of potential is related to the scalar potential in Maxwell's equations, and not to the vector potential. As such, the above potential deals with the longitudinal electrical field $\mathbf{E}_{\parallel}(\mathbf{r},t)$, and does not affect directly the transversal electrical field $\mathbf{E}_{\perp}(\mathbf{r},t)$.

Within the Bohmian theory, I study the active region (open system) from Bohmian conditional wave functions. I define $\psi(x,t;t_i,E)$ as a wave packet (Bohmian conditional wave function) with central energy E injected from the left contact at time t_i with positive central momentum. To be exact, the wave-packet at time t_i is located at a central position x_{left} deep inside the left reservoir. Identically, I get $J(x,t;t_i,E)$ as the current density in the x direction linked to $\psi(x,t;t_i,E)$. Form such state, I can compute the Bohmian velocity from (3.4) and introduce it into (5.27). I can also transform the sum over electrons as a an integral $\sum_{i=1}^{N(t)} \rightarrow \beta \int_{-\infty}^{t} dt_i \int_0^L dx |\psi_i(x,0)|^2$. Notice that β is a constant that determines number of electrons injected by second (with units of s^{-1}). This parameter is proportional to the lateral area of device (the more lateral area, the more electrons injected). I consider electrons injected from $t_i = -\infty$ until $t_i = t$ (Electrons injected after t cannot have any effect on the current). I only consider electrons at each position inside the active region (from $x = 0$ to $x = L$) with $|\psi_i(x,0)|^2$ the density probability of electrons in each position x. As a result, the total current from (5.27) (considering only one injecting energy for simplicity) will be:

$$I^{(f)}(E,t) = \beta\, \frac{e}{L} \int_0^{\infty} dE\, f(E)\, g(E) \int_{t_i=-\infty}^{t} dt_i \int_{x=a}^{b} dx \cdot J^{(f)}(x,t;t_i,E). \tag{8.7}$$

Here I have added the superindex (f) indicating the external frequency in (8.6). To

obtain a more compact notation, I define the Displacement Current Coefficient as:

$$D^{(f)}(E,t) = \beta\frac{1}{L}\int_{t_i=-\infty}^{t} dt_i \int_{x=a}^{b} dx \cdot J^{(f)}(x,t;t_i,E). \tag{8.8}$$

Note that in equation (8.8) the injection time t_i is fundamentally different from the observation (measurement) time t. And now, if I consider different injecting central energies E, the energy integral of equation 8.7 can be written with a shape similar to the Landauer model in (8.1):

$$I^{(f)}(t) = q\int_{0}^{\infty} dE\, f(E)\, g(E)\, D^{(f)}(E,t). \tag{8.9}$$

The Displacement Current Coefficient $D^f(E,t)$ in DC conditions For DC scenarios where I have $V_{ext}(x,t) \approx V_{ext}(x)$, I know that the wave function injected at the injecting time t_i and evaluate at the observation time $t = 0$ is identical to a wave packet injected at $t_i = 0$ and evaluated at $t - t_i$, meaning that an offset of time t_i has no effect so that $\psi(x, t - t_i; 0, E) = \psi(x, t; t_i, E)$, then (8.8) can be rewritten as

$$\begin{aligned} D^{(f=0)}(E,t)/\beta &= \frac{1}{L}\int_{x=a}^{b} dx \int_{t_i=-\infty}^{0} dt_i J^{(f)} f(x,t;t_i,E) \\ &= \frac{1}{L}\int_{x=a}^{b} dx \int_{t_i=-\infty}^{0} dt_i J^{(f)} f(x,t-t_i;0,E) \\ &= \frac{1}{L}\int_{x=a}^{b} dx T(E) = T(E), \end{aligned} \tag{8.10}$$

where the have used the definition of $T(E)$ in (8.2). At low frequencies, the probabilities (8.2) is equal to (8.8) divided by the constant β. The constant β with units s^{-1} is needed because $D^{(f)}(E,t)$ has units of s^{-1}.

8.4 The Displacement Current Coefficient with transversal field

In this section, I want to generalize the Displacement Current Coefficient $D^{(f)}(E,t)$ when the electron-photon interaction is considered. To do so, I take again the total current (5.27) and again I change the sum to a continuous integral
$\sum_{l=1}^{N(t)} \rightarrow \beta\int_{-\infty}^{0} dt_i \int_{0}^{L} dx \int_{-\infty}^{\infty} dq |\Psi^{(f)}(x,q,t,t_i,E)|^2$. Now, I am interested only on the velocity of the electron in the x direction. Since the coherent interaction depends also on the variable q, I have added an extra integral on q. This means that I consider

many electrons simultaneously in the device. Many of them with the same wave packet preparation, assuming them to be independent between each other. Since I compute each electron interacting with the electromagnetic filed, all possible values of q and x distributed from $|\Psi^{(f)}(x,q,t,t_i,E)|^2$ has to be considered. Then, following the same steps as in the previous computation, the total current through (8.7) will be

$$I^{(f)}(t) = \beta\frac{e}{L}\int_0^\infty dE\, f(E)\, g(E) \int_{-\infty}^{t}\int_0^L\int_{-\infty}^{\infty} dt_i\, dx\, dq\, J^{(f)}(x,q,t;t_i,E). \tag{8.11}$$

Again, to have a more compact notation, in a parallel procedure as done in (8.8), I define:

$$D^{(f)}(E,t) \equiv \beta\frac{1}{L}\int_{-\infty}^{t}\int_0^L\int_{-\infty}^{\infty} dt_i\, dx\, dq\, J^{(f)}(x,q,t;t_i,E). \tag{8.12}$$

so that it is possible to define the total current, similarly to (8.9):

$$I^{(f)}(t) = \int_0^\infty dE\, f(E)\, g(E)\, D^{(f)}(E,t), \tag{8.13}$$

Let us now provide a practical tool to be able to use (8.12) in a more effective way for a simplified system. The results of this simplified system will be shown in Chapter 12.

8.4.1 Practical computation

The practical model of (6.25) evolves two coupled electron wave functions in the physical space x, through $\psi_A(x,t)$ and $\psi_B(x,t)$, which are respectively related to an electron in the absence of a photon inside the optical cavity, and to an electron in the presence of a photon in the optical cavity. Then, by using the standard definition of the quantum current, I have:

$$\begin{aligned}
J(x,t;t_i) &= \int dq\, J(x,q,t;t_i) = \int dq \frac{\hbar}{m}\,\mathbb{I}\mathrm{m}\left(\frac{\partial\Psi^*(x,q,t)}{\partial x}\Psi(x,q,t)\right)\\
&= \frac{\hbar}{m}\int dq\,\mathbb{I}\mathrm{m}\left(\frac{\partial\psi *_A (x,t)}{\partial x}\phi_0^{(\gamma)*}(q) + \frac{\partial\psi_B^*(x,t)}{\partial x}\phi_1^{(\gamma)*}(q)\right)\cdot\\
&\cdot\quad \mathbb{I}\mathrm{m}(\psi_A(x,t)\phi_0^{(\gamma)}(q) + \psi_B(x,t)\phi_1^{(\gamma)}(q))\\
&= \frac{\hbar}{m}\,\mathbb{I}\mathrm{m}\left(\frac{\partial\psi_A^*(x,t)}{\partial x}\psi_A(x,t)\right) + \frac{\hbar}{m}\,\mathbb{I}\mathrm{m}\left(\frac{\partial\psi_B^*(x,t)}{\partial x}\psi_B(x,t)\right)\\
&= J_{A,i}(x,t) + J_{B,i}(x,t).
\end{aligned} \tag{8.14}$$

Where I used the orthonormality of $\phi_0^{(\gamma)}(q)$ and $\phi_1^{(\gamma)}(q)$, that is $\int \phi_1^{(\gamma)}(q)\,\phi_0^{(\gamma)}(q)\,dq = \int \phi_1^{(\gamma)}(q)\,\phi_0^{(\gamma)}(q)\,dq = 0$. Finally, the total current (in the physical space x) of the electron-photon system evolving fully coherently can be estimated using the new (extended) displacement current coefficient $D^{(f)}(E,t)$ as:

$$D^{(f)}(E,t) \equiv \beta \frac{1}{L} \int_0^L \int_{t=-\tau}^{0} dx\, dt_i \left(J_{A,i}(x,t) + J_{B,i}(x,t) \right). \tag{8.15}$$

The two electron components, related to two different states of the optical cavity, both contribute to the current. In this way, an external harmonic signal at frequencies in the optical domain can be studied in its effects on the conductivity of the active region of a device. The numerical estimation of $D^{(f)}(E,t)$ for an optical cavity with determined frequency ω_γ in resonance with a two-level electron system is shown in Chapter 12. The result will be shown first in function of the injection energy E in DC conditions, then in high frequency AC condition for a fixed injection energy E.

Part IV

Results

Chapter 9

Coherent Transport of Electrons with Transversal Field

In this chapter, I report results from the numerical simulation of the models explained in Chapter 6. The system will be first described by the electron wavefunction $\psi(x,t)$ guided by the semiclassical modelling of electron-photon interaction, with the equation of motion given by (6.11) and the Hamiltonian $\hat{H}_S$.

Secondly the system will be described by the 2D fully-quantum wavefunction $\Psi(x,q,t)$ from (6.18), guided by the quantum equation of motion (6.17) and Hamiltonian $\hat{H}_Q$. This last one is actually represented by the electron in 1D system $\psi(x,t)$ from (6.22), guided by the 1D quantum equation of motion (6.25).

The nomenclature used in the chapter and in the rest of the results will use the capital Ψ when the wavefunction describes the state of both electrons and photons, while I will use ψ when referring to the electron alone. In both cases, the justification of using pure states in a many-body system as an RTD, instead of density matrixes, is explained in the theory, developing the concept of Bohmian conditional wave function, in Chapter 4. The different parameters or subindexes will specify more information about the wave packets. To denote an energy eigenstate of the electron system alone or the photon alone, used as a base, I will write the symbol ϕ.

The results of this chapter are reproduced or adapted from:

- M. Villani, G. Albareda, C. Destefani, X. Cartoixà, X. Oriols, "Scattering in terms of Bohmian conditional wave functions for scenarios with non-commuting energy and momentum operators", *Entropy*, vol. 23, no. 4, p. 408, 2021;
- M. Villani, C. Destefani, X. Cartoixà, M. Feiginov, X. Oriols, "THz displacement

current in nanodevices with coherent electron-photon interaction", 2022. (Submitted)

9.1 Classical electromagnetic field

In this section, I consider a Gaussian wavefunction $\psi(x,t)$ injected inside the simulation box and interacting with the RTD device whose structure is shown in Fig. 9.1(a), with quantum well of 16 nm, barrier thickness 2 nm, mass $m = 0.041\, m_0$ and barrier height 0.5 eV. The DC transmission probability of the RTD structure is shown in Fig. 9.1(b).

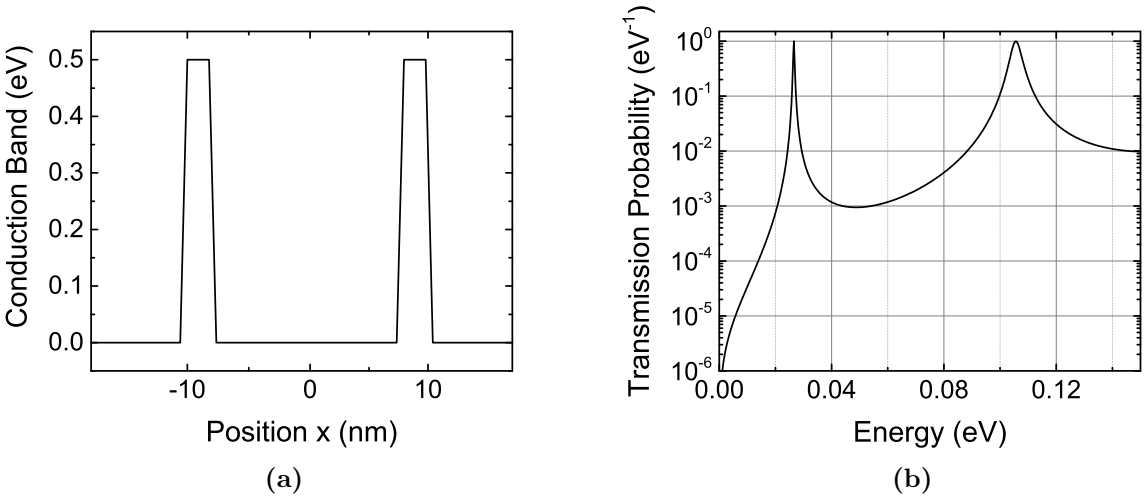

Figure 9.1: (a) Conduction band of the RTD device with quantum well of 16 nm, barrier thickness 2 nm, constant electron mass $m = 0.041\, m_0$, barrier height 0.5 eV (b) DC transmission probability in function of injection energy E, where the bottom energy level is $E_0 = 26$ meV, and the second excited level $E_1 = 104$ meV.

The transmission probability shown in Fig. 9.1(b) reveals the bottom energy eigenstate of the quantum well at energy $E_0 = 26$ meV and the first excited eigenstate at energy $E_0 = 103$ meV. From now on I define the energy difference between the two states as $E_G = E_1 - E_0$. The wavepacket will be injected from the left with a central energy $E = 103$ meV to occupy the first excited level of the quantum well.

The numerical estimation of the evolution of the electron wavefunction $\psi(x,t)$ is guided by the equation of motion equation (6.11), and Hamiltonian $\hat{H}_S$ (6.10). The related charge density $P_S(x,t) = |\psi(x,t)|^2$ is shown in Fig. 9.2. The semiclassical electromagnetic field $q(t) \propto cos(\omega_\gamma t)$ forces the quantum well to oscillate with frequency $f_\gamma = \omega_\gamma/2\pi = E_G/\hbar$. In (6.12) the interactions strength γ is fixed as $\gamma_s = 1.33$ meV/nm.

In particular in Fig. 9.2 light-matter interaction is activated in an adiabatic way at the beginning of the interaction time $t_s = 0.2\,\text{ps}$, where $\tau_s = 0.1\,\text{ps}$ is the duration of the light-matter interaction, and in this case is the time used for the adiabatic activation of the interaction. So that the semiclassical term H_I in (6.12) is: $H_I = -ex\frac{\gamma_s}{\sqrt{\omega}}q(t)\Theta(t)$, with $\Theta(t) = (t - t_s)/\tau_s$ and Θ the Heaviside function.

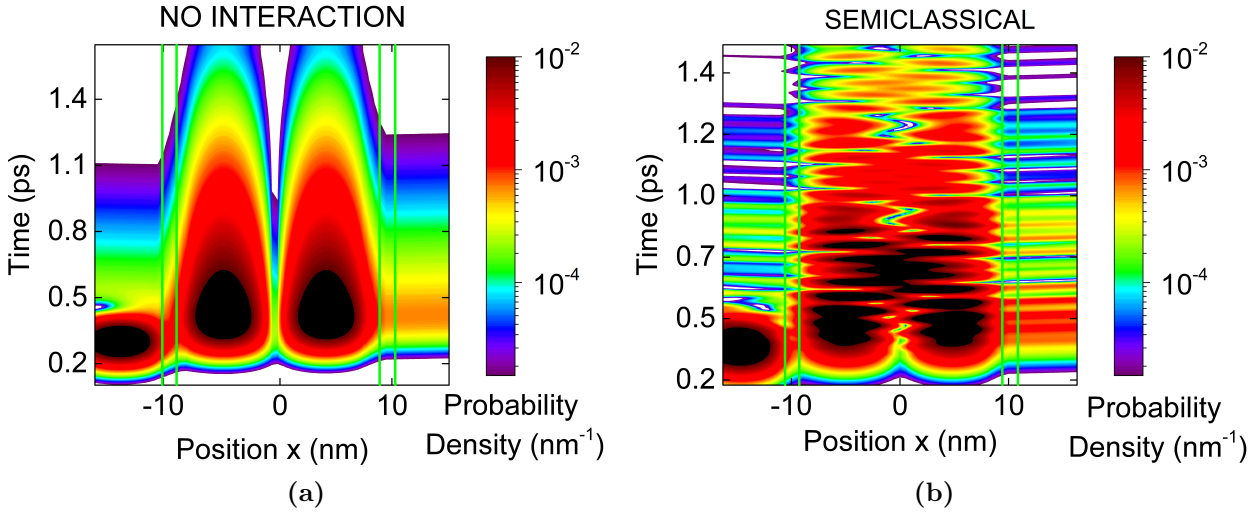

Figure 9.2: Spatial distribution of the charge associated with the wavefunction $\psi(x,t)$ (a) with null strength $\gamma_s = 0$ of electron-photon interaction, (b) with light-matter interaction with $\gamma_s = 1.33\,\text{meV/nm}$, activated at time $t_s = 0.2\,\text{ps}$ and activated adiabatically until time $t_s + \tau_s = 0.3\,\text{ps}$. Interacting with a double barrier structure shown in Fig. 9.1(a). The Rabi oscillation is observed when the interaction between electron and electromagnetic field is activated in (b).

In Fig. 9.2(a) I see the Gaussian wave packet occupying the second state of the quantum well, where with null strength $\gamma_s = 0$ of the light-matter interaction is considered. On the contrary, in Fig. 9.2(b), when the mentioned semi-classical light-matter interaction is activated, the wavefunction $\psi(x,t)$ shows oscillations of the charge at $t > t_s > 0.2\,\text{ps}$. In fact, I see oscillations at two different frequencies.

The first frequency is due to the dipole oscillation forced by the term $q(t) \propto cos(\omega_\gamma t)$ with frequency $f_\gamma = 18\,\text{THz}$. However, I observe also a lower frequency of oscillations. Since the field is in resonance with the quantum well $f_\gamma = E_G/\hbar$, the oscillation of $q(t)$ produces also Rabi oscillations [124, 125]. This is observed at frequency $f_{R,s} = 5.18\,\text{THz}$. This oscillation respects the conditions, $f_{R,s} = \gamma_s|d_x|/\hbar$, where the dipole is approximated between the two bottom eigenstates of the quantum well $d_x = L\int \phi^*_{E_1}(x)x\phi_{E_0}(x)dx$, that with $L = 16\,\text{nm}$ is $d_x = -2.88\,\text{nm}$.

9.2 Quantum electromagnetic field

Now I will provide results for what concerns the quantum description of the electron-photon interaction (both electron and electromagnetic fields are quantum). My goal is to describe the evolution of the electron-photon system described by $\Psi(x,q,t)$ in the $\{x,q\}$ degrees of freedom, evolved in (6.17), but in its simplified version, which is (6.25), as explained in Chapter 6. In order to compare this with results of the previous Section 9.1, where only the x degrees of freedom can be represented, I define $P_Q(x,t)$ as:

$$\begin{aligned} P_Q(x,t) &= \int dq\, |\Psi(x,q,t)|^2 \\ &= \int dq\, (\psi_A(x,t)\phi_1^{(\gamma)}(q) + \psi_B(x,t)\phi_0^{(\gamma)}(q))^* \cdot ((\psi_A(x,t)\phi_1^{(\gamma)}(q) + \psi_B(x,t)\phi_0^{(\gamma)}(q))) \\ &= |\psi_A(x,t)|^2 + |\psi_B(x,t)|^2, \end{aligned} \tag{9.1}$$

where I have used the wave functions $\psi_A(x,t)$ and $\psi_B(x,t)$ defined in (6.22), whose equations of motion are (6.25). I have also defined $\phi_0^{(\gamma)}(q)$ as the ground energy eigenstate of the harmonic oscillator (zero photons) and $\phi_1^{(\gamma)}(q)$ as the first energy eigenstate of the harmonic oscillator (one photon) in the quantum description of the wave nature of the electromagnetic field. Notice that $P_Q(x,t)$ can be understood as diagonal element of a reduced density matrix $P_Q(x,t) = \rho(x',x,t)|_{x'=x'}$ with:

$$\begin{aligned} \rho(x',x,t) &= \int dq\, \Psi^*(x',q,t)\Psi(x,q,t) \\ &= \int dq\, (\psi_A(x',t)\phi_1^{(\gamma)}(q) + \psi_B(x',t)\phi_0^{(\gamma)}(q))^* \cdot ((\psi_A(x,t)\phi_1^{(\gamma)}(q) + \psi_B(x,t)\phi_0^{(\gamma)}(q))) \\ &= \psi_A^*(x',t)\psi_A(x,t) + \psi_B^*(x',t)\psi_B(x,t). \end{aligned} \tag{9.2}$$

Notice that $\psi_A(x,t)$ and $\psi_B(x,t)$ are both needed, not only one, to describe the system in the orthodox language $\rho(x',x,t)$. The reason, explained in the previous chapters, is that it is not possible to describe an open system with orthodox pure states. Or, to be more precise, the state $\psi_A(x,t)$ alone, or the state $\psi_B(x,t)$ alone, are not a good physical description of the electron. Both are needed in an orthodox formulation to describe the electron system, as it is an open system. Notice that under a Markovian approximation, when observing only the system at the initial and final times, I could say that the system is initially described by $\psi_A(x,t)$ and finally by $\psi_B(x,t)$ alone. This would be accurate, however, it would be an approximation unable to provide information about the evolution in the intermediate times, during the transition.

We consider initially that the electromagnetic field is described by the zero-photon

wave function $\phi_0^{(\gamma)}(q)$. The Gaussian wavefunction $\psi(x,t)$ is then associated to the zero photon state in the optical cavity, which in (6.22), means $\psi(x,t=0)=\psi_A(x,t=0)$.

We consider the Gaussian wavefunction $\psi(x,t)$ interacting with the RTD device shown in Fig. 9.1(a). The wavepacket is injected, again, with a central energy equal to the second state of the quantum well $E=E_1=104\,\text{meV}$. The total charge estimated with (9.1) is shown in Fig. 9.3(a) without light-matter interaction, and (b) with light-matter interaction. The interaction, guided by the equation of motion (6.25), and the frequency of the photons is in resonance with the quantum well: $\omega_\gamma = E_G/\hbar$. To compare this result with the previous one I use the same strength of the electron-electromagnetic field interaction $\gamma_q=\gamma_s=\gamma=1.33\,\text{meV/nm}$. The resonance of the photon with the energetic difference between the two eigenstates E_G enables a Rabi oscillation that is observed in Fig. 9.3(b).

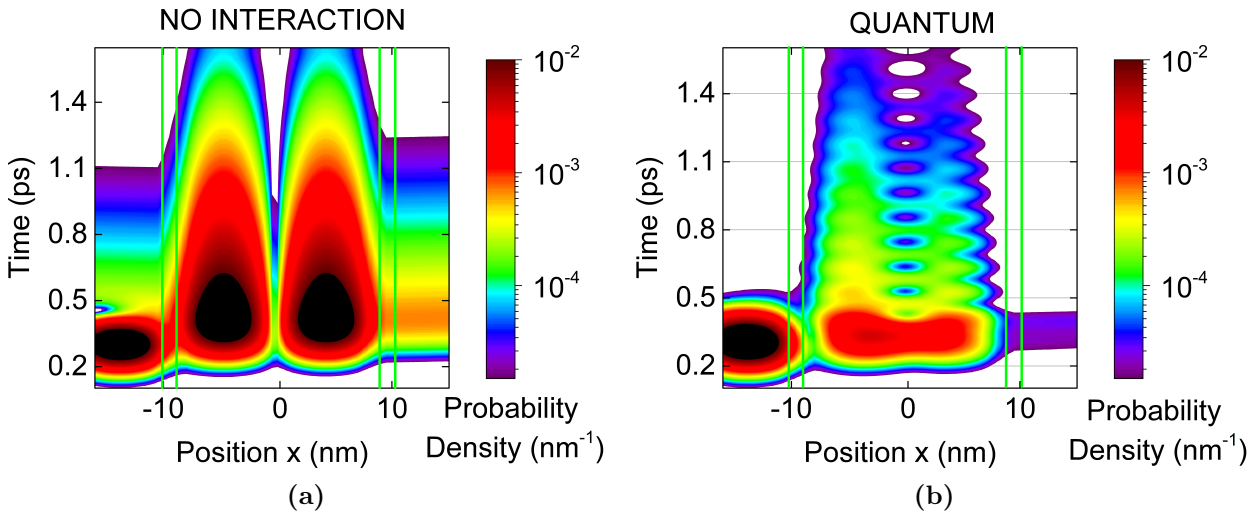

Figure 9.3: Spatial distribution of the charge associated with the wavefunction $\psi(x,t)$ (a) with null strength $\gamma=0$ of electron-photon interaction, (b) with electron-photon interaction with $\gamma=1.33\,\text{meV/nm}$. Both interacting with the double barrier structure shown in Fig. 9.1(a). The Rabi oscillation is observed when the interaction between electron and photon is activated in (b).

9.2.1 Rabi oscillation

We now want to further study the presence of these Rabi oscillations in RTDs. I consider now a Gaussian wavepacket $\psi(x,t)$ injected in the RTD device shown in Fig. 9.4(a), with quantum well of 10 nm, barrier thickness 2 nm, mass $m=0.041\,m_0$, where m_0 is the mass of the free electron $m_0=9.109\cdot10^{-31}\,\text{Kg}$, barrier height 0.5 eV.

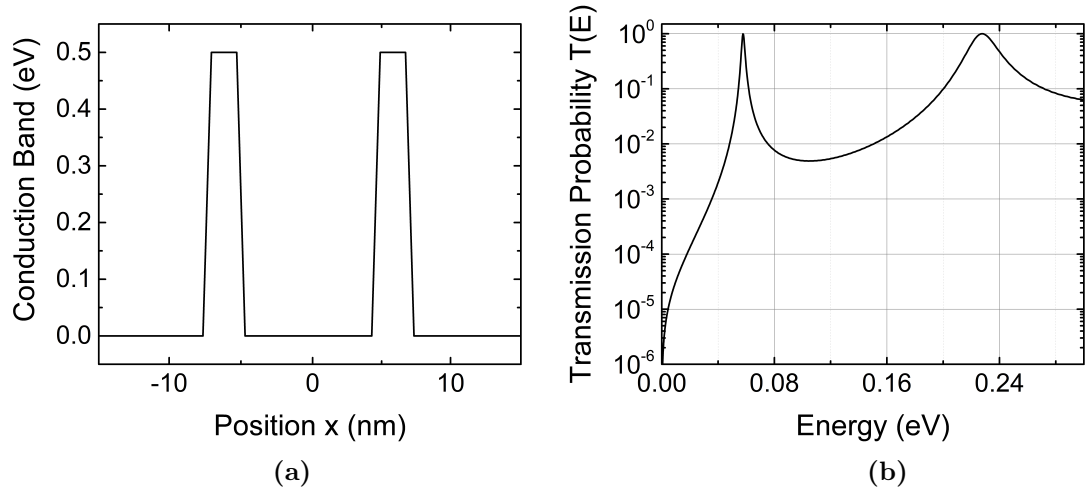

Figure 9.4: (a) Conduction band of the RTD device with quantum well of 10 nm, barrier thickness 2 nm, mass $m = 0.041\, m_0$, barrier height 0.5 eV (b) DC transmission probability in function of injection energy E, bottom energy level $E_0 = 58$ meV, and second energy level $E_1 = 235$ meV.

The new RTD structure includes a quantum well with width of $L = 10$ nm. This value is chosen to be different from the ones of Fig. 9.1 to increase the energy spacing between the eigenstates and improve the "quality" of the Rabi oscillations. The transmission probability in Fig. 9.4(b) shows the two quantum well eigenstates. The bottom energy eigenstate of the quantum well $\phi_{E_0}(x)$ has energy $E_0 = 58$ meV and the second eigenstate $\phi_{E_1}(x)$ is at energy $E_1 = 235$ meV.

Next, to estimate how much of the probability of the electron-electromagnetic field system inside the well can be assigned to the presence of one photon (associated to $\psi_B(x,t)$ in (6.22)) or its absence (associated to $\psi_A(x,t)$ in (6.22)), I define the occupation probabilities of each state relative to the occupation of the bottom state or second eigenstates of the quantum well, with the following practical description. I define the importance of each energy in the quantum well in the description (in the superposition) of $\psi_A(x,t)$ and $\psi_B(x,t)$ as:

$$c_A(E,t) = \int_0^L \psi_A(x,t)\phi_E^*(x)dx \quad , \quad c_B(E,t) = \int_0^L \psi_B(x,t)\phi_E^*(x)dx. \tag{9.3}$$

Then, I define the probabilities of the energy eigenstates with electrons related to the *one-photon case*:

$$P_{B,0}(t) = \frac{1}{N}\int_0^{\frac{E_0+E_1}{2}} |c_A(E,t)|^2 dE \quad , \quad P_{B,1}(t) = \frac{1}{N}\int_{\frac{E_0+E_1}{2}}^{\infty} |c_A(E,t)|^2 dE, \tag{9.4}$$

and the same for the eigenstates of the the electron related to the *zero-photon case*:

$$P_{A,0}(t) = \frac{1}{N}\int_0^{\frac{E_0+E_1}{2}} |c_A(E,t)|^2 dE \quad , \quad P_{A,1}(t) = \frac{1}{N}\int_{\frac{E_0+E_1}{2}}^{\infty} |c_A(E,t)|^2 dE. \tag{9.5}$$

The wave functions $\phi_E(x)$ are the energy eigenstates of the electron Hamiltonian H_0 in (6.5). These definitions are needed because I are dealing with an open system where the distribution of energies allowed to the electrons is continuous, even tough the highest probability appears at the resonant energies $E = E_0$ and $E = E_1$. Please remind that I am only interested in the probability inside the barrier region with spatial limits given by $0 < x < L$. Also, a normalization constant N, is included ensuring that $P_{A,0}(t)+P_{A,1}(t)+P_{B,0}(t)+P_{B,1}(t) = 1$ at any time (to exclude the probabilities outside the quantum well). In the following Fig. 9.5 the meaning of the probabilities defined in (9.4) and (9.5) is represented schematically with the four different possible states of the system, which will take the role of the base of the electron-photon system. The evolution is again driven by (6.25), with $\gamma_q = 7.9\,\text{meV/nm}$, and the dipole is $d_x = -1.66$, due to the new geometry of Fig.9.4.

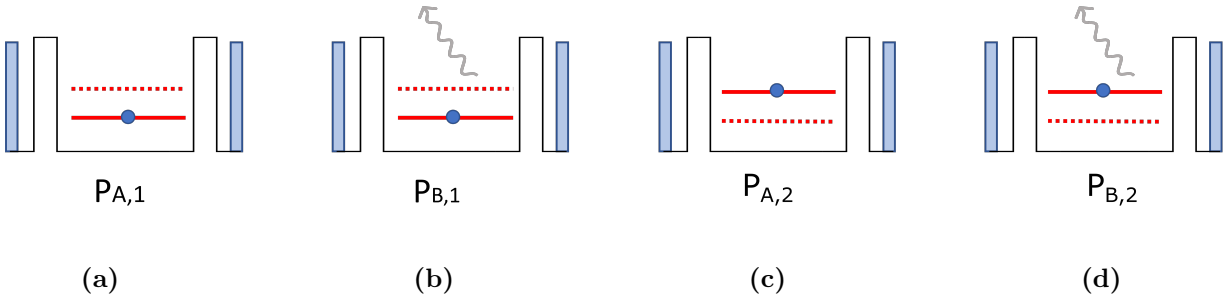

Figure 9.5: Schematic representation of all the states that I assume to be possible within the simple two electron states and two photon states representation. The light blue squares represent the optical cavity, while the black line is the RTD device double barrier structure. Red horizontal lines represent the electron energy eigenstates $\phi_{E_0}(x)$ and $\phi_{E_1}(x)$ of the quantum well, used to define the electron wavefunction $\psi(x,t)$, while the gray arrow shows the presence of a photon inside the optical cavity. The electron-photon wavefunctions $\Psi(x,q,t)$ will always be a combination of two or more of these fours states, each one associated with a probability defined in (9.4) and (9.5).

The evolution of probabilities $P_{A,0}, P_{B,0}, P_{A,1}$ and $P_{AB,1}$, from (9.4),(9.5) for a wavefunction $\psi(x,t)$ undergoing Rabi oscillation inside a quantum well of Fig. 9.4(a), is shown in Fig. 9.6, here I see the exchange of probability from $P_{B,0}$ to $P_{A,1}$, which tells us that the Rabi oscillation is taking place with periodic change of probability between the two states shown in Fig. 9.5(b) and Fig. 9.5(c). In fact the Rabi frequency respects the condition $f_{R,q} = 2\sqrt{\gamma}_q|d_x|/\hbar 20\,\text{THz}$.

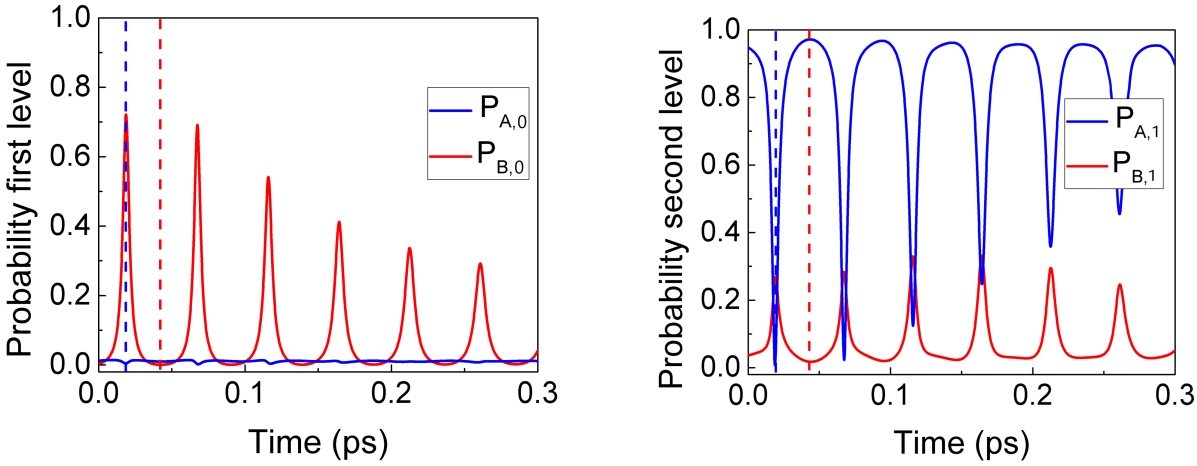

(a) **(b)**

Figure 9.6: (a) evolution of probabilities for the wavefunction to occupy the bottom state $P_{A,0}$ (blue line) and $P_{B,0}$ (red line) at $0 < E < (E_0 + E_1)/2$ (b) evolution of probabilities for the wavefunction to occupy the second state $P_{A,1}$ (blue line) at and $P_{B,1}$ at energies $(E_0 + E_1)/2 < E < \infty$ defined in (9.5),(9.4) for the case that the initial Gaussian wavepacket $\psi(x,t)$ is injected in the second state of the quantum well. Most of the probability of the electron wavefunction $\psi(x,t)$ is oscillating from $P_{B,0}$ (red line in (a)) to $P_{A,1}$ (blue line in (b)). This probability oscillation is the signature of the Rabi oscillation.

It is now interesting to see how the previous results will change if the frequency of the photons involved in the discussion is not in resonance with the mentioned energy E_G of the electrons. In particular, I consider now photons with an energy $2E_G$. I expect the light-matter interaction to switch off, because of the lack of resonance. The wavepacket is again injected in the RTD structure with energy $E = 234\,\text{meV}$ to occupy the second level of the quantum well so that it would have enough energy to emit the photon. In particular, in this non-resonant case, the evolution of probabilities defined in (9.4) and (9.5) does not show periodic oscillation. This means that the electron-photon interaction is not activated so that the electron and the photon evolve independently. These results can also be understood from the fact that the total energy of the system has to be conserved. In other words, $E_0 + 2E_G > E_1$, thus, the absorption of one photon by the electron ground state is not possible in this case, while in the previous case the absorption was possible because the energy conservation law red $E_0 + E_G = E_1$.

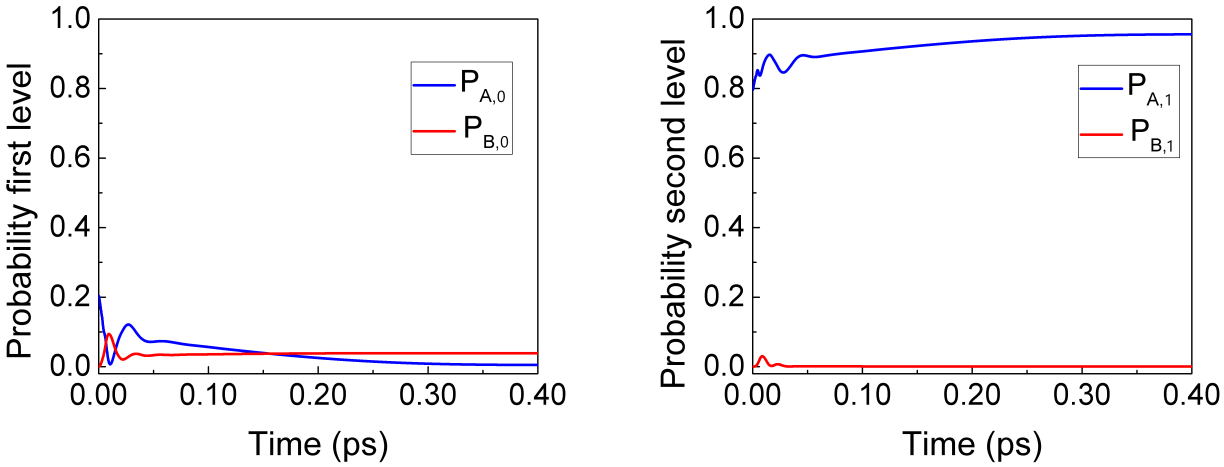

(a) **(b)**

Figure 9.7: (a) evolution of probabilities for the wavefunction to occupy the bottom state $P_{A,0}$ (blue line) and $P_{B,0}$ (red line) at $0 < E < (E_0 + E_1)/2$ (b) evolution of probabilities for the wavefunction to occupy the second state $P_{A,1}$ (blue line) at and $P_{B,1}$ at energies $(E_0 + E_1)/2 < E < \infty$ defined in (9.5),(9.4) for the case that the initial Gaussian wavepacket $\psi(x,t)$ is injected in the second state of the quantum well (so that at $t = 0$, $P_{A,1} \approx 1$). Here I show the non-resonant case where $f_\gamma = 2E_G/h$. It is clear that most of the probability is maintained in $P_{A,1}$, since the electron and the optical cavity are far from resonance.

Chapter 10

Non-coherent Transport of Electrons with Transversal Field

In this chapter, I analyze the quantum electron interacting in a non-coherent way with the quantum transversal electromagnetic field. I remind that I named as non-coherent the model of the electron-photon interaction when I use the Bohmian conditional wave function and I approximate its equation of motion from simple arguments based on conservation of momentum or conservation of energy. In particular, the non coherent treatment, explained in Chapter 7, is done using the energy exchange model in (7.10) and the momentum exchange model in (7.6). Additionally, similar results will be shown in the Wigner function representation, explained in (4.7). For comparison, the Wigner representation will be first shown with a coherent treatment (without approximations), and then non-coherently.

The results of this chapter are reproduced or adapted from:

- M. Villani, G. Albareda, C. Destefani, X. Cartoixà, X. Oriols, "Scattering in terms of Bohmian conditional wave functions for scenarios with non-commuting energy and momentum operators", *Entropy*, vol. 23, no. 4, p. 408, 2021;
- M. Villani, X. Oriols, "Can Wigner distribution functions with collisions satisfy complete positivity and energy conservation?", *Journal of Computational Electronics*, vol. 20, no. 6, p. 2232–2244, 2021.

10.1 Collisions with the Bohmian conditional wavefunction

In this section, I show results of the non-coherent evolution of electron-photon interaction presented in Section 7. First for a flat potential case, and then for an arbitrary potential one, in this case the RTD device of Fig. 9.4. In both cases I will compare the *momentum exchange model* of (7.4) to the *energy exchange model* of (7.9). The scattering is assumed to happen at time t_s, with the interaction taking place from time t_s to time $t_s + \tau_s$.

10.1.1 On the electron energy and momentum definitions

To properly compare the momentum and energy models, I assume that the change of the expectation value of the electron ΔE due to interaction with a photon with energy $E_\gamma = E(t_s + \tau_s) - E(t_s) = \Delta E$ is comparable to a change of the momentum with $p_\gamma = p(t_s + \tau_s) - p(t_s)$ satisfying:

$$p_\gamma = p(t_s + \tau_s) - p(t_s) = \frac{\sqrt{2mE(t_s + \tau_s)}}{\hbar} - \frac{\sqrt{2mE(t_s)}}{\hbar}. \tag{10.1}$$

Where p_γ is the momentum needed to have a change in energy of E_γ of the electron wavefunction $\psi(x,t)$. If (10.1) is verified, then the *momentum exchange model* of (7.4) and the *energy exchange model* of (7.9) are equivalent. But, now, the pertinent question is: can the momentums and energies of the electrons inside the device be always well-defined? The same question, in more technical words: Do the momentum and energy operators always commute?

Let us answer this question before showing the numerical result. For a arbitrary wave function $\psi(x,t)$, I can always compute the expectation value of the energy $\langle E(t) \rangle$ through (7.8), and of the momentum $\langle p(t) \rangle$ through (7.3). However, a change of energy ΔE in the expectation value of the energy corresponds to a change of momentum of the kind Δp only if electron energy eigenstates $\phi_E(x)$ are also momentum eigenstates $\phi_K(x)$. This is satisfied the energy and momentum operators commute: $[p, H_0] = 0$.

The typical quantum mechanical momentum operator in the position representation $p = -i\hbar\frac{\partial}{\partial x}$ commutes with the Hamiltonian H_0 when there is are spatial variations on the potential profile; for example, in the presence of a null potential profile. However, in the presence of a position-dependent arbitrary potential $V(x)$, the Hamiltonian operator is $H_0 = -\frac{\hbar}{2m}\frac{\partial^2}{\partial x^2} + V(x)$, and the commutator of the energy operator with the momentum operator will different, in general, from zero:

$$[p, H_0] = -i\hbar \frac{\partial}{\partial x} V(x) \neq 0. \tag{10.2}$$

This result will be very relevant in this chapter when I discuss collisions inside a typical device with a space-dependent conduction band; for example, the RTD used in my examples.

In particular, if momentum and energy do not commute I have the following situation depicted in Fig. 10.1. Let us consider an initial wave packet at a time $t = t_s$, before the collision, located in a flat potential where energy and momentum operators do commute. Then, $\psi(x, t_s)$ is characterized by a energy eigenstates distribution $a(E, t_s)$ with a Gaussian shape with small dispersion σ_E, and the expectation value $\langle E(t_s) \rangle$ (from (7.8)) so that I conclude that the energy of the initial electron is (roughly) well-defined. Identically, I can expect a similar behavior for the momentum given by a Gaussian shape with dispersion σ_p, and momentum eigenstates distribution $b(k, t_s)$, with expectation value $\langle p(t_s) \rangle$ (from (7.3)). So, I conclude, again, that the momentum of the electron is (roughly) well-defined at this initial time. This is represented in Fig. 10.1 by the red Gaussian wave packets in energy and momentum.

Then, the wave function interacts with the arbitrary potential $V_{ext}(x, t)$, where the time dependence t is not needed in this discussion, but it is kept to maintain generality. During this time I applied our collision model (either momentum exchange or energy exchange). But, now, because of the spatial dependence of $V_{ext}(x, t)$ it is not possible to have well-defined momentum and energy after the scattering. This is schematically shown in Fig. 10.1, and numerically validated in the following section where its consequences for quantum transport are discussed in detail. To bring additional proof this will also be shown with a Wigner representation, and with a different RTD structure, in Section 10.2.

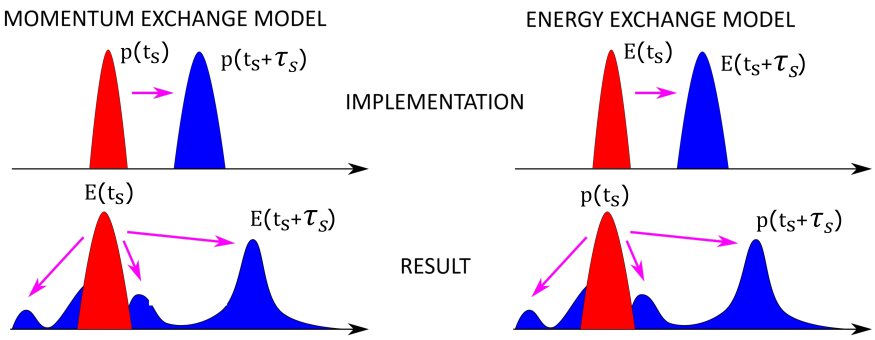

Figure 10.1: Schematic representation of the evolution of the energy and momentum components in the *momentum exchange model* (left figure) of (7.4) and *energy exchange model* (right figure) of (7.9). On the top figures I show the implemented transition, on the bottom figures I show the consequent creation of a new energy or momentum spectra.

Any non-coherent algorithm should be aware of this fundamental limitation to estimate simultaneously the energy and the momentum of a wave packet. In fact, since electrons are governed by the Hamiltonians that are the energy operators (not momentum operators), it is much more reasonable to expect a roughly well-defined energy for an electron, rather than a well-defined momentum. In such a way, an energy-exchange algorithm for collisions is much more physically acceptable than a momentum-exchange one. The conclusion is that those approaches that manipulate the momentum (like the Wigner function in the phase space) will have important difficulties to deal with collisions in a proper way.

Electron-photon interaction in case of flat potential

As just said, non-coherent algorithms based on either the momentum or energy exchange in a flat potential condition lead to equivalent results. Here I consider the electron Bohmian Conditional Wavefunction $\psi(x,t)$ interacting with a photon, with the interaction modelled with the *momentum exchange algorithm* of (7.4), whose probability distribution $|\psi(x,t)|^2$ is shown in Fig. 10.2(a). Then the scattered electron Bohmian Conditional Wavefunction $\psi(x,t)$ is modelled with the *energy exchange algorithm* of (7.9), whose probability $|\psi(x,t)|^2$ evolution is shown in Fig. 10.2(b). The expectation value of the velocity of the wavepacket is increased as a consequence of the *absorption* of a photon with energy $E_\gamma = 100\,\text{meV}$ and momentum $p_\gamma = 1.704 \cdot 10^8\, m^{-1}$, at the arbitrary scattering time $t_s = 15\,\text{fs}$. Clearly in this case the two models are fully equivalent.

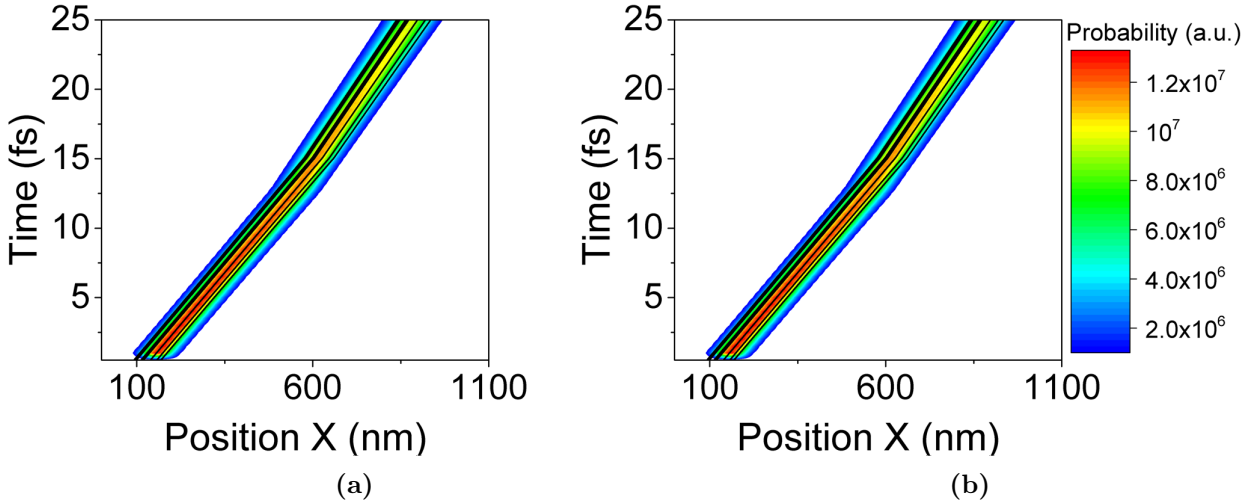

Figure 10.2: Evolution of the probability density $|\psi(x,t)|^2$, in flat potential conditions, with initial energy 58 meV, absorbing a photon at time $t_s = 15$ fs (a) using the momentum exchange model of (7.4) to absorb a photon with momentum $p_\gamma = 1.704 \cdot 10^8\, m^{-1}$ (b) using the energy exchange model of (7.9) to absorb a photon with energy $E_\gamma = 100$ meV.

In Fig. 10.3 the same comparison is done with the Bohmian Conditional Wavefunction $\psi(x,t)$, in the case of *emission* of a photon with energy $E_\gamma = 100$ meV and momentum $p_\gamma = 1.704 \cdot 10^8\, m^{-1}$. The equivalence shown in Fig. 10.2 is also clear looking at Fig. 10.3(a), which show the probability density $|\psi(x,t)|^2$ scattered with the *momentum exchange algorithm* of (7.4), and comparing it with Fig. 10.3(b), which show the probability density scattered with the *energy exchange algorithm* of (7.9).

In both figures the expectation value of the velocity of the wavepacket is decreased at the scattering time $t_s = 12$ fs. This equivalence is due to the fact that the momentum and energy operator commute in the case of a flat potential, as anticipated in subsection 10.1.1.

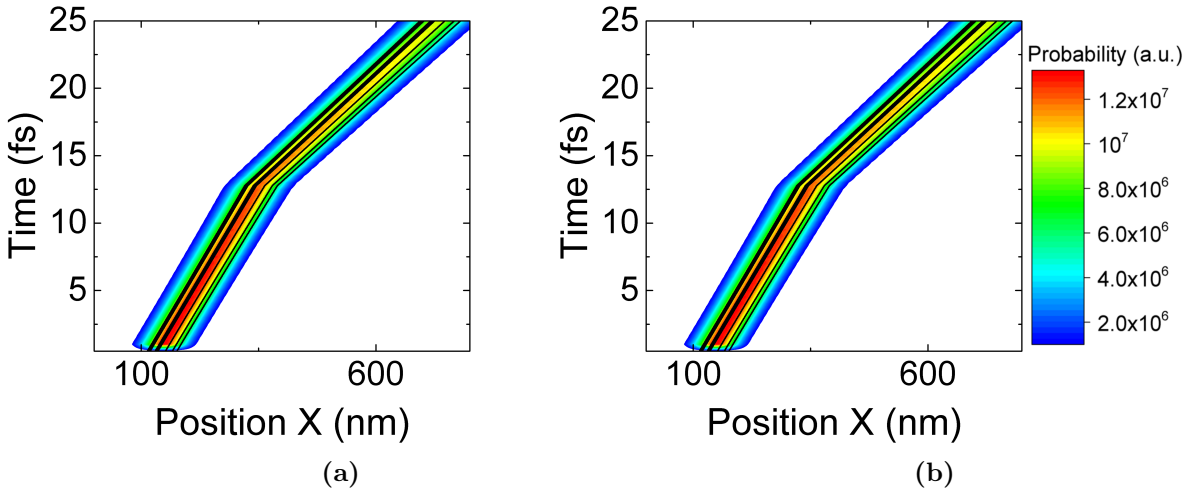

Figure 10.3: Evolution of the probability density $|\psi(x,t)|^2$, in flat potential conditions, emitting a photon at time $t_s = 15\,\text{fs}$ (a) using the momentum exchange model of (7.4) to emit a photon with momentum $p_\gamma = 1.704 \cdot 10^8\, m^{-1}$ (b) using the energy exchange model of (7.9) to emit a photon with energy $E_\gamma = 100\,\text{meV}$.

10.1.2 Momentum exchange model in case of arbitrary potential

In this subsection, I show the same result as Fig. 10.2 and 10.3 but in the presence of the arbitrary potential shown in Fig. 9.4.

We now show the unphysical result obtained when using a *momentum exchange model* to model electron-photon non-coherent interaction in the presence of an arbitrary potential $V_{ext}(x,t)$. I consider an electron Bohmian Conditional Wavefunction $\psi(x,t)$, which is injected in the active region in the presence, as I said, of an arbitrary potential. The evolution is described by (7.4), which in this case performs a simple shift of amount $p_\gamma = 2.529 \cdot 10^8\, m^{-1}$ (momentum of the photon) of the expectation value of momentum of the wavepacket, so that $p_\gamma = \langle p(t_s + \tau_s)\rangle - \langle p(t_s)\rangle$. In the arbitrary potential case this is *not* equivalent to a shift of $E_\gamma = 176\,\text{meV}$, because of the presence of the RTD structure. In particular, in Fig. 10.4 the wavepacket is injected in the bottom level of the quantum well $V_{ext}(x,t)$ shown in Fig. 9.4 with energy $E_{inj} = E_0 = E(t_s) = 58\,\text{meV}$ and momentum $p_{inj} = p(t_s) = 2.507 \cdot 10^8\, m^{-1}$, occupying the bottom state state $\phi_{E_0}(x)$ of the quantum well. In Fig. 10.4(a) the wavepacket is shown without scattering, to compare it with the following result in Fig. 10.4(b) where the wavepacket undergoes scattering, at time $t_s = 250\,\text{fs}$, consisting of *absorption* of a photon with resonant energy $E_\gamma = E_G$. The distribution of the momentum eigenstates $b(k, t_s + \tau_s)$ forming the base

of the wavefunction has a well-defined Gaussian shape, since the *momentum exchange model* of (7.4) is used, but now the distribution of the energy components $a(E, t_s + \tau_s)$ is not Gaussian any more, as schematically shown in Fig. 10.1.

The first effect of this is that some of the components of $a(E, t_s + \tau_s)$ has non-null occupation probability of energy eigenstates $\phi_E(x)$ so that, when included in the calculation of expectation value of the energy $\langle E(t_s + \tau_s)\rangle$ in (7.8) does violate the energy conservation:

$$E_\gamma = \frac{\hbar^2 p_\gamma^2}{2m} = \frac{\hbar^2 \langle p(t_s)\rangle^2}{2m} - \frac{\hbar^2 \langle p(t_s + \tau_s)\rangle^2}{2m} \neq \langle E(t_s)\rangle - \langle E(t_s + \tau_s)\rangle. \tag{10.3}$$

Additionally a non-Gaussian shape of $a(E, t_s + \tau_s)$ means a mixing of energy eigenstates $\phi_E(x)$ whose combination is not continuous in its spatial distribution and this creates the spatial oscillations visible in 10.4(b) after the scattering time $t_s = 250\,\text{fs}$. On the other hand the non-coherent *emission* of a resonant photon with the same algorithm (7.4) is shown Fig. 10.5, where the wavepacket is injected with energy equal to the second energy state of the quantum well $E(t_s) = E_1 = 235\,\text{meV}$ and momentum $p(t_s) = 5.036 \cdot 10^8\, m^{-1}$.

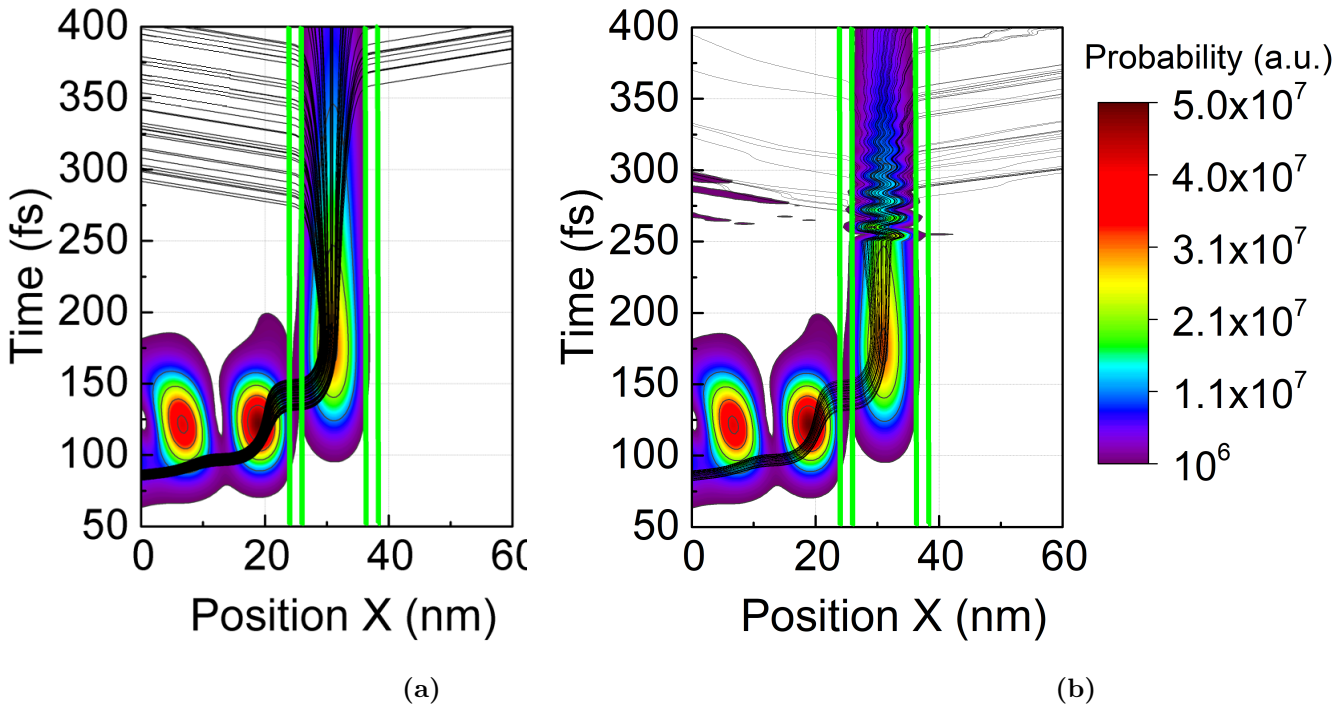

Figure 10.4: Spatial distribution of the electron probability density $|\psi(x,t)|^2$ (a) unperturbed electron evolving in time interacting with the quantum well (b) electron evolving in time interacting with the quantum well, absorbing a photon with momentum $p_\gamma = 2.529 \cdot 10^8\, m^{-1}$. Green vertical lines show the position of the RTD barriers.

In Fig. 10.5(a) the wavepacket is shown without scattering, to compare it with the following result in Fig. 10.5(b) where the wavepacket undergoes scattering, consisting of *emission* of a photon at the arbitrary time $t_s = 125\,\text{fs}$. The momentum behaves as in the previous photon absorption case, maintaining its Gaussian well-defined shape, and again this builds additional unphysical components in the superposition of the energy eigenstates used as the base of the wavefunction.

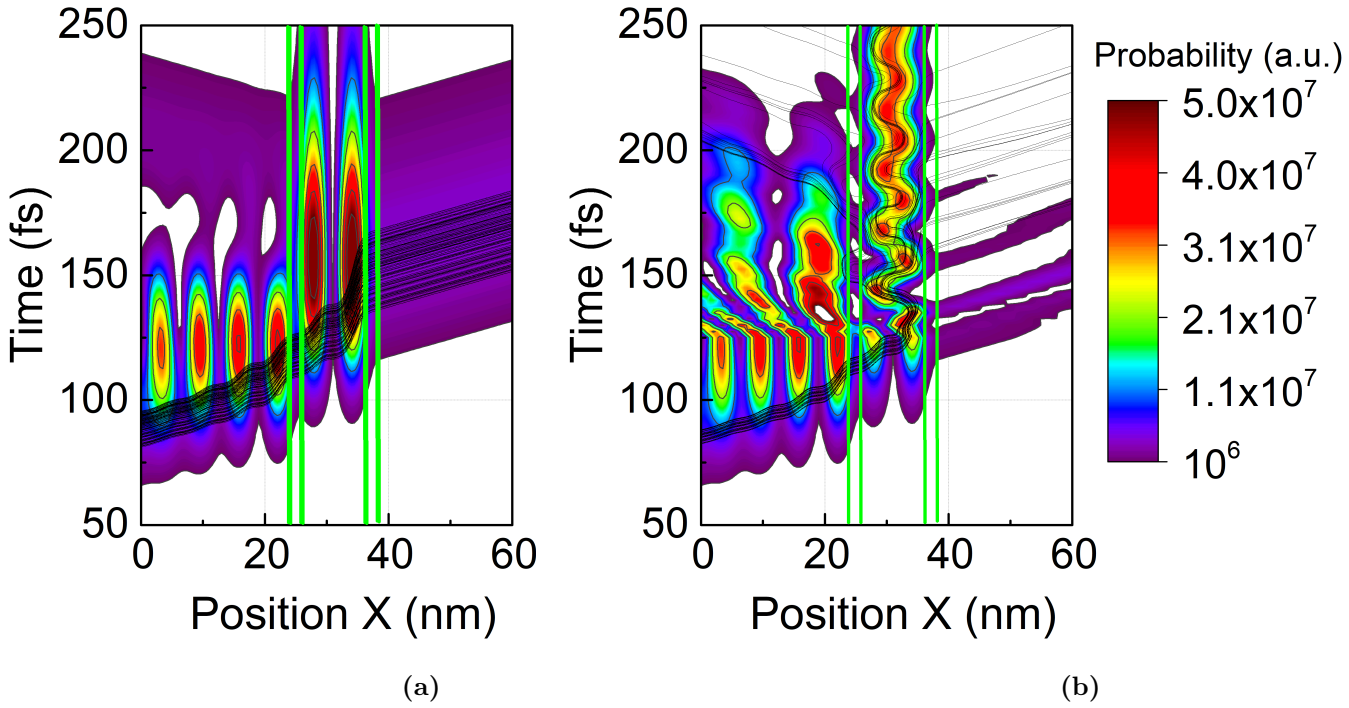

Figure 10.5: Spatial distribution of the electron probability density $|\psi(x,t)|^2$ (a) unperturbed electron evolving in time interacting with the quantum well (b) electron evolving in time interacting with the quantum well, emitting a photon with momentum $p_\gamma = 2.529 \cdot 10^8\, m^{-1}$ at time $t_s = 125\,\text{ps}$. Green vertical lines show the position of the RTD barriers.

As I have said, the momentum exchange in arbitrary potential is unphysical because it violates the total conservation of energy, which would be otherwise guaranteed by the coherent evolutions of wave packets from Hamiltonian (energy) operators. The conclusion is that those approaches that manipulate the momentum can provide unphysical results. As an example of these unphysical results in the literature are the oscillations simulated in the quantum well of an RTD which have been used to wrongly predict RTDs as intrinsic THz oscillators.

10.1.3 Energy exchange model in case of arbitrary potential

Now I apply the *energy exchange model* described in (7.9) to show a proper implementation of a non-coherent evolution of the system describing electron-photon interaction. I consider the same case shown in Fig. 10.4, with a single-electron wavepacket injected in the bottom state with mean energy $E_{inj} = E_0 = 58\,\text{meV}$ in the same RTD device shown in Fig. 9.4. The electron is absorbing a resonant photon, with energy $E_\gamma = E_G = 176\,\text{meV}$, where the variation in energy of the electron is modelled with (7.9). The result is shown in Fig. 10.6(b), where first the probability density $|\psi(x, t_s)|^2$ shows one maximum one maximum inside the quantum well, meaning that the bottom eigenstate $\phi_{E_0}(x)$ is occupied and $\langle E(t_s)\rangle = E_0$. Then, after the scattering time $t_s = 160\,\text{fs}$ the wavepacket is occupying the second state $\phi_{E_1}(x)$, and its related probability $|\psi(x, t_s + \tau_s)|^2$ shows two maxima inside the quantum well, which indicates that that $\langle E(t_s + \tau_s)\rangle = E_1$. The behaviour of probability density is synonymy of an effective absorption of a resonant photon with energy $E_\gamma = E_G$ inside the quantum well. For comparison, in Fig. 10.6(a) the same wavepacket is shown to evolve without undergoing scattering, so that $\langle E(t_s)\rangle = \langle E(t_s + \tau_s)\rangle = E_0$ occupying the bottom state of the quantum well for the whole simulation time.

The energy components of the Bohmian Conditional Wavefunction before, $a(E, t_s)$, and after the scattering, $a(E, t_s + \tau_s)$, are shown in Fig. 10.7(a) for the momentum exchange model of (10.7) and in Fig. 10.7(b) for the energy exchange model of (7.9). In Fig. 10.7(a) the $a(E, t_s + \tau_s)$ does not have any more the Gaussian shape of $a(E, t_s)$, with components that go up to $0.8\,eV$, much larger than the energy inside the whole electron-photon system, which can give, at best, an electron energy of $E_{max} = E_2 = 234\,\text{meV}$. All the additional unphysical components shown in red in Fig. 10.6(a) are the reason of the oscillation of the charge in 10.4. This is a result deriving from the non commutability of the energy and momentum operators in (10.2). On the other hand, in Fig. 10.6(b) the Gaussian shape is maintained in the transition from $a(x, t_s)$ with expectation value $\langle E(t_s)\rangle = E_0$ to $a(x, t_s + \tau_s)$ with expectation value $\langle E(t_s + \tau_s)\rangle = E_1$.

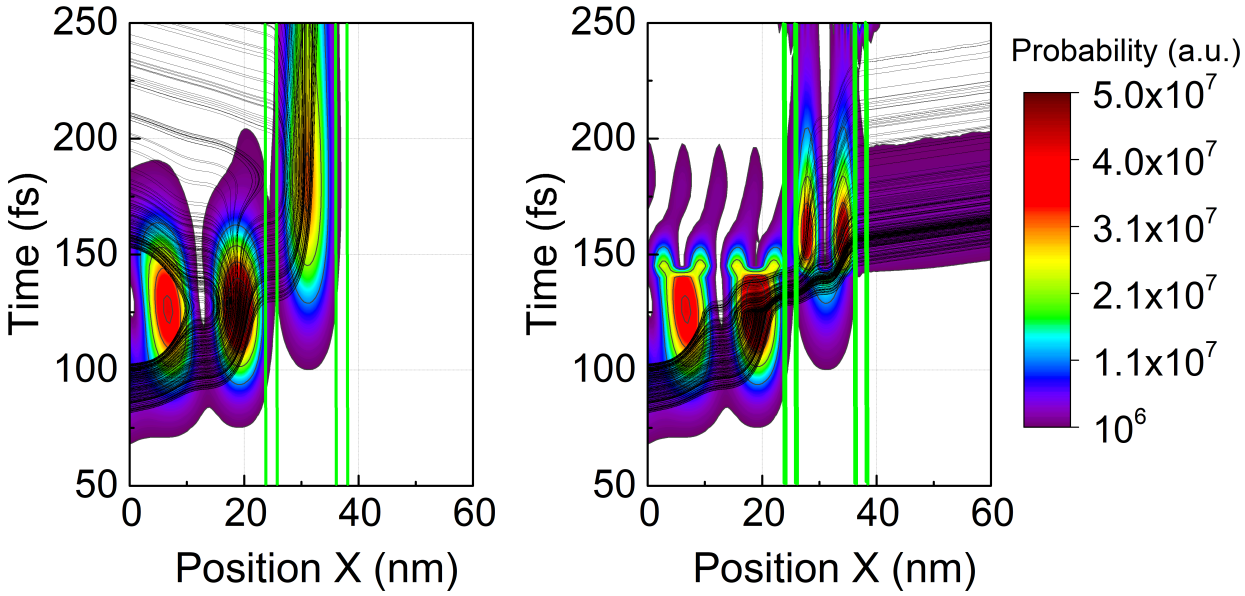

Figure 10.6: Spatial distribution of the electron probability density $|\psi(x,t)|^2$ interacting with the quantum well of Fig. 9.4, (a) unperturbed electron evolving in time interacting with the quantum well (b) electron evolving in time interacting with the quantum well of Fig. 9.4, while absorbing a photon with resonant energy $E_\gamma = E_1 - E_0 = 176\,\text{meV}$, at time $t_s = 160\,\text{ps}$. Green vertical lines show the position of the RTD barriers.

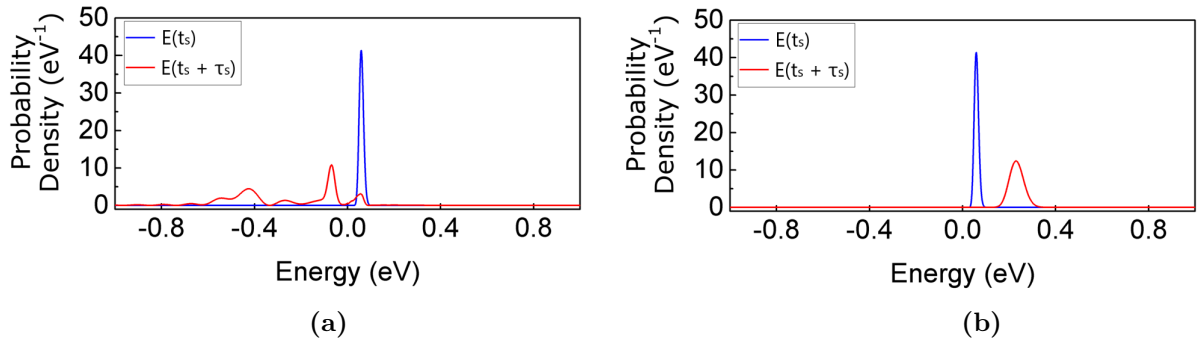

Figure 10.7: Energy components of the electron wavefunction $\psi(x,t)$ (a) evolved with the momentum exchange model, before the scattering event at $t = t_s$ (in blue) and after the scattering event at $t = t_s + \tau_s$ (in red), related to evolution of Fig. 10.4, (b) evolved with the energy exchange model, before the scattering event at $t = t_s$ (in blue) and after the scattering event at $t = t_s + \tau_s$ (in red), related to evolution of Fig. 10.6.

In Fig. 10.8 I take into consideration the wavepacket $\psi(x,t)$ injected in the second energy level, with expectation value of the energy $E_{inj} = E_1 = 234\,\text{meV}$. The wavepacket is now shown to emit a photon, with energy $E_\gamma = E_G = 176\,\text{meV}$, where the interaction is modelled with the energy exchange model of (7.9). The result is shown in Fig. 10.8(b), where the second eigenstate $\phi_{E_1}(x)$ is initially occupied, so that $\langle E(t_s)\rangle = E_1$ and then

after the scattering time $t_s = 150\,\text{fs}$ the wavepacket is occupying the bottom eigenstate $\phi_{E_0}(x)$, with one maxima inside the quantum well, so that $\langle E(t_s + \tau_s)\rangle = E_0$. This indicates the emission of a resonant photon inside the quantum well. For comparison, in Fig. 10.6(a) the same wavepacket is shown to evolve without undergoing scattering.

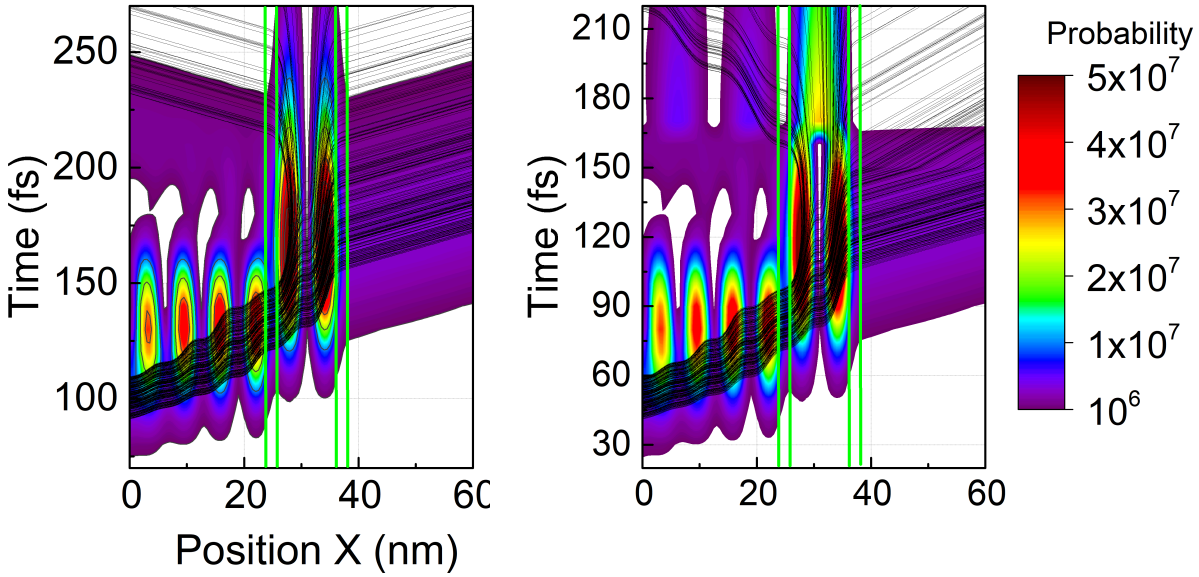

(a) **(b)**

Figure 10.8: Spatial distribution of the electron probability density $|\psi(x,t)|^2$ interacting with the quantum well of Fig. 9.4, (a) unperturbed electron evolving in time interacting with the quantum well (b) electron evolving in time interacting with the quantum well of Fig. 9.4, while emitting a photon with resonant energy $E_\gamma = E_1 - E_0 = 176\,\text{meV}$, at time $t_s = 150\,\text{ps}$. Green vertical lines show the position of the RTD barriers.

10.2 Collisions with the Wigner function

In this section, I analyse the Wigner Function description in its ability to implement a proper non-coherent electron-photon interaction. The Boltzmann-Wigner model of (4.8) is the tool used to introduce collision in the Wigner representation, and the bibliography that tries to properly implement a physically sound collision operator keeps expanding by the year. As already anticipated in Sec. 4.2 the most well-known problem when the collision operator is defined within the Wigner function description is to guarantee the condition of complete positivity of the probability. I will analyse how the condition of energy conservation is also often violated when a Wigner description is used if the collision operator is not properly defined. One reason for this is well known and explored in bibliography [51, 111, 113], and is deriving from analogous issues of the Density Matrix

description, which is Wigner's father representation, as explained in Sec. 4.2, in (4.19). A second reason which makes conservation of energy problematic will be observed in this thesis and was analysed in [113]. This reason is linked to the already mentioned non-commutability of the momentum $\hat{p}$ and energy $\hat{H}$ operators (10.2) when an arbitrary potential $V_{ext}(x,t)$ is included in the simulation box. This problem will affect any phase-space description in the implementation of a non-coherent system, but I anticipate that is a problem with a practical nature: while conceptually it is always possible to implement scattering in an open system defined in a phase-space $\{x,p\}$, in practice this needs the definition of a rather complicated collision operator $\hat{C}$, to overcome the problem of non-commutability shown in Fig.10.7.

10.2.1 Example for coherent model

To give additional results to compare the coherent approach with a non-coherent ones, I consider, also in the Wigner description, the coherent evolution of a Wigner function $f_W(x,k,t)$ interacting with a RTD structure shown in Fig. 10.9, with quantum well of 16 nm, barrier thickness 2 nm, electron mass $m = 0.041\, m_0$, barrier height 0.3 eV. The RTD device with this structure has a bottom energy level $\phi_{E_0}(x)$ with energy $E_0 = 23\,\text{meV}$, and the second state $\phi_{E_1}(x)$ with eigenenergy $E_1 = 96\,\text{meV}$. The RTD is interacting with an optical cavity which hosts two-photon states $\phi_0^{(\gamma)}(q)$ related to the vacuum state, and $\phi_1^{(\gamma)}(q)$ related to the first excited state of the optical cavity.

The optical cavity is assumed to only host perfectly monochromatic states with frequency ω_γ and resonant with the energy eigenstates of the quantum well: $E_G = \omega_\gamma/\hbar = 76\,\text{meV}$.

For a coherent implementation of electron-photon interaction within the Wigner description, I use equations (6.25) to evolve the wavefunction (6.22). The evolution is guided with the interaction strength $\gamma_q = 1.33\,\text{meV/nm}$. The evolution of (6.22) is represented in its Wigner representation, estimated with (4.7) on the whole wave function $\Psi(x,q,t)$ with the degree of freedom q integrated. From a computational point of view, the Wigner function $f_W(x,k,t)$ describing the open system of is computed form the density matrix $\rho(x,x',t)$ defined in (9.2), which give a total Wigner function equal the Wigner function computed form $\psi_A(x,t)$ plus the Wigner function computed from $\psi_B(x,t)$.

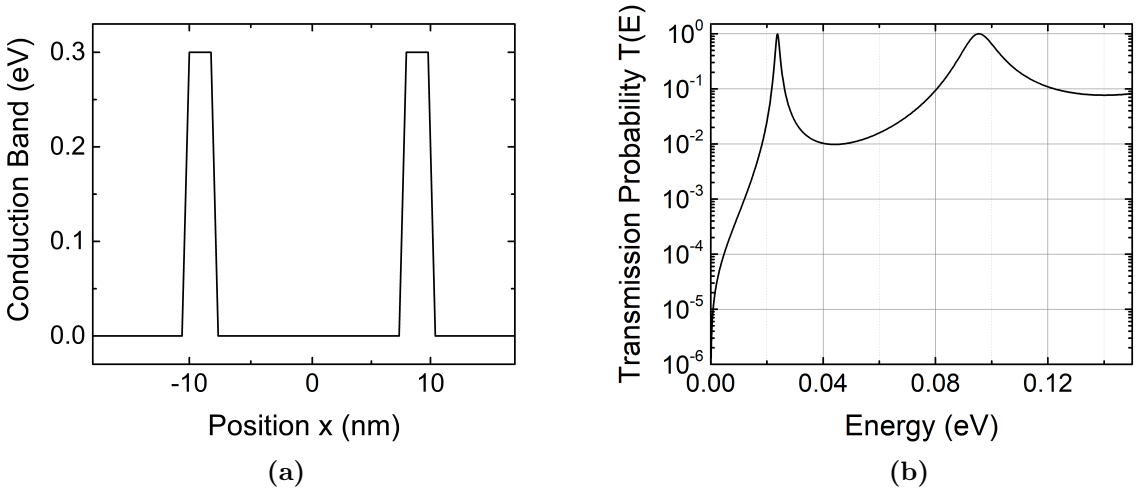

Figure 10.9: (a) Conduction band of the RTD device with quantum well of 16 nm, barrier thickness 2 nm, constant electron mass $m = 0.041\, m_0$, barrier height 0.3 eV (b) DC transmission probability in function of injection energy E, bottom energy level $E_0 = 23$ meV, second level $E_1 = 96$ meV.

The initial Wigner function is related to the wavefunction $\psi(x,0) = \psi_A(x,t)$ in (6.22), meaning that initially there is no photon in the optical cavity. The initial wavefunction is injected in the second level of the quantum well, so that $\psi(x,0) \approx \phi_{E_1}(x)$ and $E_{enj} = E_0 = 23$ meV. In Fig. 10.10 I show the result of the evolution of the Wigner function $f_W(x,k,t)$, the system is evolving from the top figures to the bottom ones, on the left column I show the Wigner function $f_W(x,k,t)$ in its typical $\{x,k\}$ phase-space, while in the right column I show the projection along the x and k axes, and along the kinetic energy $E = \hbar^2 k^2/2m$. In Fig. 10.10(a) $f_W(x,k,t)$ is injected deep into the contact, with central position $x = -90\, nm$, far away from the double barrier structure, the expectation value of the energy is $E_{inj} = 23$ meV, as can be seen to the red Gaussian distribution in the $\{x,p\}$ space, far away from the two vertical green lines. Then in Fig. 10.10(c) and (d) the $f_W(x,k,t)$ is entering inside the active region mostly occupying the bottom eigenstate in the quantum well, as I can notice the single peak inside the double barrier structure in the bottom part of Fig. 10.10(d). Finally in Fig. 10.10(e) and (f) the Wigner function $f_W(x,k,t)$ is interacting with the optical cavity, and inside the quantum well it occupies the second eigenstate, as can be observed by the double peak of the probability in the charge in the bottom of Fig.10.10(f).

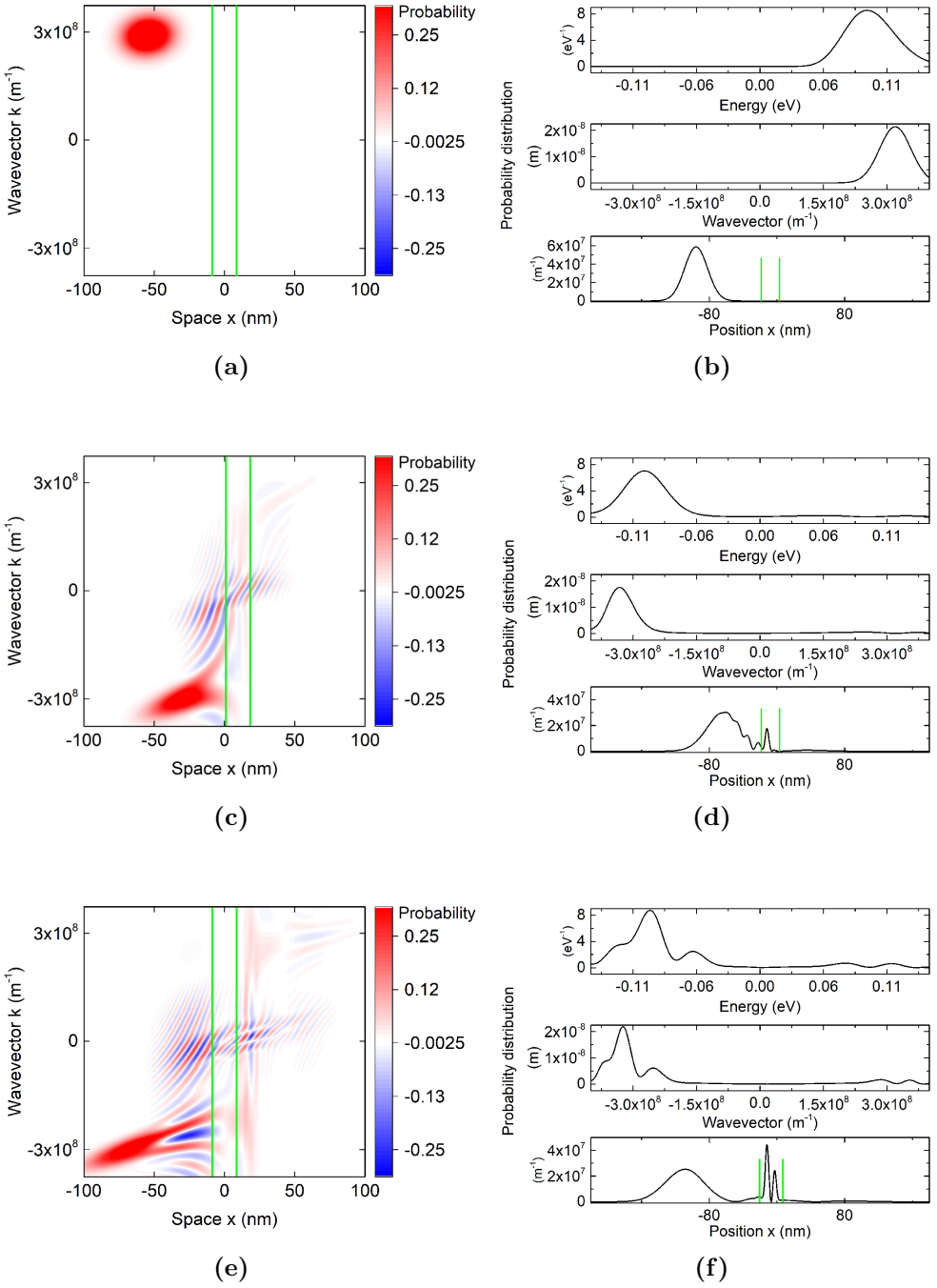

Figure 10.10: Wigner function of the total electron wavefunction interacting with a double barrier structure (green lines), at different times of its evolution: (a) at the beginning of the evolution, (c) when first entering inside the double barrier structure with $\langle E(t) \rangle = 23\,\text{meV}$, (d) after absorbing a photon, so that the electron energy is $\langle E(t) \rangle = 96\,\text{meV}$. In (b), (d), (f) are shown projections along the energy (top), momentum (middle) and position (bottom) axis of the Wigner transform respectively of (a), (c), and (d).

Electron-photon interaction in case of flat potential

To show that the momentum exchange model is not problematic for the Wigner function given particular conditions, I try the Boltzmann-Wigner equation in flat potential condition, $V_{ext}(x,t) = 0$. The result is shown in Appendix D, where in Fig. D.1, in flat potential conditions the momentum exchange (non-coherent) model of (7.4) is used to simulate the absorption of a photon in one electron described by the Wigner function $f_W(x,k,t)$. The Wigner function $f_W(x,k,t)$ maintains a well-defined gaussian shape of the momentum components during the scattering from Fig.D.1(b), showing the Wigner function at at $t = t_s$, to D.1(d) showing the Wigner function at at $t = t_s + \tau_s$.

10.2.2 Momentum exchange model in case of arbitrary potential

In this section, I use the Wigner representation of the Bohmian Conditional Wavefunction evolved using the momentum exchange and the energy exchange algorithms presented respectively in (7.4) and (7.9), in the presence of an arbitrary potential $V_{ext}(x,t) \neq 0$. In Fig. 10.1 I show the rising of the same issues of the previous Section 10.1, where the momentum exchange algorithm is used for photon emission or absorption by an electron that interacts with a double barrier structure. In this case the structure is the one shown in Fig. 10.9, with quantum well of 16 nm, barrier thickness 2 nm, constant electron mass $m = 0.041\, m_0$, barrier height 0.3 eV.

The change of the expectation value of the momentum of the Winger function $f_W(x,k,t_s)$ of the Bohmian Conditional Wavefunction is equivalent to the most diffused algorithm used for scattering in the Wigner description, which, by the nature of this description, is based on evolution in space and momentum. In Fig. 10.11(a) the Wigner function of the Bohmian Conditional Wavefunction with initial injection momentum $p(t_s)$ is impinging against the double barrier structure whose position is indicated by the vertical green lines.

The Gaussian wavepacket interacts with a photon with momentum $p_\gamma = p(t_s + \tau_s) - p(t_s) = \frac{\sqrt{2mE_1}}{\hbar} - \frac{\sqrt{2mE_0}}{\hbar}$ while it evolves in space, where E_1 and E_0 are the second eigenenergy and the bottom energy of the double barrier structure. In Fig. 10.11(b) the Wigner function $f_W(x,k,t_s)$ is shown to have initial expectation value of the energy of $E_{inj} = \langle E(t_s)\rangle = E_0 = 23\,\text{meV}$ (see top figure), equivalent to (mostly) occupying the first eigenstates of the quantum well, because one peak in the probability is visible (see bottom image of Fig. 10.11(b)). When the majority of the wavefunction is inside the quantum well, the emission of a photon of momentum p_γ is taking place. In Fig. 10.11(c)

the scattered Wigner function $f_W(x, k, t_s + \tau_s)$ is shown, and its projections along the x and k axis show the problems of implementation the momentum exchange algorithm. In fact the expectation value of the momentum (and of the energy) of the Wigner function is not changing from $f_W(x, k, t_s)$ in Fig. 10.11(b) to the one in $f_W(x, k, t_s + \tau_s)$ in 10.11(d). This is also visible in the charge distribution, where in both 10.11(b) and (d) the same bottom eigenstates of the quantum well si occupied. This means that after the scattering, I have $\langle E(t_s + \tau_s)\rangle \neq E_1$, so that the energy conservation is violated, and $\langle E(t_s + \tau_s)\rangle \neq \langle E(t_s)\rangle + E_\gamma$.

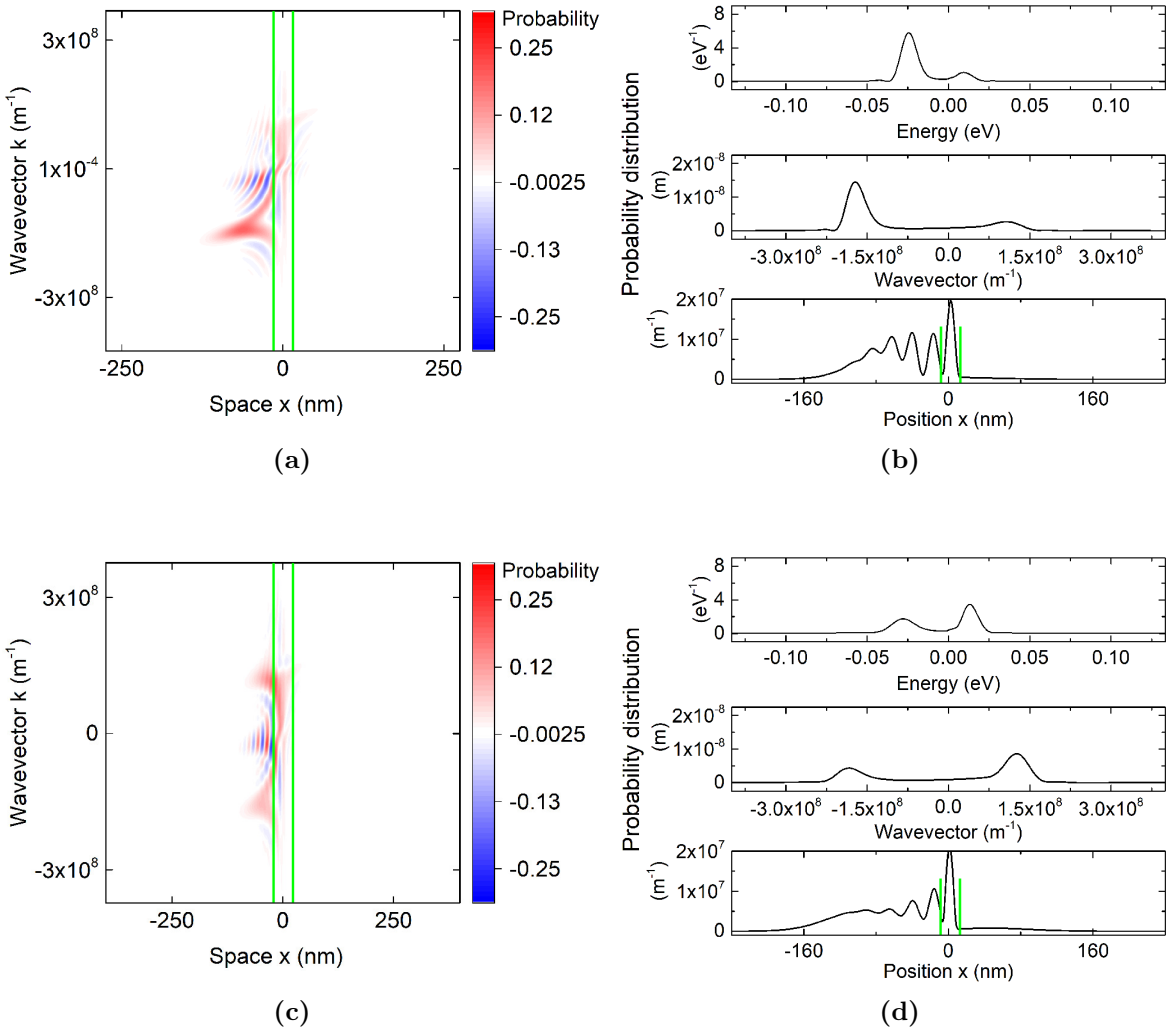

Figure 10.11: Wigner function for photon absorption in a double barrier structure evolved with the *momentum exchange model* (7.4): (a) before scattering ($f_W(x, k, t_s)$), injected in the bottom level $E_{inj} = E_0 = 23\,\text{meV}$ and (c) scattered ($f_W(x, k, t_s + \tau_s)$) by emitting a photon with resonant energy $E_\gamma = E_G = E_1 - E_0 = 73\,\text{meV}$, where E_1 and E_0 is the bottom and second energy eigenstates of the quantum well. In (b) and (d) I show projections along the energy (top), momentum (middle) and position (bottom) axis of the Wigner functions respectively of the Wigner function (a) and (c). The green lines show the position of the double barrier structure.

Equivalent results are observed when the photon is emitted, as in Fig. 10.12. Here initially the Wigner function $f_W(x, k, t_s)$ is injected with momentum $p(t_s)$, equivalent to the energy $E_{inj} = \langle E(t_s) \rangle = E_1 = 0.96\,\text{meV}$, which is equivalent to the energy eigenvalue of the second state in the quantum well, as it is proved by the charge distribution at the bottom of Fig. 10.12(b). After the scattering, Fig. 10.12(c) and (d) show the same expectation values of energy and momentum, and the same charge distribution of Fig. 10.12(a) and (b). Again I have violated the conservation of energy $\langle E(t_s + \tau_s) \rangle \neq \langle E(t_s) \rangle - E_\gamma$.

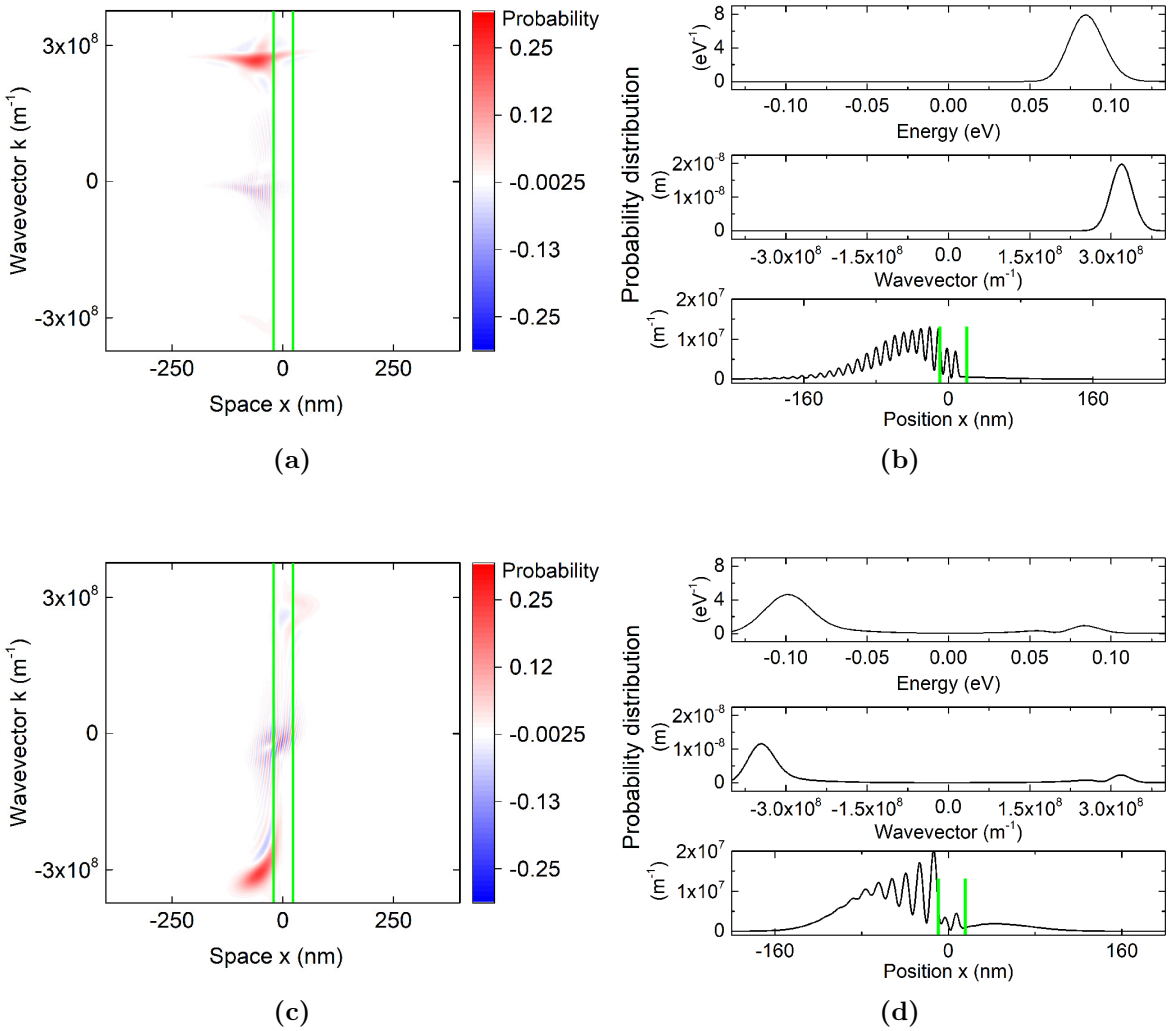

Figure 10.12: Wigner function for photon emission in a double barrier structure evolved with the *momentum exchange model* (7.4): (a) before scattering ($f_W(x, k, t_s)$), injected in the second resonant level $E_{inj} = E_2 = 96\,\text{meV}$ and (c) scattered ($f_W(x, k, t_s + \tau_s)$) by emitting a photon with resonant energy $E_\gamma = E_G = E_1 - E_0 = 73\,\text{meV}$, where E_1 and E_0 is the bottom and second energy eigenstates of the quantum well. In (b) and (d) I show projections along the energy (top), momentum (middle) and position (bottom) axis of the Wigner functions respectively of the Wigner function (a) and (c). The green lines show the position of the double barrier structure.

10.2.3 Energy exchange model in case of arbitrary potential

In this section, I use the Wigner representation scattered with the energy exchange algorithm in (7.9), in the presence of an arbitrary potential $V_{ext}(x,t) \neq 0$. shown in Fig. 10.9, with quantum well of 16 nm, barrier thickness 2 nm, constant electron mass $m = 0.041\, m_0$, barrier height 0.3 eV. This algorithm will be applied to the same Wigner function $f_W(x,k,t)$ of the previous Fig. 10.11 and 10.12. As for the case of the wave-function representation, I expect the model of (7.9) to provide an effective algorithm for non-coherent electron-photons scattering. The result is shown in Fig. 10.13 for the absorption of a photon with energy $E_\gamma = 73$ meV. In Fig.10.13 (a) and (b), the Wigner function $f_W(x,k,t_s)$ initially has expectation value of the energy of $\langle E(t_s)\rangle = 23$ meV (see top figure), which is equivalent to (mostly) occupying the bottom state of the quantum well. In fact, only one peak in the probability is visible (see bottom figure 10.11(b)). Then in Fig. Fig.10.13 (c) and (d) after the scattering at time the Wigner function $f_W(x,k,t_s+\tau_s)$ is occupying the second state of the quantum well, and I have $\langle E(t_s+\tau_s)\rangle = E_1$. In fact, all of the energy and momentum components are shifted at higher values, respecting the energy conservation: $\langle E(t_s+\tau_s)\rangle = \langle E(t_s)\rangle + E_\gamma = E_0 + E_\gamma = E_1 = 96$ meV.

The same result can be shown for photon emission. In Fig.10.13 (a) and (b), the Wigner function $f_W(x,k,t_s)$ has initial expectation value of the energy of $E(t_s) = 23$ meV. And only two peaks in probability are present in the bottom figure 10.11(b)). Then in Fig. 10.13 (c) and (d) after the scattering the Wigner Function $f_W(x,k,t_s+\tau_s)$ is occupying the bottom state of the quantum well. This shows that the energy conservation is respected, since $E(t_s+\tau_s) = E(t_s) - E_\gamma = E_1 - E_\gamma = E_0 = 23$ meV.

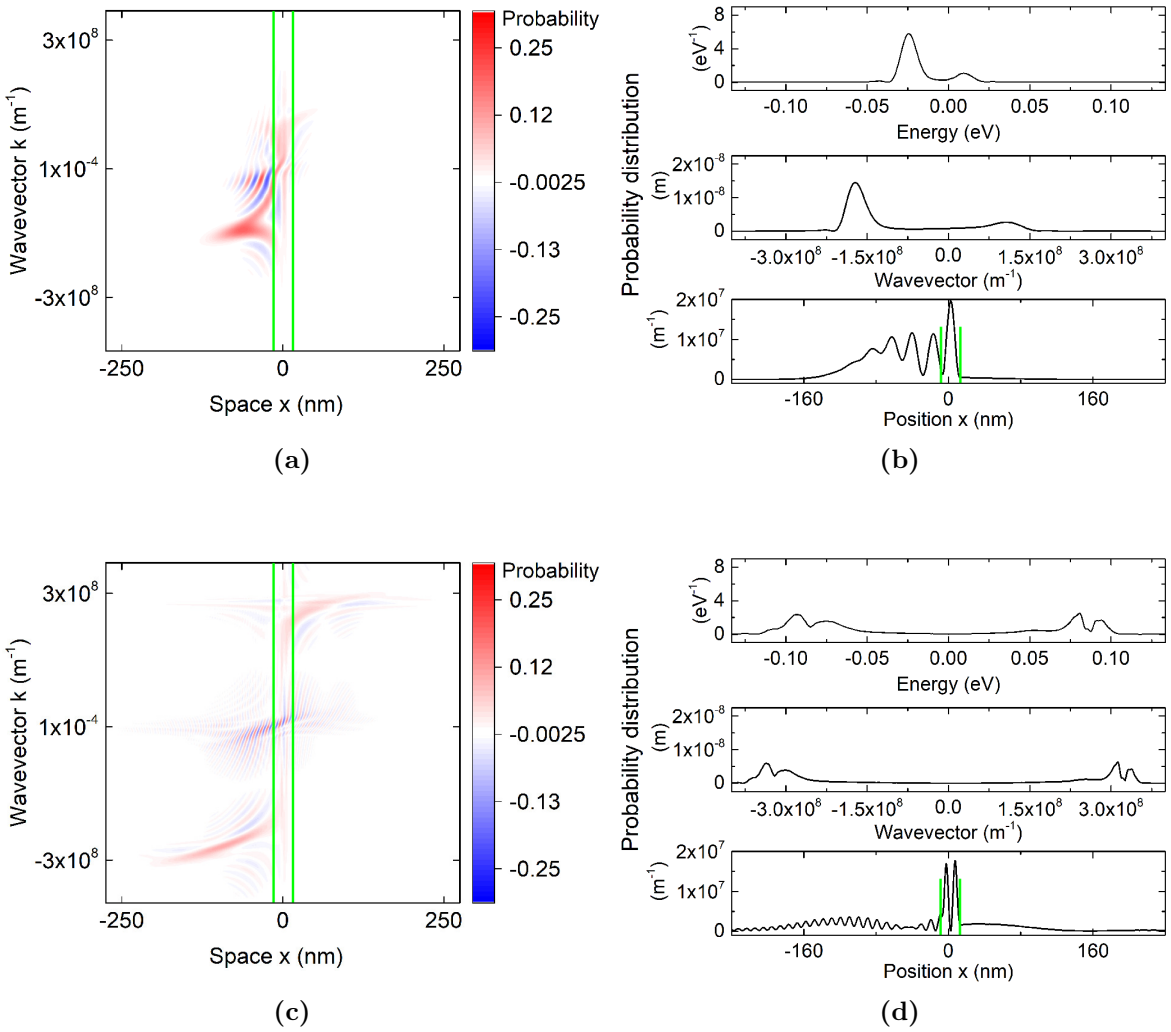

Figure 10.13: Wigner function for photon absorption in a double barrier structure evolved with the *energy exchange model* (7.9): (a) before scattering ($f_W(x, k, t_s)$), injected in the second resonant level $E_{inj} = \langle E(t_s)\rangle = E_0 = 23\,\text{meV}$ and (c) scattered ($f_W(x, k, t_s + \tau_s)$) by emitting a photon with resonant energy $E_\gamma = E_G = E_1 - E_0 = 73\,\text{meV}$, and occupying the second eigenstate of the quantum well with $\langle E(t_s + \tau_s)\rangle = E_1 = 96\,\text{meV}$. In (b) and (d) I show projections along the energy (top), momentum (middle) and position (bottom) axis of the Wigner functions respectively of the Wigner function (a) and (c). The green lines show the position of the double barrier structure.

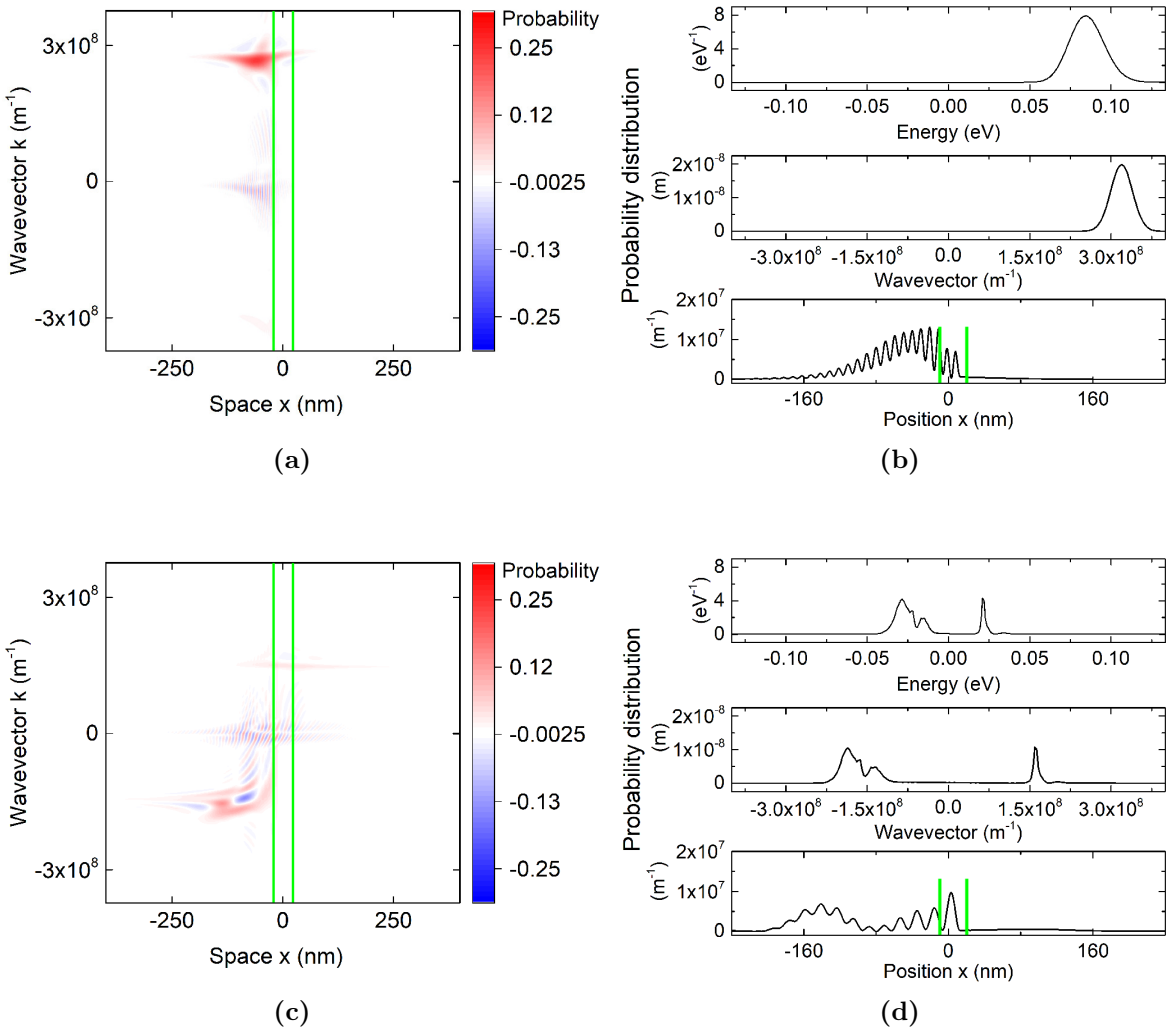

Figure 10.14: Wigner function for photon emission in a double barrier structure evolved with the *energy exchange model* (7.9): (a) before scattering ($f_W(x,k,t_s)$), injected in the second resonant level $E_{inj} = \langle E(t_s)\rangle = E_1 = 96\,\text{meV}$ and (c) scattered ($f_W(x,k,t_s+\tau_s)$) by emitting a photon with resonant energy $E_\gamma = E_G = E_1 - E_0 = 73\,\text{meV}$, and occupying the second eigenstate of the quantum well with $\langle E(t_s+\tau_s)\rangle = E_0 = 23\,\text{meV}$. In (b) and (d) I show projections along the energy (top), momentum (middle) and position (bottom) axis of the Wigner functions respectively of the Wigner function (a) and (c). The green lines show the position of the double barrier structure.

Finally in Fig.10.15 I compare the expectation value of the electron energy $\langle E(t)\rangle$ for the Wigner function $f_W(x,k,t)$. The value of the energy for the coherent evolution shown in Fig. 10.10, evolved with (6.25), and then converted in the Wigner function description with (4.7), is the black dashed line. This is compared with the change of the expectation value of the energy from the charge evolution shown in Fig. 10.13 and 10.14, both evolved with the energy exchange model of (7.9), and then represented in the Wigner function with (4.7).

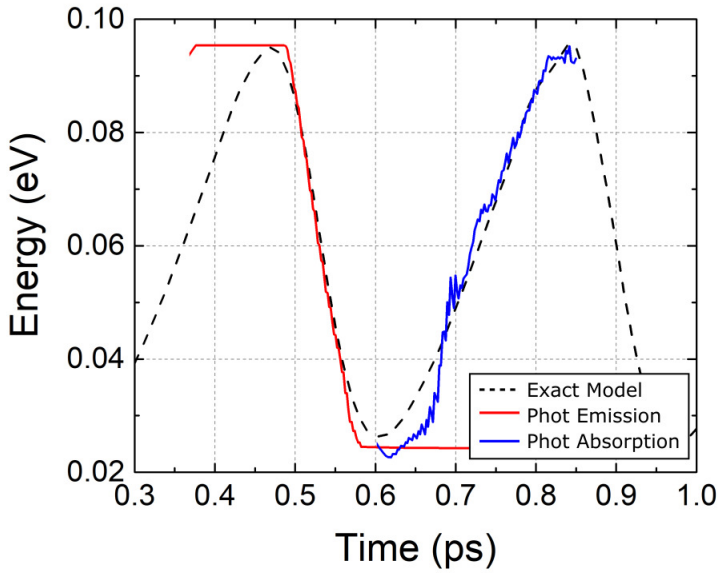

Figure 10.15: Evolution of the expectation value of the energy of the Wigner Functions. The dashed line shows the evolution for the coherent photon-electron interaction model in Fig. 10.10. The coherent and non-coherent models are shown to be equivalent in the expectation value of the energy, both for emission and for absorption of a photon (respectively red and blue lines). The equivalence in time is artificially fixed by the choice of a proper adiabatic transition for the non-coherent electron-photon interaction.

I conclude by repeating that, in principle, the Wigner function can develop a model to include scattering, but the typical Boltzmann collision operator can provide unphysical results because it is based on a momentum exchange that does not satisfy conservation of energy during the scattering process. Such lack of conservation of energy can generate, for example, the unphysical oscillation of the charge in the well of the RTD, as seen in Fig. 10.5. In fact, such unphysical oscillations have been used in the literature to erroneously predict intrinsic THz oscillators build from RTD.

Chapter 11

Displacement current coefficient without transversal field

In this chapter I show results related to the estimation of the Displacement Current Coefficient $D^{(f)}(E,t)$ defined in (8.8). This estimation will be done for a double barrier RTD device whose structure will be explained later. First I will consider the DC condition, for a comparison of the Displacement Current Coefficient $D^{(f)}(E,t)$ with the transmission probability $T(E)$ typical of the Landauer model. This comparison will be done in function of input bias and then in function of the injection energy of the electron wavefunctions $\psi(x,t)$. Secondly, the AC regime will be studied in the frequency range from 10 GHz up to 8 THz, with a qualitative analysis of the small-signal response of the RTD device first in the time domain, with a focus on the frequencies from 350 GHz to 2 THz, and then in the frequency domain through the mentioned Displacement Current Coefficient.

The results of this chapter are reproduced or adapted from:

- M. Villani, S. Clochiatti, W. Prost, N. Weimann, X. Oriols, "There is Plenty of Room for THz Tunneling Electron Devices Beyond the Transit Time Limit", *IEEE Electron Device Letters*, vol. 42, no.2, p. 224-227, 2021.

11.1 Simulation setup

Let us first introduce the simulation setup used all along this chapter. The simulation of the Displacement Current Coefficient $D^{(f)}(E,t)$ as in (8.8) is performed by injecting a train of non-interacting single-electron Gaussian wavepackets $\psi(x,t;t_i)$, with given expectation value of the energy, which I define as injection energy $\langle E(t=0)\rangle = E_{inj}$. The

parameter t_i in $\psi(x,t;t_i)$ specifies at what time the electron was located deep in the left reservoir (far from the active region). The active region is the RTD structure shown in Fig. 11.1, with quantum well width of 1.7 nm, barrier thickness 1.7 nm, constant electron mass $m = 0.067\,m_0$, barrier height 0.5 eV. Each Gaussian's injection energy determines the energy dependency inside the Displacement Current Coefficient $D^{(f)}(E,t)$, so that I will from now on say $E_{inj} \equiv E$, then each wavefunction is evolved with the Hamiltonian H_0 in (6.5). The single-electron current density, $J(x,t;t_i)$, needed in (8.8) , is estimated from $\psi(x,t;t_i)$ with the typical definition (3.3).

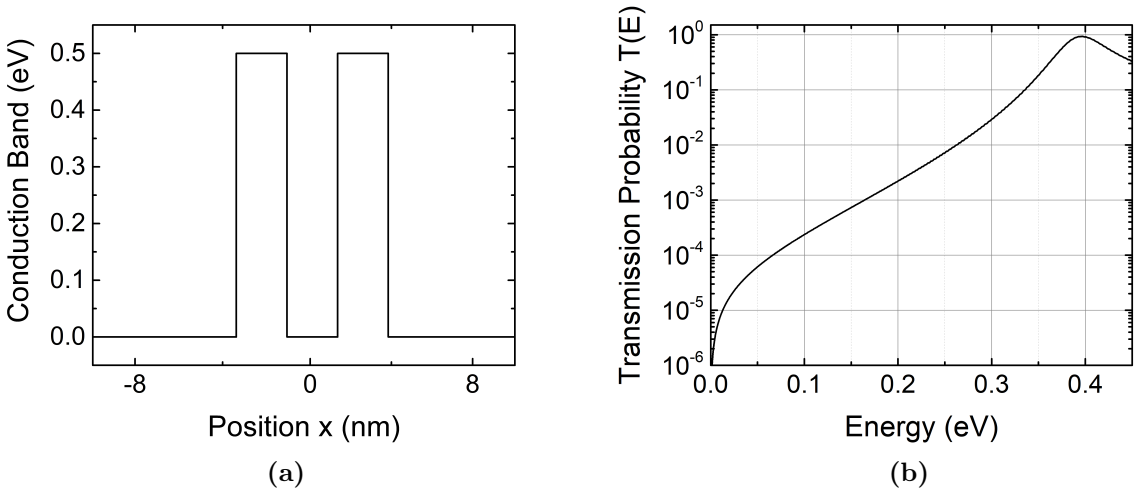

Figure 11.1: (a) Conduction band of the RTD device with quantum well width of 1.7 nm, barrier thickness 1.7 nm, constant electron mass $m = 0.067\,m_0$, barrier height 0.5 eV(b) DC transmission probability in function of injection energy E, bottom energy level $E_0 = 396$ meV, second eigenstate is not shown as it is beyond the reach of the Fermi distribution function at room temperature and zero bias conditions.

I remind the reader that from (8.5) the RTD device's drain contact oscillates give an external sinusoidal signal $V_{in}(t) = V_0 \cdot cos(2\pi f \cdot t + \theta)$ with given external frequency f, which determines the f apex of the Displacement Current Coefficient $D^{(f)}(E,t)$, and phase θ. The steady-state of a device is defined as a working frequency f respecting the relationship $f << 1/\tau$, where τ is the (average) transit time of carriers inside the active region. For the device in Fig. 11.1, without electron-photon interaction, the transit time is estimated to be around $0.3\,ps$. In fact in the practical implementation of (8.8), the ∞ value in the integral, which dictates the simulated time t_{max} for each single-electron current $J(x,t;t_i)$, is reduced to just satisfy being greater than τ. In the numerical simulation, I will use $t_{max} = 0.4$ ps. I underline that the exact estimation of the transit time in the model (8.8) is not needed for an accurate simulation, as the time-dependent evolution of $\psi(x,t)$ will naturally include this time in the simulation, and

as already said, the role of t_{max} is just giving the time-dependent wavefunction enough time, t_{max}, to enter and leave the wave function in a natural way. Regarding the quasi-static regime, from the transit time of $\tau \approx 0.3\,\text{ps}$, I know that for an input frequency of $f > 1\,\text{THz}$ the device is fully above the transit time limit.

11.2 Device in DC condition

In this section I show some numerical results where I excite the device with input signal frequency of $f = 1\,\text{GHz}$, in (8.6), which can be considered to be steady-state conditions. I call $D^{(f=0)}(E,t)$ the value of the Displacement Current Coefficient $D^{(f)}(E,t)$ estimated in steady-state conditions. In the frequency analysis I will better define the limit of this condition, however here I stay in a safe low frequency condition. The train of independent single-electron wavefunctions $\psi(x,t;t_i)$ is injected with different central energies, to observe how the *transmission probability* $T(E)$ and the Displacement Current Coefficient $D^{(f)}(E,t)$ compare. I have already shown in (8.10) that, by construction it is easy to show that for $f \to 0$, I have $D^{(f)}(E,t) \to T(E)$. In fact, in Fig. 11.2 it can be seen how the two parameters perfectly coincide when this low-frequency signal (black dashed line) is applied on the RTD device. The two coefficients are shown for different injection energies E. Additionally here I assume $\beta = 1\,\text{s}^{-1}$ in (8.8). Here is shown that $T(E)$ from (8.2) and the Displacement Current Coefficient $D^{(f)}(E,t)$ from (8.8) have good agreement.

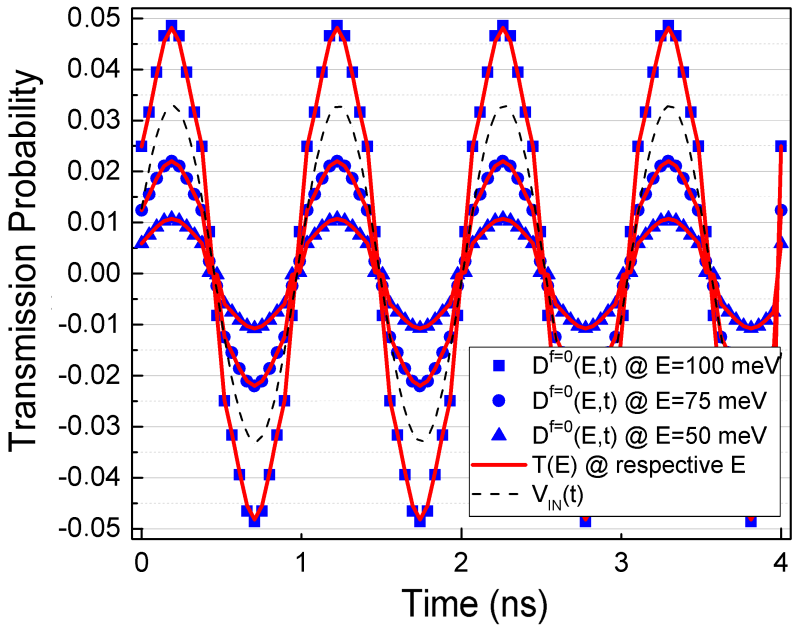

Figure 11.2: The transmission probability $T(E)$ (red line) as in (8.2), compared with the Displacement Current Coefficient $D^{(f)}(E,t)$(blue shapes) as in (8.8), estimated for the same RTD device whose potential profile is shown in Fig. 11.1. The estimation is done for different injection energies, in function of time, under an input signal with frequency $f = 1\,\text{GHz}$ (black dashed line).

The energy analysis in DC conditions is shown in the following result of Fig. 11.3 where the transmission probability $T(E)$, is confronted with the Displacement Current Coefficient $D^{(f)}(E,t)$ in function of the injection energy E, estimated with no applied bias and in DC condition (with $f = 1\,\text{GHz}$).

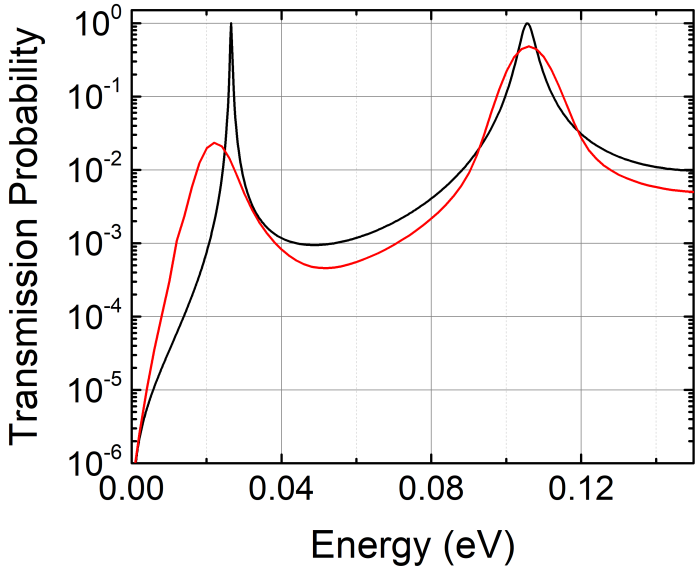

Figure 11.3: Transmission probability $T(E)$ (black line) from (8.2) and Displacement Current Coefficient $D^{(f)}(E,t)$ (red line) from (8.8) in function of the injection energy E for the structure in Fig.11.1, in DC conditions. The additional broadening of the Displacement Current Coefficient $D^{(f)}(E,t)$ derives from the non-zero energy dispersion $\sigma_E = 15\,\text{meV}$ of the injected Gaussian wavepackets $\psi(x,t;t_i)$ used to estimate (8.8). This also gives problems in estimating the Displacement Current Coefficient $D^{(f)}(E,t)$ for injection energies E below 30 meV as numerical problems rise.

11.3 Device in AC condition

In this section and the following, I estimate the Displacement Current Coefficient $D^{(f)}(E,t)$ for the RTD device of Fig.11.1, here I show the evolution of the output, for a harmonic input signal as in (8.6), with amplitude $V_0 = 0.01\,V$ and different frequencies f. The input signal (8.6) influences the potential profile $V_{ext}(x,t)$ through (8.5). This will influence the evolution of the t_i-train of electron wavefunctions $\psi(x,t;t_i,E)$ with the Hamiltonian H_0 in (6.5). The analysis of the output is first done in a time domain, where the output current will be estimated using (8.7) in function of time. Secondly, the same coefficient is estimated in function of frequency f of the input signal, by defining a small-signal conductance $Y_{11}(f)$. For both the following results the injection energy of the wavefunction is $E = 50\,\text{meV}$. I remind that the single-band time-dependent Displacement Current Coefficient $D^{(f)}(E,t)$ is directly proportional to the output current $I^{(f)}(t)$ as in (8.9).

11.3.1 Time domain analysis

In Fig. 11.4, the output current related to the energy band of $E = 0.05\,\text{eV}$ is shown as a function of time. The amplitude of the input signal $V_{in}(t)$ shown in (8.6) has amplitude

$V_0 = 0.01\,\mathrm{V}$, while the frequency f varies. The resulting conduction band $V_{ext}(x,t)$ evolves oscillating the RTD device as in (8.5). The simulation shows that the output current can vary strongly when the input frequency moves in the domain from 350 GHz to 2 THz. I will discuss each frequency comparing it with the inverse of the (average) transit time $\tau \approx 0.3\,ps$.

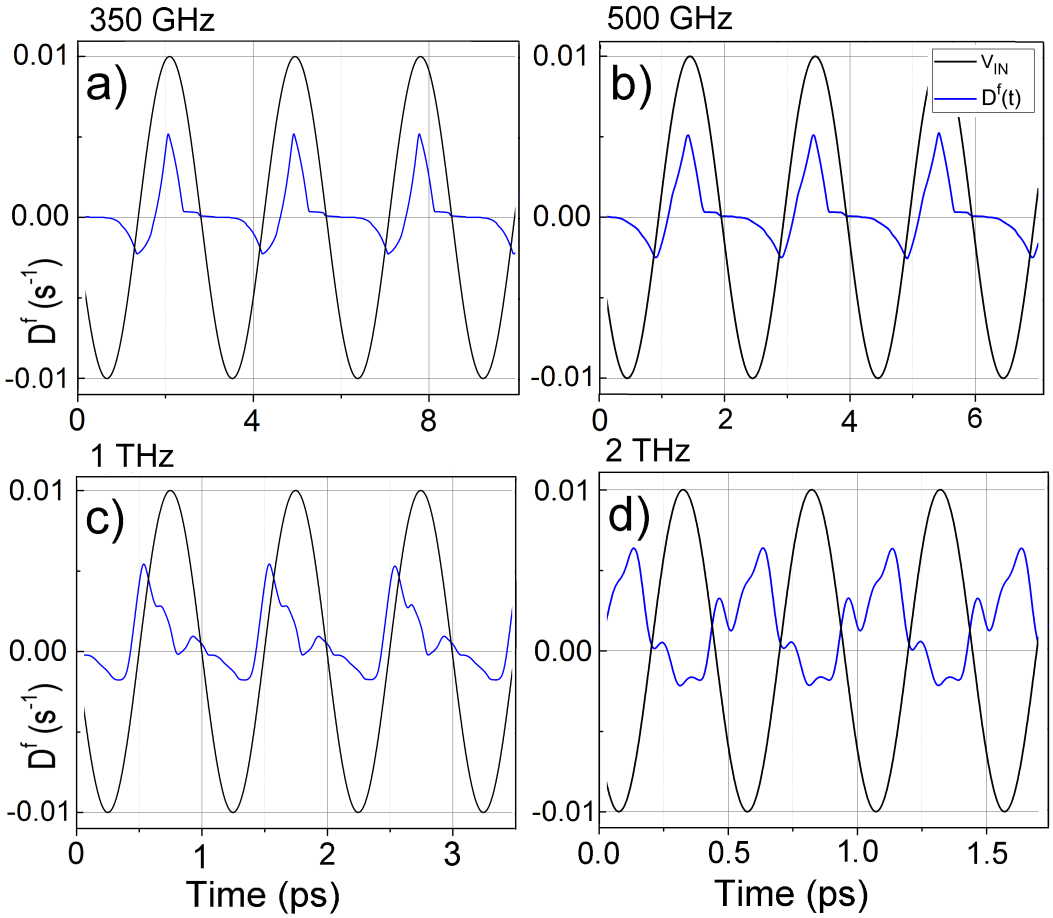

Figure 11.4: Time-dependent output current of the RTD calculated at the injection energy of 0.05 eV, for different frequencies of the input signal, shown in function of time. (a) $f = 350\,\mathrm{GHz}$, (b) $f = 500\,\mathrm{GHz}$, (c) $f = 1\,\mathrm{THz}$, (d) $f = 2\,\mathrm{THz}$. The input signal is represented by the continuous black line.

For low frequency, in Fig.11.4(a) the behaviour of the output current is similar to what I expect looking at the transmission probability $T(E)$. Since at this input signal I have $f \approx 0.1 \cdot \frac{1}{\tau}$, the low working frequency makes the device reproduce the strong non-linearities of the DC characteristics. Single-electron currents will simply be transmitted or reflected following what is the DC bias.

The output current of Fig.11.4(b) show a slight increase in the non-linear behaviour, but the output current $I(t)$ is still easily linked to the value of the input signal, and the conductance is still mostly positive.

In Fig.11.4(c), the working frequency is approaching the inverse of the (average) tran-

sit time, as $f \approx 0.4 \cdot \frac{1}{\tau}$. The output current $I(t) \approx D^{(f)}(E,t)$ shows non-linearities and additional components that are not expected in the DC behaviour of this device. The physical origin of these components is the interference between electrons injected at different times t_i which have evolved with different effective potential profiles since this will be different for every time interval $[t-\tau, t]$, where τ is the (average) transit time of electrons in the active region. Since I assumed all electrons to be independent, the interference is happening in the integral of (8.8), where all the single-electron currents are summed to create unexpected patterns of the output current.

In Fig.11.4(d) I have a frequency almost equal to the inverse of the (average) transit time: $f \approx 0.66 \cdot \frac{1}{\tau}$. The output current's behaviour is clearly non-linear because all of the single-electron currents $J(x,t;t_i)$ that have a role in the creation of the output current are different between each other, as the potential profile is very different at each time t_i in the range $[t-\tau, t]$. In other words, each electron injected at a different time t_i will have a very different memory of the behaviour of the potential profile. Moreover, I remind the reader that the electron's (average) transit time is of the order of $\tau = 0.3\,\text{ps}$, and since the time scale of Fig.11.4(d) is around 1.5 ps, one electron will occupy the active region for a good portion of the period of the input signal, and will "see" different shapes of the potential profile as in (8.5). This is another reason why having a simple linear relationship between the input signal $V_{in}(t)$ and output total current $I(t) \approx D^{(f)}(E,t)$ at any time t looks to be rather unreasonable.

We underline that while this is only a partial and qualitative analysis of the behaviour of the output current of a single energy band inside the device, in Fig. 11.4(c) and (d) I reveal that the definition of the Displacement Current Coefficient $D^{(f)}(E,t)$ is opening the possibility of predicting the output current of the RTD device well beyond the quasi-static condition, without the need of assuming a linear behaviour of the device.

11.3.2 Frequency domain analysis

In Fig. 11.5 I show results taken from publications [136, 137], and I will extend the explanation of the Displacement current coefficient and its meaning. To build a frequency analysis of the Displacement Current Coefficient $D^{(f)}(E,t)$ I use a small-signal model. For an applied DC bias V_DC I get a DC current I_{DC}. Then, the steady-state (complex) small-signal conductance $Y_{11}(f)$ is the relationship between the input voltage $V_{in}(t)$ from (8.6) and the output signal from the Displacement Current Coefficient $D^{(f)}(E,t)$ from (8.8) when the DC current I_{DC} is subtracted. The real and imaginary components of

$Y_{11}(f)$ describe, in linear domain, the (complex) output current $\mathbf{I}^{(f)}(t)$ when a (complex) input AC small-signal $\mathbf{V}_{in}(t)$ is used. The frequency f of the input signal is considered a parameter in the computation of the admittance $Y_{11}(f)$. When the linear domain between current and voltage is verified, the input and output signal present well-known behaviour and only two phases of the sinusoidal output signal are relevant [138]. I define $I_R^{(f)}(t) = \mathbb{R}\mathrm{e}(I^{(f)}(t))$ and $I_I^{(f)}(t) = \mathbb{I}\mathrm{m}(I^{(f)}(t))$ as the real and imaginary parts of a complex current $\mathbf{I}^{(f)}(t)$ as:

$$\begin{aligned}
\mathbf{I}^{(f)}(t=0) - I_{DC} - jI_{DC} &= I_R^{(f)}(t=0) - I_{DC} + j[I_I^{(f)}(t=0) - I_{DC}] \\
&= Y_{11}(f) \cdot V_0\, e^{2\pi f t} \\
&= Y_{11}(f) \cdot V_0[\cos(2\pi f t) + j\sin(2\pi f t)] \\
&= Y_{11}(f) \cdot V_0[\cos(2\pi f t) + j\cos(2\pi f t - \pi/2)] \\
&= I_0^{(f)}(t=0) - I_{DC} + j[I_{-\pi/2}^{(f)}(t=0) - I_{DC}], \qquad (11.1)
\end{aligned}$$

where $t = 0$ is an arbitrary time that fixes at what time to observe the different current corresponding to different phases θ_i. Thus, I see that what I call first a complex current $\mathbf{I}^{(f)}(0)$ is, in fact, computed from a unique simulation of a real current $I^{(f)}(t)$ and observing it at different times (implying different θ). For example, $I_R^{(f)}(t=0)$ (also defined as $I_0^{(f)}(t=0)$) correspond to $I^{(f)}(t=0)$ for an input voltage $V_{in}(t) = V_0 cos(2\pi f t)$, while $I_I^{(f)}(t=0)$ (also defined as $I_{-\pi/2}^{(f)}(t=0)$) correspond to $I^{(f)}(t=1/(2f)$ for the same input voltage $V_{in}(t) = V_0 cos(2\pi f t)$. Notice that any other phase θ can also be computed, while for a linear system these two phases are enough. Finally using the Displacement Current Coefficient $D^{(f)}(E,t)$ in (8.8), the $Y_{11}(f)$ parameter is estimated with the following definition [138–140]:

$$\begin{aligned}
Y_{11}(f) &= \left(\frac{I_R^{(f)}(t=0) - I_{DC}}{V_0}\right) + j\left(\frac{I_I^{(f)}(t=0) - I_{DC}}{V_0}\right) \\
&= \left(\frac{I_0^{(f)}(t=0) - I_{DC}}{V_0}\right) + j\left(\frac{I_{-\pi/2}^{(f)}(t=0) - I_{DC}}{V_0}\right) \\
&= q\int_{-\infty}^{\infty} dE \cdot g(E) \cdot f(E) \cdot \left[\left(\frac{D_0^{(f)}(E,t) - T(E)}{V_0}\right) + j\left(\frac{D_{-\pi/2}^{(f)}(E,t) - T(E)}{V_0}\right)\right] \\
&= \mathbb{R}\mathrm{e}(Y_{11}(f)) + \mathbb{I}\mathrm{m}(Y_{11}(f)). \qquad (11.2)
\end{aligned}$$

Here, to simplify the notation, I define positive energies E as those belonging to electrons injected from the left and negative energies E for those electrons injected from the right.

For an applied DC bias, the Fermi-Dirac distribution $f(E)$ changes for negative and positive energies. As before, $D_0^{(f)}(E,0)$ and $D_{-\pi/2}^{(f)}(E,0)$ mean the Displacement Current Coefficient $D^{(f)}(E,t)$ estimated from the input signal has respectively the phase $\theta_i = 0$ and $\theta_i = -\pi/2$.

As I have mentioned, the whole procedure of the computation of the Y_{11} parameter is based on the assumption that the device is linear. Then, knowing these two phases of the response will reveal the value of the conductance at any phase of the period. To explore any non-linear behaviour that is expected following the qualitative results of Fig. 11.4, I need to estimate the Displacement Current Coefficient $D^{(f)}(E,t)$ at other phases. For example, at this opposite phase: $\theta_i = -\pi$, leading to the current $I_{-\pi}^{(f)}(t=0)$. Since the harmonic input signal V_{in} in (8.6) gives $\cos(2\pi ft) = -\cos(2\pi ft - \pi)$, in literature it is known that, in linear domain, $I_0^{(f)}(t=0) = -I_{-\pi}^{(f)}(t=0)$ This condition is in fact the indication that a small signal-model can be used to predict in a compact way the value of the output current $I^{(f)}(t)$ at any time t. On the other hand, the inequality $I_0^{(f)}(t=0) \neq -I_{-\pi}^{(f)}(t=0)$ reveals non-linearities of the device. I argue in this thesis that these non-linearities are not a drawback, but just a new opportunity to get richer THz devices, since it indicates additional components created in the spectrum of the output signal. However, what is lacking is a model for the device working at high-frequency to predict these non-linearities, to enable engineering. For more details about the meaning of Displacement Current Coefficient $D^{(f)}(E,t)$ and possibilities opened by this study of high-frequency nanodevices, I recall [139]. Finally, in Fig. 11.5, the three different phases of the Displacement Current Coefficient $D^{(f)}(E,t)$: $D_0^{(f)}(E,t) \approx \mathbb{R}\mathrm{e}(Y_{11})$, $D_{-\pi/2}^{(f)}(E,t) \approx \mathbb{I}\mathrm{m}(Y_{11})$ and $D_{-\pi}^{(f)}(E,t)$ are plotted as a function of the input frequency f in (8.6)(8.5) in the range from 10 GHz to 10 THz, estimated for a single injection energy band at $E = 0.05$ eV. In this figure, four different frequency domains can be observed, for each domain, I will analyse the behaviour of each one of these three phases components of the Displacement Current Coefficient $D^{(f)}(E,t)$. But first, let me define the four frequency regimes:

- Linear Regime $f < 100\,\mathrm{GHz}$, where the $D^{(f)}(t)$ coefficient is equivalent to the transmission probability of the device at a given energy $T(E)$. For small enough input signal, the RTD behaves in a linear way.
- Non-linear THz regime $100\,\mathrm{GHz} < f < 10\,\mathrm{THz}$. The frequency is so high that for a (finite) small input voltage, the RTD is no longer linear.
- Electromagnetic regime $f > 10\,\mathrm{THz}$. Here additional component and Γ_m in Eq

(5.20) becomes relevant, and the device goes out of the Darwin approximation explained in Chapter 5. So that the definition of the total current $I(t)$ (5.26), which neglect this component, loses its validity, and any prediction given by the model presented in (8.8) start to be inaccurate.

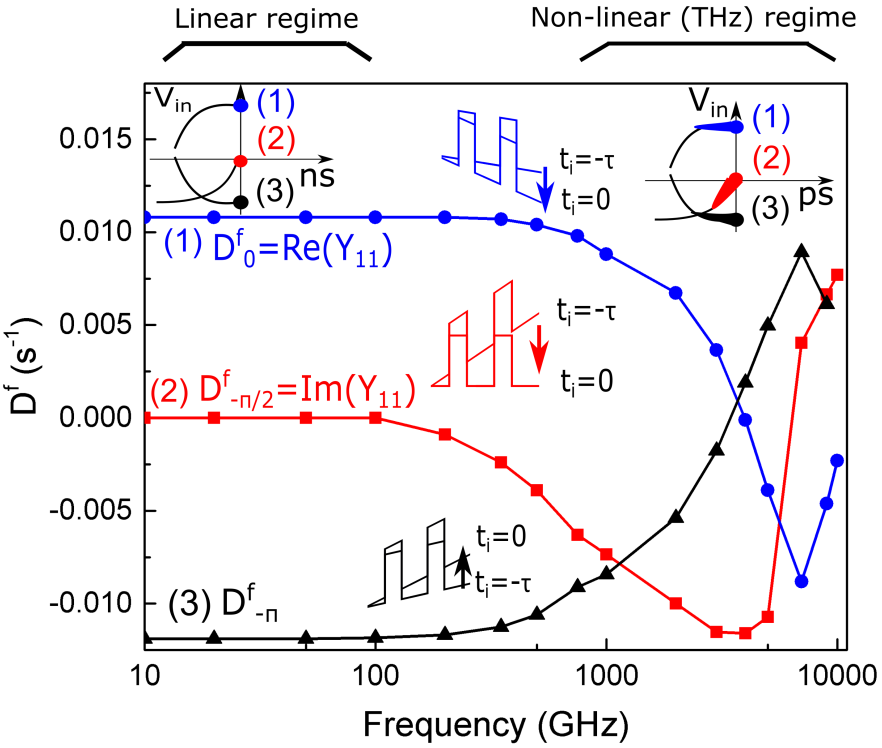

Figure 11.5: Displacement Current Coefficient $D^{(f)}(E,t)$ for the RTD in Fig. 11.1 for different input frequencies f and estimated for all three phases $\theta = 0, \theta = -\pi/2$ and $\theta = -\pi$. Result from [136]. © 2021 IEEE.

The behaviour of all the phases of $D^{(f)}(t)$ can be explained keeping in mind that the current observed at time t holds memory about all electrons injected at all times $[t-\tau, t]$, and the device's memory has the length of the (average) transit time τ. The behaviour of the current can be explained by simple visualization of the evolution of the Conduction Band $V_{ext}(x,t)$ (defined in (8.5)) during the (average) transit time, so that I will compare $V_{ext}(x,t)$, the conduction band at the observation time, with $V_{ext}(x,t-\tau)$, the latest relevant value of the conduction band which still has a role in determining the output current at the measurement time t, because of the memory conserved by electrons along the (average) transit time τ. As already said in Chapter 5.1, in (8.5) I will now avoid to include the Coulomb electron-electron interaction $U(x,t)$. This approximation will only add complexity to the result of this section. I define $V_{SD}(t)$ as the value of the input signal at time t, equal to $V_{in}(x=b,t) - V_{in}(x=a,t)$, where a and b are the position

of interfaces of the active region respectively with the source and drain contact. I also assume the source to be connected with a ground contact, so that $V_{in}(x = a, t) = 0$ and $V_{SD}(t) = V_{in}(x = b, t)$. Where $V_{in}(x, t)$ was defined in (8.6).

Linear regime In linear regime, I have $E_c(t) \approx E_c(t - \tau)$, and the three lines of Fig. (11.5) are: $D_0^{(f)}(E, t) = T_{DC}(E - V_0)$, $D_{\pi/2}^{(f)}(E, t) = T_{DC}(E)$, $D_{\pi}^{(f)}(E, t) = T_{DC}(E + V_0)$. In fact, in this regime, the Landauer model perfectly quantifies the transmission probability of the active region.

Non-linear THz regime In the non-linear THz regime, $E_c(t) \neq E_c(t - \tau)$, and the RTD shows a much richer phenomenology. The behaviour of the three phases can be explained as follow:

- For $D_0^{(f)}(E, t)$, I know that the input signal will behave in the following way: $V_{SD}(t) > V_{SD}(t - \tau)$. So, looking at the instantaneous values of the transmission probability, $T(E)|_t < T(E)|_{t-\tau}$. Performing the time integral in 8.7, the value of $T(E)|_{t-\tau}$ will be more and more relevant for the estimation of $I^{(f)}(t)$ as the frequency increases. As a consequence, $D_0^{(f)}(E, t)$ will decrease, as in the blue line in Fig.11.5.

- For $D_{-\pi}^{(f)}(E, t)$, because of the phase, I have that $V_{SD}(t) < V_{SD}(t - \tau)$. So that $T(E)|_t > T(E)|_{t-\tau}$. Gain, the value of $T(E)|_{t-\tau}$ will be more and more relevant for the estimation of $I^{(f)}(t)$ as the frequency increases. And for this phase, $D_{-\pi}^{(f)}(E, t)$ will increase, as in the black line in Fig.11.5.

- For $D_{-\pi/2}^{(f)}(E, t)$, the input signal is at the maximum of its derivative so that its frequency dependence is higher than the other phases. In fact, this phase is the first one to be affected by the high frequency of the input signal as in the red line in Fig.11.5. Depending on the phase ($\phi = 0$ or $\phi = 2\,\pi$), I can either observe an increase or decrease of this parameter as input frequency increases.

All the variations observed here are just showing a delay of the system with respect to the input signal. This phenomenon is included in the estimation of the cut-off frequency of the device as the input frequency f approaches the inverse of the (average) transit time.

The non-linearity We can observe that the value of $D_{-\pi}^{(f)}(E,t)$ changes from its DC value $D_{-\pi}^{(f=0)}(E,t)$ at the relatively low input frequency of $f = 200\,\text{GHz}$, while $D_0^{(f)}(E,t)$ changes from its DC value $D_0^{(f=0)}(E,t)$ at higher frequencies at around $f = 500\,\text{GHz}$. The reason for $D_0^{(f)}(E,t) \neq -D_{-\pi}^{(f)}(E,t)$ is the memory of the device, which can be held for the (average) transit time τ, and is non-symmetrical for the two opposite phases. Please remind that the relevant single-electron currents $J(x,t;t_i)$ for the current measured in $I^{(f)}(t)$ are the ones related to electrons that were injected at times $[t-\tau,t]$.

This is because for this particular phase (see blue line in Fig.11.5) I will have $V_{SD}(t-\tau) < V_{SD}(t)$ (see the small blue double barrier structure in Fig.11.5). As a consequence the instantaneous transmission probability will be higher at time t than the one at time $t-\tau$, and a different amount of charge will enter inside the RTD at these two different times: $J(x,t;t_i) > J(x,t-\tau,;t_i)$. Thus, the measured charge at time t will be less influenced by the *smaller* amount of charge entered at time $t-\tau$, decreasing the strength of the memory and thus the frequency dependence.

For the opposite phase $D_{-\pi}^{(f)}(E,t)$ (black line in Fig.11.5) has higher frequency dependence because since $V_{SD}(t-\tau) > V_{SD}(t)$ (see the black blue double barrier structure in Fig.11.5), and the amount of charge entered in the active region at time $t-\tau$, $J(x,t-\tau;t_i)$, will be higher than the one entering at the observation time t: $J(x,t;t_i) < J(x,t-\tau;t_i)$. This behaviour leads to higher dependency on the memory, in comparison with the opposite phase, and this will increase the frequency dependence,as observed in Fig. (11.5).

Memory-related effects in ballistic and non-ballistic devices The memory-related effects explained in the previous paragraph is conceptually valid for any electron device. This is the reason why eventually at high enough frequency any device has a non-linear behaviour. The main difference between a ballistic device, such as a Resonant Tunnelling Diode, and a non-ballistic resistor is the memory of the device. While for the RTD the memory is held for a time τ, any non-ballistic device holds memory only for its electron free-flight time τ_f, determined by the scattering rate. Surely, $\tau > \tau_f$, so that the non-linear regime that I explained here is much more important for ballistic devices than for resistive ones. However, it is relevant to conclude that this is just a physical difference, not a conceptual one.

The summary of this chapter is identical to the title of the article that I have recently published on this topic. Up to now, tunnelling electron devices have basically been engineered to work at frequencies not overcoming the inverse of the electron transit time. The behaviour of such tunnelling electron devices below the transit time can be easily

predicted with quasi-static tools like the transmission coefficient, but "There is Plenty of Room for THz Tunnelling Electron Devices Beyond the Transit Time Limit".

Chapter 12

Displacement current coefficient with transversal field

In this chapter I show the numerical simulation of the Displacement Current Coefficient $D^{(f)}(E,t)$ defined in (8.8), but modified as explained in Section 6.3.2, where the electron is interacting with an external electromagnetic field so that the whole wave function is $\Psi(x,q,t)$ with x a degree of freedom of the electron and q a degree of freedom of the (transversal part of the) electromagnetic field. The interaction is described coherently, first in a semiclassical way following (6.13), and then in a fully quantum way, following (6.25). These two analyses will be done in both DC and AC conditions, and in the latter conditions, I will show a characterization in the frequency domain, using the definition of the device admittance from (11.2), and doing an analysis similar to the one done in Chapter 11.

The results of this chapter are reproduced or adapted from:

- M. Villani, C. Destefani, X. Cartoixà, M. Feiginov, X. Oriols, "THz displacement current in nanodevices with coherent electron-photon interaction", 2022. (Submitted)

12.1 Simulation setup

I now take into consideration the RTD device whose conduction band $E_c(x)$ is shown in Fig. 12.1(a) with quantum well of 16 nm, barrier thickness 2 nm, constant electron mass $m = 0.041\, m_0$, barrier height 0.5 eV. In Fig. 12.1(b) the related transmission coefficient $T(E)$ is shown. I remind that the distance between the energy eigenstates is defined as $\mathrm{E}_G = E_1 - E_0 = 78$ meV. A photon with this energy has frequency $f_\gamma = E_G/h = 18$ THz.

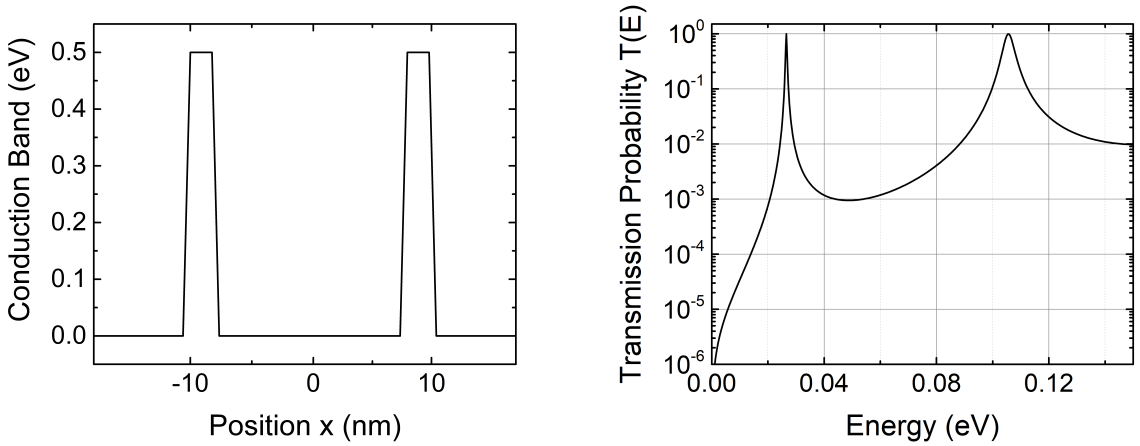

Figure 12.1: (a) Conduction band of the RTD device with quantum well of 16 nm, barrier thickness 2 nm, constant electron mass $m = 0.041\, m_0$, barrier height 0.5 eV (b) DC transmission probability in function of injection energy E, bottom energy level $E_0 = 26$ meV, second level $E_1 = 104$ meV.

12.2 Device in DC condition

In this section, the Displacement Current Coefficient $D^{(f)}(E,t)$ is estimated in DC conditions for different injection energies. The electron wavefunction is injected at different injecting times t_i and different energies E. In the semiclassical treatment of the electromagnetic field, $\psi(x,t;t_i,E)$ is the wave function of the electron, while in the quantum treatment of the electromagnetic field the electron, together with the photon, is defined as $\Psi(x,q,t;t_i,E)$.

12.2.1 Classical electromagnetic field

Here I consider the semiclassical light-matter interaction, so that the wavefunction $\psi(x,t;t_i,E)$ is guided by the Hamiltonian H_S in (6.13). As a result I have the electron described as a quantum particle, interacting with a classical electromagnetic field, with a matter-light interaction strength $\gamma_s = 1.33$ meV/nm in (6.16). Additionally, for the DC analysis, I compute the displacement current coefficient with null frequency $f = 0$ as in (8.5), with $E_c(x)$ shown in Fig. 12.1. Then the Displacement Current Coefficient $D^{(f)}(E,t)$ is estimated using (8.8) for an interaction with the classical electromagnetic field with frequency $\omega_\gamma = 2\pi Cdot18$ THz, acting in the injected wavepackets $\psi(x,t;t_i)$ with the Hamiltonian (6.13). Both results are shown in 12.2. Again to make this comparison I assume $\beta = 1\,\mathrm{s}^{-1}$ in 8.8.

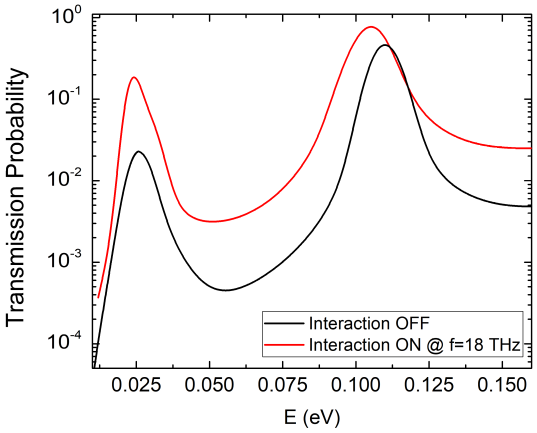

Figure 12.2: $D^{(f)}(E,t)$ coefficient estimated in DC conditions in function of the injection energy E, with inclusion of coherent semiclassical light-matter interaction.

The changes between $D^{(f=0)}(E,t)$ with and without the interaction with the classical EM filed are quite minimal. Again, the estimation of the transmission coefficient at low frequency, below 30 meV, suffers because of the use of wave packets when the mean energy E approaches the standard deviation σ_E.

12.2.2 Quantum electromagnetic field

Here I consider the quantum light-matter interaction, so that the wavefunction $\Psi(x,q,t;t_i,E)$ is guided by the equation of motion (6.25) including the electron-photon coherent interaction, with electron-photon interaction $\gamma_q = 1.33\,\text{meV/nm}$ in (6.16), a time-independent external potential $V_{ext}(x,t)$ as in (8.5), with $E_c(x)$ shown in Fig. 12.1. Then the Displacement Current Coefficient $D^{(f)}(E,t)$ is estimated using (8.15). The initial injection is $\psi_A(x,0) = \psi(x,0)$ and $\psi_B(x,t) = 0$ defined in (6.22), so that I consider an initial state related to the vacuum state of the electromagnetic field, meaning that initially the no-photon case is considered. I also add that the injected wavefunction $\psi(x,t)$, consisting of a Gaussian wavepacket of energy eigenstates, has standard deviation in energy equal to $\sigma_E = 15\,\text{meV}$, because of this reason, injection energies E below 30 meV pose numerical problems in the proper definition of an injected wavepacket. This is done for several injection energies E from 0.01 eV to 0.16 eV, and because of the DC condition, I have that $D^{f=0}(E,t) \to T(E)$. In Fig. 12.3 I show the resulting $D^{f=0}(E,t)$ for different photon frequencies ω_γ. The goal is to observe that the electron-photon interaction changes the resonant energy of the whole electron-photon structure.

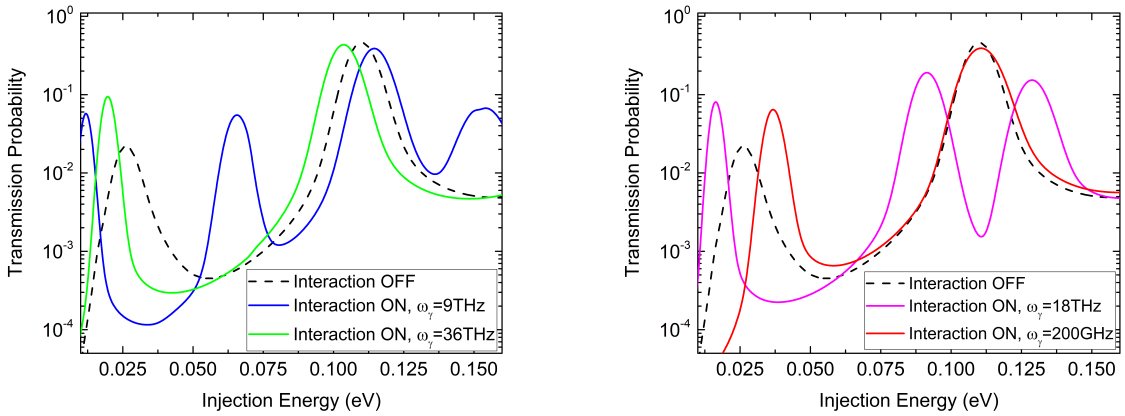

Figure 12.3: $D^{(f)}(E,t)$ coefficient estimated in DC conditions in function of the injection energy E, with inclusion of coherent electron-photon interaction, interacting with resonant (in magenta) and strongly non resonant (in red) photons, all compared with the non-interacting case (black dashed line).

Fig. 12.3(a) the non-interacting case (black dashed line) is compared with the interacting case with photon energy out of resonance with the quantum well. In particular, in the case $\omega_\gamma = 0.5E_G/\hbar = 2\pi \cdot 9\,\text{THz}$ (blue line), additional peaks appear concerning the non-interacting case. This is explained by knowing that each peak is related to an energy eigenvalue of the 2D Hamiltonian (6.17), even if in a particular case. The middle peak is created by the sum of the energies of the bottom state of the quantum well with the first excited state of the optical cavity (presence of a photon). This means that $E_p = E_0 + \omega_\gamma\hbar = E_0 + 0.5E_G/\hbar = 65\,meV$. This is the second peak from the left at $E_p = 65\,\text{meV}$ in the blue line of Fig. (12.3)(a). Again for Fig. 12.3(a), in the case $\omega_\gamma = 2E_G/\hbar = 2\pi \cdot 36\,\text{THz}$ (green line), minimal change is observed in the structure of the transmission probability, because the high energy given by the photon goes beyond the energy window represented here. However, the standard deviation of the injected wavepackets σ_E may bring some components of the energy base to change the peak of a small amount of around 10 meV.

In Fig. 12.3(b) I will first explain the behaviour of the red line, as here the photon frequency is $\omega_\gamma = 200\,\text{GHz}$, far away from the value needed for resonance. The result is a very good equivalence between the interacting model with low photon frequency $\omega_\gamma = 200\,\text{GHz}$ and $\gamma_q = 1,33\,\text{meV/nm}$ and the non-interacting model with $\gamma_q = 0$. Then the magenta line shows the $D^{(f=0)}(E,t)$ coefficient, for the case of electron-photon coherent interaction with (6.17) (like for all this subsection 12.2.2), but now interacting with a resonant photon: $\omega_\gamma = E_G/\hbar = 2\pi \cdot 18\,\text{THz}$. This result should be compared with the

one in Fig. (12.2) red line in the previous subsection, which was resonant too, but for the semiclassical interaction of (6.13). Notice that the magenta line shows a splitting of the main peak of the red and black dashed lines. This splitting is a well-known result in the photonics community [124], [125], but it is unknown in the framework of electronic engineering. I are observing a phenomenon that is typical of photonics, using as the figure of merit the total current, instead of observing photons. The splitting itself is due to the fact that the coherent electron-photon interaction creates two degenerate states, which are the ones that were schematically shown in 9.5 (b) and (c). In fact, in Fig. 12.3 inside the well at energy $E = E_1 = 104\,\text{meV}$ I have the behaviour of Fig.9.3(b), which is the Rabi oscillation between two states, these states have different energies created by quantum mechanics, which creates the splitting.

12.3 Device in AC condition

Now I take into consideration a AC condition of the potential profile $V_{ext}(x,t)$, defined in (8.5). The electron wavefunction $\psi(x,t)$ is evolved in the RTD device shown in 12.1, ad interacting with a electromagnetic field. The light-matter interaction is modelled both as semiclassical by using the Hamiltonian $\hat{H}_S$ as in (6.10), with interaction strength $\gamma_s = 1.33\,\text{meV/nm}$ and as quantum by using the Hamiltonian $\hat{H}_Q$, whose equation of motion are (6.25), with interaction strength $\gamma_q = 1.33\,\text{meV/nm}$. The high frequency analysis is done as in Chapter 11, in Fig. 11.5, where the Displacement Current Coefficient $D^{(f)}(E,t)$ is defined at three different phases θ of the input signal: $D_0^{(f)}(E,t), D_{-\pi/2}^{(f)}(E,t), D_{-\pi}^{(f)}(E,t)$. And this is linked to the estimation of the high frequency conductance as in (11.2). The input signal, as defined in (8.6), acting on the potential profile $V_{ext}(x,t)$ as in (8.5), has amplitude $V_0 = 0.01\,\text{V}$, and different frequencies f in the range $[200\,\text{GHz}, 2\,\text{THz}]$. Finally, the electron wavefunctions are always injected in the second eigenstate of the quantum well of Fig. 12.1, with injection energy $E_{inj} = E_1 = 104\,\text{meV}$, which in the model of the Displacement Current Coefficient $D^{(f)}(E,t)$ determines the energy dependence, so that in the notation I will assume $E_{inj} \equiv E$. In Fig. 12.4 I show the result of this analysis in function of different input frequencies.

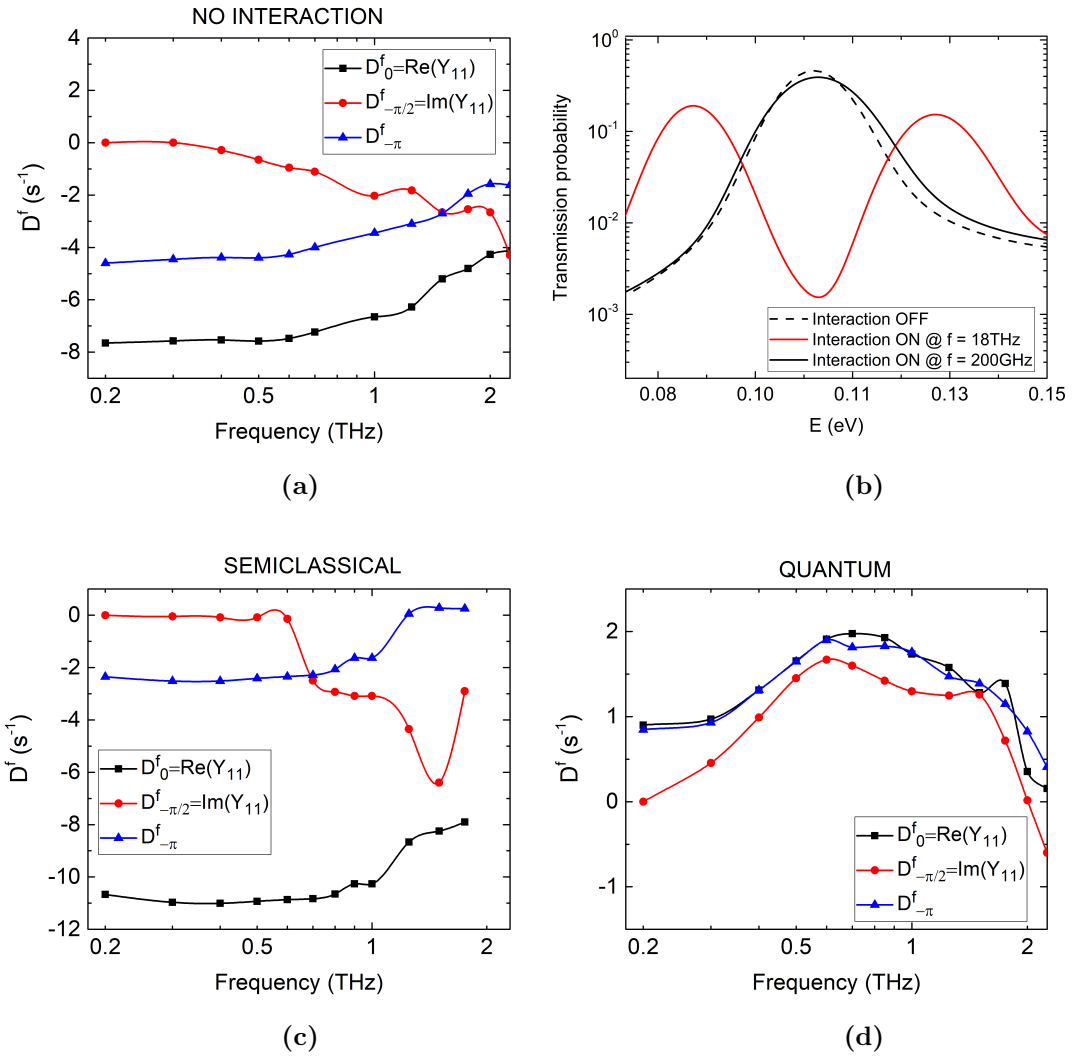

Figure 12.4: $D^{(f)}(E,t)_0, D^{(f)}(E,t)_{-\pi/2}, D^{(f)}(E,t)_{-\pi}$ coefficients estimated for electron wavefunction $\psi(x,t)$ injected at energy equal to the second eigenstate of the quantum well $E = E_1 = 104\,\text{meV}$ (a) for non-interacting case (c) for interacting case with the semiclassical light-matter model of (6.13) (d) interacting for fully quantum light-matter model of (6.17). (b) show a zoom of the result of Fig. 12.3(b) around the energy of injection of the electron wavefunction, resonant with the second eigenstate of the quantum well $E = E_1 = 104\,\text{meV}$.

The evolution of the system shown in Fig. 12.4 at low frequency $f = 200\,\text{GHz}$ is coherent with the results shown in Fig. 12.2 and 12.3(b). We already talked, in the previous Chapter 11, about the origin of the high frequency non-linearities of a ballistic device, predicted by the $D^{(f)}(E,t)$ coefficient, and observed by the inequality $D_0^{(f)}(E,t) \neq -D_{-\pi}^{(f)}(E,t)$. Now I observe how the result shown in Fig. 12.4 is coherent with the results of Fig. 12.2 and 12.3. I remind that all electrons injected in the current at any time $[t, t-\tau]$ contribute with the total current.

Low-frequency analysis For the low frequency of $f = 200\,\text{GHz}$, considered to be $f << 1/\tau$, the result of Fig. 12.4(a), showing the estimation of the Displacement Current Coefficient $D^{(f)}(E,t)$ without electron-photon interaction, with $\gamma_q = 0$, is coherent with the result of the DC estimation in the dashed line of Fig. 12.3 around the injection energy $E = 0.104\,\text{eV}$. This result is zoomed in in Fig. 12.4(b). The dashed line shows a higher transmission for the phase where the system is in resonance. This is the case of the red line in Fig.12.4(a), which shows $D^{(f)}(E,t)_{-\pi/2}$. Then, the same dashed line in in Fig.12.4(b) shows lower transmission when the phase of the input signal is at $\theta = 0$ or $\theta = -\pi$, since the system is out of resonance. In particular, the higher value of $D^{(f)}(E,t)_{-\pi}$ at $f = 200\,\text{GHz}$ is probably due to the non-symmetry of the peak of the dashed line in Fig.12.4(b), around the resonance energy $E = 104\,\text{meV}$.

A similar analysis can be done for Fig.12.4(c), for the case of interaction of the electron with the electromagnetic field modelled with a semiclassical equation of motion of Hamiltonian H_S in (6.13). The DC transmission coefficient is the red line in 12.2, and the resonant energy, linked to $D^{(f)}(E,t)_{-\pi/2}$ give a higher value of said coefficient at $f = 200\,\text{GHz}$, in comparison with the coefficient related to other two phases.

A different analysis is done for the $D^{(f)}(E,t)$ for quantum electron interaction with a quantized electromagnetic field. Here the transmission probability for the resonant case, which dictates $\omega_\gamma = E_G/\hbar$, is shown zoomed around $E = 104\,\text{meV}$ in the red line in Fig.12.4(b). The new shape of the transmission coefficient in DC for the quantum interaction case, with a local minimum of the transmission probability around the injection energy, is the reason why I see $D_0^{(f=0)}(E,t) \approx D_{-\pi}^{(f=0)}(E,t) > D_{-\pi/2}^{(f=0)}(E,t)$. In fact, the resonant case now has a disadvantage with respect to the non-resonant cases.

High-frequency analysis Beside the low-frequency analysis, I remind the reader when the frequency is $f \approx 1/\tau$, the current at time t,influenced by any potential profile at time $[t, t-\tau]$, can be affected by the memory hold by ballistic electrons. It is possible to give a explanation on the behaviour of the $D^{(f)}(E,t)_{-\pi/2}$ coefficient in Fig.12.4(a) as frequency increases. Since $D_{-\pi/2}^{(f=0)}(E,t) > D_0^{(f=0)}(E,t)$, ss the transmission probability is more and more dependent on potential profiles at time $t-\tau$ the Displacement current coefficient $D_{-\pi/2}^{(f)}(E,t)$ is going to decrease as the frequency increases, which is the behaviour of the red line of Fig.12.4(a). This is also happening for the red line of Fig.12.4(c). Additionally, deriving from the inequality $D_{-\pi/2}^{(f=0)}(E,t) > D_0^{(f=0)}(E,t)$ and $D_{-\pi/2}^{(f=0)}(E,t) > D_{-\pi}^{(f=0)}(E,t)$ for the non-interacting case, we can expect the Displacement Current Coefficient $D^{(f)}(E,t)$ related to the two other phases to increase with the fre-

quency, as the memory of the memory at time $t - \tau$ is related to higher transmission probability. This is in fact observed in the blue and black lines both in Fig.12.4(a) and (c).

Part V

Conclusions

Goal of this thesis

The THz gap, defined as the frequency between 100 GHz and 10 THz, is highly attractive to build a new generation of telecommunication technology. Currently, sources of electromagnetic radiation in this domain are inefficient and/or not portable. To tackle this lack of reliable radiation sources, in this thesis I propose a framework to extend the static view of tunnelling electron devices into higher THz frequencies. At such higher frequencies, the so-called displacement current (usually ignored in quantum electron devices) becomes more important than the traditional particle current. In addition, at such THz frequencies, the energy of the transversal electromagnetic fields interacting with the electrons needs to be quantized. With a proper modelling of such new phenomena, novel performances in THz electron devices can be predicted. The new modelling tools introduced in this thesis for tunnelling electron devices at THz frequencies pave the way for new capabilities of engineering devices in the THz gap. In particular, I specify three big conclusions.

- **Displacement Current Coefficient** For properly modelling the THz gap, the electrical current has to include two components, the particle and the displacement currents. In this thesis I introduce a new tool, called the Displacement Current Coefficient, to include the displacement current component in the description of quantum tunnelling devices at THz frequencies in a simple Landauer-like approach.

  I use the Displacement Current Coefficient to study the performance of a double barrier Resonant Tunnelling Diode (RTD) in the THz gap. First, in DC or steady-state conditions, the Displacement Current Coefficient is shown to be equivalent to the traditional Transmission coefficient of the Landauer model. This result tells us that, as expected, the displacement current component can be neglected in DC conditions. Then in AC, I estimate the small-signal conductivity of an RTD from the Displacement Current Coefficient and I show its ability to predict non-linearities at THz frequency. These non-linearities are not an unexpected result, but can now be accurately predicted and potentially engineered to improve the performance of RTD technology, or any technology based on ballistic transport, for a wide range of THz applications.

- **Quantum electron interacting with quantum electromagnetic fields** To further improve the range of applicability of the Displacement Current Coefficient,

I include a description of the transversal electromagnetic field inside the active region of the electron device. This energy of the electromagnetic field is well known to show quantization (photons) when the involved frequencies are in the THz gap. I introduce the interaction between quantum electron and quantum electromagnetic field (photon) in a time-dependent description, and I use it to estimate a new Displacement Current Coefficient. With this model, the electrical current shows new phenomena that are well-known to the photonics community, but never acknowledged in the electronic domain; for example, the splitting of the energy of the eigenstates of the quantum well of the electron device due to coherent electron-photon interaction.

Thirty years ago a revolution appears in the electron device industry when the classical view of modelling electrons were adapted to a new quantum one. The results of this thesis suggest that, now, the classical view of modelling electromagnetic fields in high-frequency electron devices needs to be adapted to a quantum view.

- **Orthodox Macroscopic or Bohmian microscopic view of electron devices?** It seems quite strange that an engineer like me wants to say something about the foundations of quantum mechanics. In general, the role of engineers is just using mature physical theories to provide practical applications to improve our society. However, is the quantum theory a mature one? On one side, it was developed more than a century ago, so it seems old enough to become a mature theory. On the other hand, philosophers and physicists are still under a lively debate on fundamental topics, as for example what is the role of the wavefunction, is it a real object of just a probability. So, it seems that quantum mechanics is not as mature as engineers think it is. This is in fact ever more evident when photonics and electronics meet. In this regard, the present thesis has been inspired and developed under a non-orthodox understanding of quantum phenomena: the Bohmian quantum mechanics. In this theory, electrons are particles with determined positions and electromagnetic fields are just fields with determined properties. Such definition of electrons and electromagnetic fields may seem naive, but it is a revolutionary definition from the point of view of orthodox quantum mechanics. The orthodox theory says that electrons have no positions (unless one measures the position), and electrons *are* probability distributions, without any determined value. The same happens to the quantum electromagnetic fields. However I ask ourselves is it if needed to go to such lengths, to get to a description so far away to how I things at the world.

The answer is no, the Bohmian mechanics shows a path to understand the most complex phenomena with a simple and natural language of unobserved deterministic trajectories. This can fro example describe the electron interacting with a quantized electromagnetic field, studied in this thesis.

We show, in a practical example, the computational advantages of the Bohmian theory in front of the orthodox one. The modelling of electron-photon collision through orthodox tools, like the Density Matrix or the Wigner function, has many problems to ensure complete positivity and energy conservation. This is because such orthodox tools have no microscopic information about the state of a single-particle (its energy, momentum), but only macroscopic information through the wave function on all electrons together. In general (non-Markovian) scenarios, tools of orthodox mechanics forbid the use of single-particle pure states to describe the open system. On the contrary, in this thesis, such collisions can be described with the use of a single-particle pure state through the rigorous use of the Bohmian conditional wave function. The orthodox theory has renounced to a microscopic description of the properties of the electron in the active region, while the Bohmian theory provides such a microscopic view!

The overall summary of this thesis is that "There is Plenty of Room for THz Tunneling Electron Devices Beyond the Transit Time Limit". The proper engineering of the displacement current and a coherent treatment of the interaction of electrons and electromagnetic fields, brings the performance of electronic devices closer to the worlds of photonics, opening many new unexplored possibilities to close the mentioned THz gap.

Part VI

Appendices

Appendix A

Time-dependent circuit-based boundary conditions for the active region

In all the simulation done in the main text, I have assumed that the external applied voltages are directly affecting the active region, which I have simulated with great detail. But, in a real device, the external applied bias is applied very far from the active region. There are, at least, cables between the external bias and the active region. In some cases, the active region is not connected to cables only, but to a type of resonant circuit. This setup is typical of a THz oscillator used as a source for THz radiation, as explained in Chapter 2.

In this appendix, I explain how to eliminate the previous assumption (the external bias is applied directly to the active region) by implementing a self-consistent boundary conditions on the active region where the external elements (cables of resonant circuit are also simulated). Certainly, I cannot simulate such external elements with the same microscopic tools that I are doing for the active region. In a type of multiscale simulation scheme, I will use a circuit model for this external parts and still the Bohmian trajectories approach for the active region of the RTD.

The basic idea the self-consistent simulator is resumed in the scheme of Fig. A.1. Now I will describe it for the case of a simple external resonant circuit, modelling an antenna coupled to what I call the *quantum simulation box*, modelling the active region of an electron device. The quantum simulation box is characterized, besides other things, by the instantaneous potential profile $U_{ext}(x,t)$. In fact, the electron wavefunction $\psi(x,t)$ injected inside the system is evolved with the Hamiltonians described in the main text.

For example, I assume:

$$H_0 = \frac{\hbar^2}{2m}\frac{\partial^2}{\partial x^2} + U_{ext}(x,t). \tag{A.1}$$

and the ability to provide an external total current in the borders of the active region has been explicitly explained in the main text of this thesis.

The quantum simulation box is interaction, as it will be explained, with an arbitrary circuit that has an admittance $Y_c(V,f)$. Notice that in principle, the right and left circuits can be different and they can have their own external batteries. For simplicity, I consider the simple circuit shown in Fig. A.1.

At each time t, after giving the proper boundary conditions for the potentials at the borders of the active region, I get a value of the current $I_0(t)$ for the microscopic simulation of electrons in the RTD. This value of the current will give a potential at each border of the active region when coupled to the circuits given by of $V_{in}(t) = I_0(t)/Y_c(V,f)$. This computed value of $V_{in}(t)$, at each time, is the input of the quantum simulation box. In other words $V_{in}(t)$ is the potential applied by the external circuit (with its external batteries).

Here I show a schematic representation of the two simulated domains:

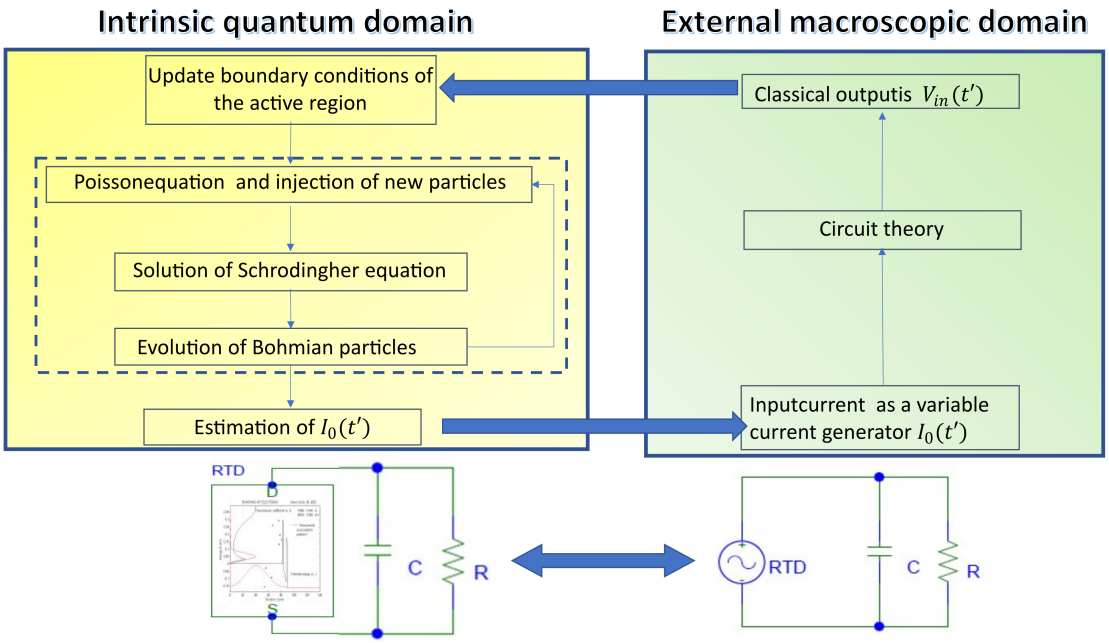

Figure A.1: Schematic representation of the two self-consistent loops implemented in this algorithm, the loo (A), evolving the quantum system, is in the dashed rectangle, while the loop (B) the self-consistent evolution of the classical and quantum system.

Here I give a step by step explanation about how the two systems interact in a self-consistent way.

(1) The quantum system in equilibrium, with potential energy $U_{ext}(x,t) = E_c(x)$, sees the injection of wavepackets following the Fermi distribution function;

(2) The quantum system self-consistently solves the Poisson and Schrödinger equations for injected electrons, so that the potential energy $U_{ext}(x,t) = E_c(x) + U(x,t)$ contains the Coulomb interaction. The potential profile will affect the evolution of N single-particle wavepacket through (A.1). Additionally, the new potential profile affects the injection rate and energy of new electrons.

(3) After several repetitions of point 2, at time t' the total current from the active region is estimated using Ramo-Shockley Theorem of (5.27) and its value, is the input I_0 of the external classical circuit.

(4) The external circuit is excited by the total current I_0, and returns the resulting potential falling on the drain and source contacts with respect to the ground, which is V_{in}.

(5) The potential V_{in} affects the potential profile of the quantum simulation box, so that $U_{ext}(x,t') = E_c(x) + U'(x,t') + e \cdot V_{in}(x,t')\frac{a-x}{L}$, at the same time t'.

(6) The new potential profile is used to estimate the injection probabilities of electron wavefunctions $\psi(x,t)$ at time t', which will be different from the one in step 1. This step restarts the loop.

We underline that only step (4) is spent in the classical domain of the external circuit, however, this influences the quantum domain in two different ways: (i) by changing the potential profile U_{ext}, and through (A.1) affecting electron dynamics, and (ii) by changing the injection of new electrons inside the simulation box.

The time scale of the two simulated domains There are two time-dependent simulations involved in this scheme:

- (A) The time dependent quantum simulation in the active region in terms of time-dependent trajectories. It has its own time-step of the simulation.
- (B) The time dependent simulation of the circuit is done by solving Kirchhoff equations.

While loop (A) has a time periodicity dictated by the sampling frequency of the solution of the Schroedinger equation, loop (B) is related to a proper sampling of the

time-dependent output current of the external circuit and its physical requirements are a proper estimation of the potential applied to V_{in} given the conductivity $Y_c(V, f)$ of the circuit. As such, to minimize the computational cost, the self-consistency of the loop (B) is usually solved after many self-consistent solutions of the (A) loops. So that the classical system interacts with the quantum active region with relatively large steps. As an example, loop (B) can be repeated each 0.1 ps, while loop (A) is repeated each 1 fs. This algorithm has been implemented in the time-dependent fully-quantum BITTLES simulator [110].

Appendix B

Bohmian treatment of the guiding wavefunction theory

In this appendix, I report a reformulation of the work of de Broglie done by Bohm in 19352 [63, 64]. The guiding wavefunction can be written in polar form, by defining $\Psi(\vec{x},t) = R(\vec{x},t)e^{iS(\vec{x},t)/\hbar}$, where if $\Psi(\vec{x},t)$ is complex, $R(\vec{x},t)$ and $S(\vec{x},t)$ are real values. Substituting the polar form in the Schrödinger equation, then the imaginary part of the new Schrödinger equation will be equal to zero and equivalent to the continuity equation (3.7):

$$\frac{\partial R^2(\vec{x},t)}{\partial t} + \sum_{i=1}^{N} \frac{\partial}{\partial x_i}\left(\frac{1}{m}\frac{\partial S(\vec{x},t)}{\partial x_i}R^2(\vec{x},t)\right) = 0. \tag{B.1}$$

On the other hand, the real part is:

$$\frac{\partial S(\vec{x},t)}{\partial t} + \sum_{i=1}^{N} \frac{1}{2m}\left(\frac{\partial S(\vec{x},t)}{\partial x_i}\right)^2 + U(\vec{x},t) - \sum_{i=1}^{N} \frac{1}{2m}\frac{\partial^2 R(\vec{x},t)}{\partial x_i} = 0, \tag{B.2}$$

which is the quantum Hamilton-Jacobi equation, and while all the first three terms compose the classical Hamilton-Jacobi equation, the fourth term on the left side is the quantum potential $\vec{Q}(\vec{x},t)$ with no classical counterpart. This is why the above equation is named quantum Hamilton-Jacobi equation.

Since the kinetic energy term related to the single particle from (B.2) has the shape:

$$K_i(\vec{x},t) = \frac{1}{2m}\left(\frac{\partial S(\vec{x},t)}{\partial x_i}\right)^2, \tag{B.3}$$

then I can easily deduce and expression for the Bohmian velocity of the i-th particle as:

$$v_i(\vec{x},t) = \frac{1}{m}\frac{\partial S(\vec{x},t)}{\partial x_i}. \tag{B.4}$$

This expression of the velocity is exactly the same velocity given by (B.4) in the main text, but written in a polar form. The way of deducing the Bohmian expression in the text has some advantages in comparison with the one used here. When it is difficult to reach a quantum Hamilton-Jacobi equation I can always look for the development done in the main text.

Appendix C

Equation of motion of the Bohmian conditional Wavefunction

In this appendix, I show how the equation of motion of the Bohmian Conditional Wavefunction. I consider a N particle system described in the Bohmian theory in N degrees of freedom by $\Psi(x_1, x_2, ..., x_N, t)$ and trajectories $\{x_1[t], x_2[t], ..., x_N[t]\}$. As in the main text, I define $\vec{x}_b = \{x_1[t], x_2[t], ..., x_{a-1}[t], x_{a+1}[t], ..., x_N[t]\}$ and I look for an equation of motion for the Bohmian Conditional wave function which will guide trajectory x_a.

C.1 Velocity of Bohmian conditional wavefunction

It can be demonstrated that the trajectory of particle a can be alternatively simulated from the many-body wavefunction $\Psi(x_a, \vec{x}_b, t)$, and from the Bohmian Conditional Wavefunction $\psi(x_a, t) \equiv \Psi(x_a, \vec{x}_b[t], t)$. As done in Appendix B, I write the Bohmian Conditional Wavefunction in polar form $\psi(x_a, t) = r_a(x_a, t)e^{is_a(x_a,t)/\hbar}$, where $s_a(x_a, t) \equiv S(x_a, \vec{x}_b, t)$ and $r_a(x_a, t) \equiv R(x_a, \vec{x}_b, t)$, and then I define the Bohmian velocity of the Bohmian Conditional Wavefunction as the spatial derivative of $S(x_a, \vec{x}_b, t)$ along the x_a degree of freedom, as suggested by (B.4),

$$\begin{aligned} v_a[t] &= \frac{1}{m}\frac{\partial S(x_a, \vec{x}_b, t)}{\partial x_a}\bigg|_{\vec{x}_b=\vec{x}_b[t]} \\ &= \frac{1}{m}\frac{\partial s_a(x_a, \vec{x}_b, t)}{\partial x_a}\bigg|_{\vec{x}_b=\vec{x}_b[t]}. \end{aligned} \tag{C.1}$$

Where the condition $\vec{x}_b = \vec{x}_b[t]$ means that I fixed the position of all the other particles in the time t, which are used as parameters. The definition of the positions as parameters is the key of the definition (4.12).

At the end of the day, the Bohmian velocity $v_a[t]$ of the a-th particle will hold information about the position of all the $N-1$ particles as indicated in the main text.

C.2 Equation of motion

To look for the equation of motion of the Bohmian Conditional Wavefunction, I know that for any single-valued function $\psi_a(\vec{x}_a,t)$ that can be solved from a Schrödinger equation, there is a potential $\tilde{U}(x_a,t)$ that can be defined in the x_a degree of freedom as [109]:

$$\tilde{U}(x_a,t) = \left.\frac{i\hbar\frac{\partial\psi(x_a,t)}{\partial t}+\frac{\hbar}{2m}\frac{\partial^2\psi(x_a,t)}{\partial x_a^2}}{\psi(x_a,t)}\right|_{\vec{x}_b=\vec{x}_b[t]}. \tag{C.2}$$

The imaginary part of this potential will be equal to zero if $\psi_a(\vec{x}_a,t)$ conserves the norm, so that, substituting the polar form, I write the imaginary part of the potential $\tilde{U}(x_a,t)$ as:

$$\mathbb{I}\mathrm{m}[\tilde{U}(x_a,t)] = \frac{\partial r^2(\vec{x},t)}{\partial t}+\sum_{i=1}^{N}\frac{\partial}{\partial x_i}\left(\frac{1}{m_a}\frac{\partial s(\vec{x},t)}{\partial x_i}r^2(\vec{x},t)\right)=0, \tag{C.3}$$

while the real part is:

$$\mathbb{R}\mathrm{e}[\tilde{U}(x_a,t)] = \frac{\partial s(\vec{x},t)}{\partial t}+\sum_{i=1}^{N}\frac{1}{2m_a}\left(\frac{\partial s(\vec{x},t)}{\partial x_i}\right)^2+U(\vec{x},t)-\sum_{i=1}^{N}\frac{1}{2m}\frac{\partial^2 r(\vec{x},t)}{\partial x_i}=0. \tag{C.4}$$

Most importantly, now I would like to link the evolution of $\psi(x_a,t)$ with the evolution of the conditional wavefunction in the shape $\Psi(x_a,\vec{x}_b[t],t) = R(x_a,\vec{x}_b[t],t)e^{iS(x_a,\vec{x}_b[t],t)}$, meaning that I would like to make explicit the dependence on all the other $N-1$ trajectories. To do so, I have to take into account all the conditional positions of the other particles $\vec{x}_b[t]$, so that, I look for the derivatives in (C.3) and (C.4), in function of $R(x_a,\vec{x}_b[t],t)$ and $S(x_a,\vec{x}_b[t],t)$:

$$\begin{aligned}\frac{\partial S(x_a,\vec{x}_b[t],t)}{\partial t} &= \left(\frac{\partial S(x_a,\vec{x}_b[t],t)}{\partial t}\right)\Big|_{\vec{x}_b=\vec{x}_b[t]}+\sum_{i=1,i\neq a}^{N}\frac{\partial S(x_a,\vec{x}_b[t],t)}{\partial x_i}v_i(\vec{x}[t],t)\\ &= \left(-\frac{1}{2m}\left(\frac{\partial S(x_a,\vec{x}_b[t],t)}{\partial x_a}\right)^2-U(x_a,\vec{x}_b[t],t)-Q_a(x_a,\vec{x}_b[t],t)\right)\Big|_{\vec{x}_b=\vec{x}_b[t]}\\ &+ \sum_{i=1,i\neq a}^{N}\frac{\partial S(x_a,\vec{x}_b[t],t)}{\partial x_i}v_i(\vec{x}[t],t),\end{aligned} \tag{C.5}$$

where I substituted the Hamilton-Jacobi of $\Psi(\vec{x},t)$ in polar form (B.2), and $U(x_a,\vec{x}_b[t],t)$ is the potential and $Q_a(x_a,\vec{x}_b[t],t)$ the quantum potential. And I can write:

$$\begin{aligned}\frac{\partial R^2(x_a,\vec{x}_b[t],t)}{\partial t} &= \left(\frac{\partial R^2(x_a,\vec{x}_b[t],t)}{\partial t}\right)\Big|_{\vec{x}_b=\vec{x}_b[t]} + \sum_{i=1,i\neq a}^{N}\frac{\partial R^2(x_a,\vec{x}_b[t],t)}{\partial x_i}v_i(\vec{x}[t],t)\\ &= \left(-\sum_{k=1}^{N}\frac{\partial}{\partial x_i}\left(\frac{1}{m}\frac{\partial S}{\partial x_i}R^2(x_a,\vec{x}_b[t],t)\right)\right)\Big|_{\vec{x}_b=\vec{x}_b[t]}\\ &+ \sum_{i=1,i\neq a}^{N}\frac{\partial R^2(x_a,\vec{x}_b[t],t)}{\partial x_i}v_i(\vec{x}[t],t), \end{aligned} \tag{C.6}$$

where I used (B.1). Many of the terms in (C.5) and (C.6) can be seen as potential terms that include the effect of all particles in the a-th trajectory. Now I divide the total Coulomb potential in:

$$U(x_a,\vec{x}_b[t],t) = U_a(x_a,\vec{x}_b[t],t) + U_b(\vec{x}_b[t],t), \tag{C.7}$$

where $U_a(x_a,\vec{x}_b[t],t)$ is the interaction with a potential external to the electron system, like the conduction band, and $U_b(\vec{x}_b[t],t)$ is the electron-electron Coulomb interaction, acting on the a-th particles, taking all the other trajectories as parameters ($\vec{x}_b = \vec{x}_b[t]$). and I define:

$$\begin{aligned} G_a(x_a,\vec{x}_b[t],t) &= U_b(x_a,\vec{x}_b[t],t) +\\ &+ \sum_{i=1,i\neq a}^{N}\left(\frac{1}{m}\left(\frac{\partial S(x_a,\vec{x}_b[t],t)}{\partial x_i}\right)^2 + Q_i(x_a,\vec{x}_b[t],t)\right)\\ &- \sum_{i=1,i\neq a}^{N}\left(\frac{\partial S(x_a,\vec{x}_b[t],t)}{\partial x_i}v_i(x_a,\vec{x}_b[t],t)\right), \end{aligned} \tag{C.8}$$

$$\begin{aligned} J_a(x_a,\vec{x}_b[t],t) &= \sum_{i=1,i\neq a}^{N}\frac{\hbar}{2R^2(x_a,\vec{x}_b[t],t)}\cdot\\ &\cdot\left(\frac{\partial R^2(x_a,\vec{x}_b[t],t)}{\partial x_i}v_i(\vec{x}[t],t) - \frac{\partial}{\partial x_i}\left(\frac{R^2(x_a,\vec{x}_b[t],t)}{m}\frac{\partial S(x_a,\vec{x}_b[t],t)}{\partial x_i}\right)\right). \end{aligned} \tag{C.9}$$

So that I rewrite (C.2) for the Bohmian Conditional Wavefunction as a sum of potentials given by different interactions between electrons:

$$i\hbar\frac{\partial\psi_a(x_a,t)}{\partial t} = \left(-\frac{\hbar}{2m}\frac{\partial^2}{\partial x^2} + U_a(x_a,\vec{x}_b[t],t) + G_a(\vec{x}[t],t) + iJ_a(\vec{x}[t],t)\right)\psi_a(x_a,t). \tag{C.10}$$

Notice that terms U_a, G_a, J_a, acting as potentials on the Bohmian Conditional Wavefunction $\phi(x_a,t)$, depended on the particular configuration of all trajectories $\vec{x}$. However

this dependence is not known for all the terms, in particular, $U(\vec{x}, t)$ is determined by the Poisson law, while terms $G_a(x_a, \vec{x}_b[t], t)$ and $J_a(x_a, \vec{x}_b[t], t)$ can be shown to be related to the exchange energy, but their dependence on the position configuration $\vec{x}$ is not straightforward.

Appendix D

Non-coherent Wigner-Boltzmann collision in flat potential

In this appendix, I show that the momentum exchange model is not problematic for the Wigner function evolved with flat potential condition, $U_{ext}(x,t) = 0$. In the following Fig. D.1, in flat potential conditions, the momentum exchange (non-coherent) model of (7.4) is used to simulate the absorption of a photon in one electron described by the Wigner function $f_W(x,k,t)$. I see from Fig. D.1(a) to (c) that the Gaussian wavepacket absorbs a photon with momentum $p_\gamma = p(t_s + \tau_s) - p(t_s) = \frac{\sqrt{2mE_1}}{\hbar} - \frac{\sqrt{2mE_0}}{\hbar}$ while it evolves in space, where E_1 and E_0 are two arbitrary energies. The change in momentum is clearly visible from Fig. D.1(b) to (d) in the projection over the momentum axis, and in the estimated energies. The same result is obtained when the energy exchange (not shown) model is used. In Fig. D.2 (a) and (c) the same Gaussian wavepacket is shown to emit a photon, and the same equivalence between momentum exchange (shown) and in energy exchange (not shown) algorithms are verified.

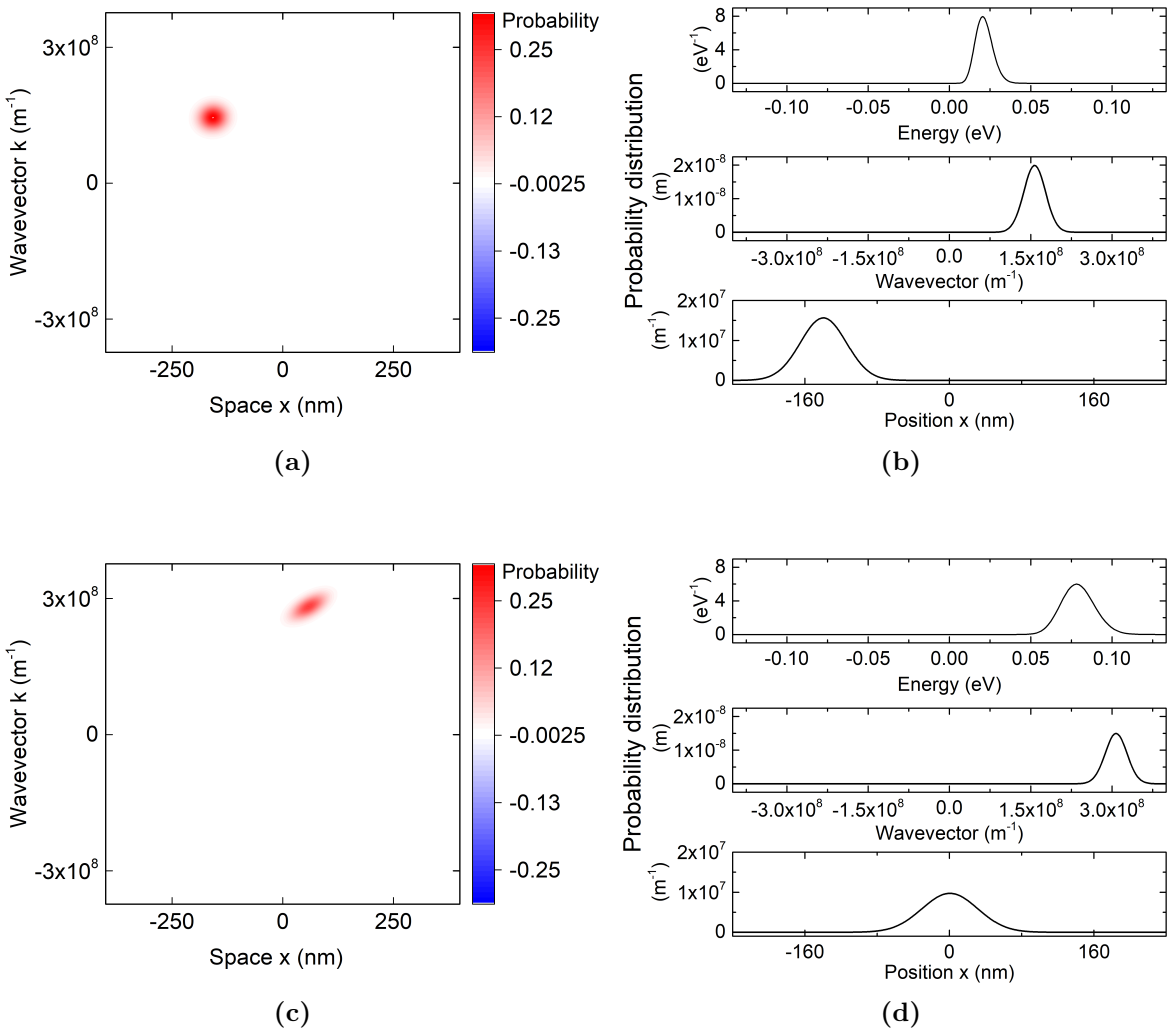

Figure D.1: Wigner function of a single-electron undergoing photon absorption in free space using the algorithm of (7.4) and alternatively (7.9): (a) before the scattering event $t = t_s$ (c) after the scattering event $t = t_s + \tau_s$ with the energy exchange and the momentum exchange algorithms, which are equivalent in free space conditions. In (b) and (d) is it possible to see projections of the Wigner function along the energy (top), momentum (middle) and position (bottom) axis respectively related to figures (a) and (c).

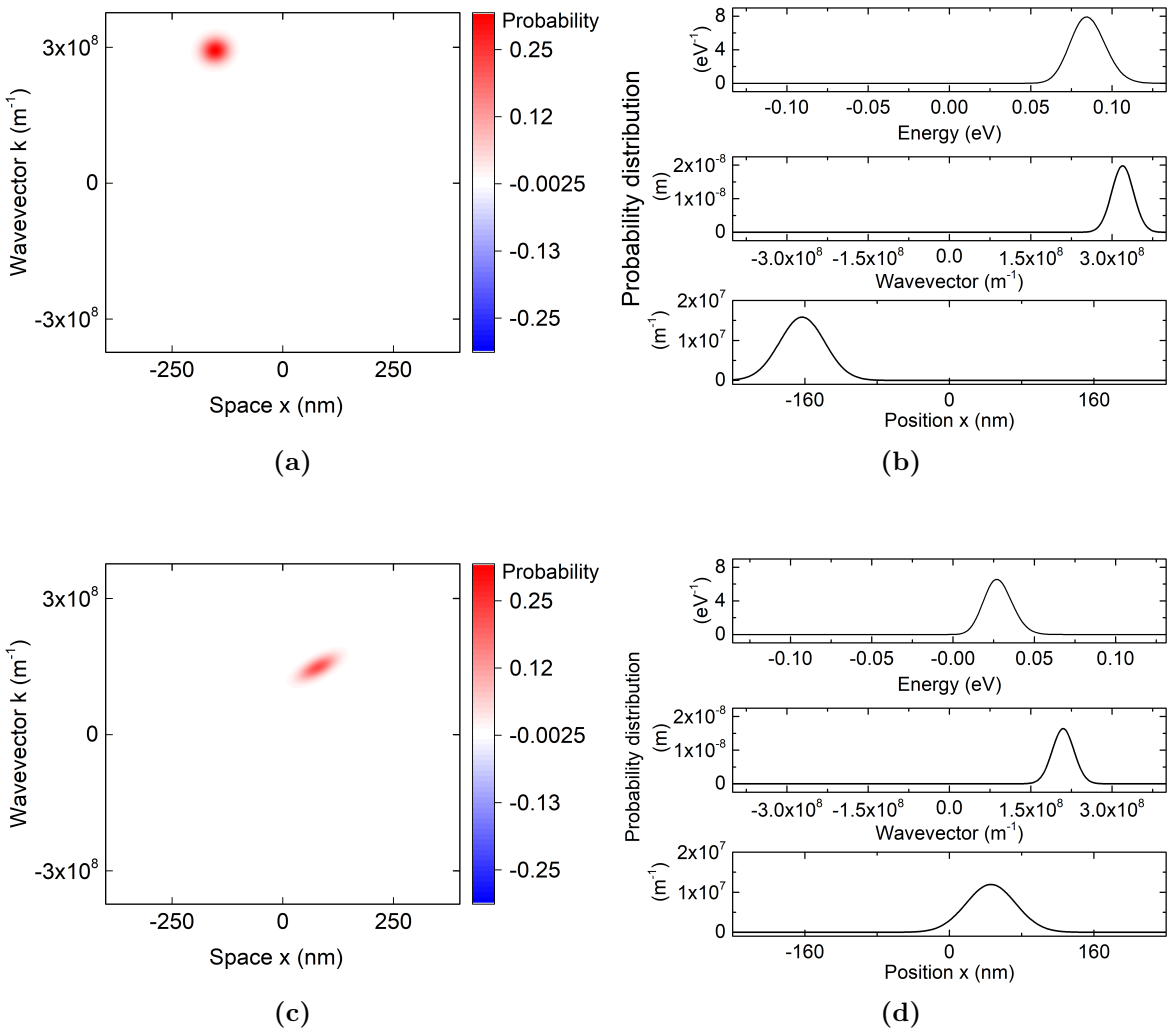

Figure D.2: Wigner function of a single-electron undergoing photon emission in free space(a) before the scattering event $t = t_s$ (c) after the scattering event $t = t_s + \tau_s$ with the energy exchange and the momentum exchange algorithms, which are equivalent in free space conditions. In (b) and (d) is it possible to see projections of the Wigner function along the energy (top), momentum (middle) and position (bottom) axis respectively related to figures (a) and (c).

Bibliography

[1] W.-G. Yeo, N. K. Nahar, R. Lee, and J. L. Volakis, "New frontiers for commercial applications of terahertz," *Proceedings of the 2011 IEEE National Aerospace and Electronics Conference (NAECON)*, pp. 5–8, 2011.

[2] S. Sung, E. R. Brown, W. S. Grundfest, Z. D. Taylor, S. Selvin, N. Bajwa, S. Chantra, B. Nowroozi, J. Garritano, and J. e. a. Goell, "THz imaging system for in vivo human cornea," *IEEE Transactions on Terahertz Science and Technology*, vol. 8, no. 1, p. 27–37, 2018.

[3] Z. D. Taylor, S. Sung, J. Garritano, N. Bajwa, B. Nowroozi, and W. Grundfest, "THz medical imaging: Current status and future outlooks," *2014 United States National Committee of URSI National Radio Science Meeting (USNC-URSI NRSM)*, pp. 1–1, 2014.

[4] K. Humphreys, J. Loughran, M. Gradziel, W. Lanigan, T. Ward, J. Murphy, and C. O'Sullivan, "Medical applications of Terahertz Imaging: A review of current technology and potential applications in biomedical engineering," *The 26th Annual International Conference of the IEEE Engineering in Medicine and Biology Society*, pp. 1302–1305, 2004.

[5] J.-I. Nishizawa, T. Sasaki, K. Suto, T. Yamada, T. Tanabe, T. Tanno, T. Sawai, and Y. Miura, "THz imaging of nucleobases and cancerous tissue using a gap THz-wave generator," *Optics Communications*, vol. 244, no. 1-6, p. 469–474, 2005.

[6] W.-G. Yeo, O. Gurel, C. L. Hitchcock, S. Park, K. Sertel, and N. K. Nahar, "Evaluation of cancer tissue morphology via THZ spectroscopic imaging: Human Lung and small intestine malignancies," *Infrared Physics and Technology*, vol. 97, p. 411–416, 2019.

[7] H.-J. Song, "Terahertz wireless communications: Recent developments including a prototype system for short-range data downloading," *IEEE Microwave Magazine*, vol. 22, no. 5, p. 88–99, 2021.

[8] H. Tataria, M. Shafi, A. F. Molisch, M. Dohler, H. Sjoland, and F. Tufvesson, "6G wireless systems: Vision, requirements, challenges, insights, and opportunities," *Proceedings of the IEEE*, vol. 109, no. 7, p. 1166–1199, 2021.

[9] S. Koenig, D. Lopez-Diaz, J. Antes, F. Boes, R. Henneberger, A. Leuther, A. Tessmann, R. Schmogrow, D. Hillerkuss, R. Palmer, and et al., "Wireless sub-THz communication system with high data rate," *Nature Photonics*, vol. 7, no. 12, p. 977–981, 2013.

[10] S. Jia, X. Yu, H. Hu, J. Yu, T. Morioka, P. U. Jepsen, and L. K. Oxenlowe, "120 GB/s multi-channel THz wireless transmission and THz receiver performance analysis," *IEEE Photonics Technology Letters*, vol. 29, no. 3, p. 310–313, 2017.

[11] M. Asada and S. Suzuki, "Room-temperature oscillation of resonant tunneling diodes close to 2THz and their functions for various application," *Journal of Infrared, Millimeter, and Terahertz Waves*, vol. 37, no. 12, p. 1185–1198, 2016.

[12] M. Feiginov, H. Kanaya, S. Suzuki, and M. Asada, "Operation of resonant-tunneling diodes with strong back injection from the collector at frequencies up to 1.46 THz," *Applied Physics Letters*, vol. 104, no. 24, p. 243509, 2014.

[13] R. A. Lewis, "A review of terahertz sources," *Journal of Physics D: Applied Physics*, vol. 47, no. 37, p. 374001, 2014.

[14] S. Preu, G. H. Döhler, S. Malzer, A. Stöhr, V. Rymanov, T. Göbel, E. R. Brown, M. Feiginov, R. Gonzalo, M. Beruete, and et al., "Principles of THz Generation," *Semiconductor Terahertz Technology: Devices and Systems at Room Temperature Operation*, p. 3–68, 2015.

[15] T. Nagatsuma, G. Ducournau, and C. C. Renaud, "Advances in terahertz communications accelerated by Photonics," *Nature Photonics*, vol. 10, no. 6, p. 371–379, 2016.

[16] G. Dodel, "On the history of far-infrared (FIR) gas lasers: Thirty-five years of research and application," *Infrared Physics and Technology*, vol. 40, no. 3, p. 127–139, 1999.

[17] E. Bründermann, A. M. Linhart, L. Reichertz, H. P. Röser, O. D. Dubon, W. L. Hansen, G. Sirmain, and E. E. Haller, "Double acceptor doped Ge: A new medium for inter-valence-band lasers," *Applied Physics Letters*, vol. 68, no. 22, p. 3075–3077, 1996.

[18] J. N. Hovenier, M. C. Diez, T. O. Klaassen, W. T. Wenckebach, A. V. Muravjov, S. G. Pavlov, and V. N. Shastin, "The p-Ge terahertz laser-properties under pulsed- and mode-locked operation," *IEEE Transactions on Microwave Theory and Techniques*, vol. 48, no. 4, p. 670–676, 2000.

[19] K. Sengupta, T. Nagatsuma, and D. M. Mittleman, "Terahertz integrated electronic and hybrid electronic–Photonic Systems," *Nature Electronics*, vol. 1, no. 12, p. 622–635, 2018.

[20] T. Nagatsuma, K. Oogimoto, Y. Yasuda, Y. Fujita, Y. Inubushi, S. Hisatake, A. M. Agoues, and G. C. Lopez, "300-GHz-band wireless transmission at 50 gbit/s over 100 meters," *2016 41st International Conference on Infrared, Millimeter, and Terahertz waves (IRMMW-THz)*, pp. 1–2, 2016.

[21] D. Cimbri, J. Wang, A. Al-Khalidi, and E. Wasige, "Resonant tunnelling diodes high-speed terahertz wireless communications - A Review," *IEEE Transactions on Terahertz Science and Technology*, p. 1–1, 2022.

[22] M. Oehme, O. Kirfel, J. Werner, M. Kaschel, E. Kasper, and J. Schulze, "Antimony doped si esaki diodes without post growth annealing," *Thin Solid Films*, vol. 518, no. 6, 2010.

[23] R. Duschl, O. Schmidt, G. Reitemann, E. Kasper, and K. Eberl, "High room temperature peak-to-valley current ratio in si based esaki diodes," *Electronics Letters*, vol. 35, no. 13, p. 1111, 1999.

[24] V. Gružinskis, J. H. Zhao, P. Shiktorov, and E. Starikov, "Gunn Effect and THz Frequency Power Generation in n - n - n GaN Structures," *Materials Science Forum*, vol. 297-298, p. 341–344, 1998.

[25] S. Pérez, T. González, D. Pardo, and J. Mateos, "Terahertz Gunn-like oscillations in InGaAs/InAlAs planar diodes," *Journal of Applied Physics*, vol. 103, no. 9, p. 094516, 2008.

[26] A. Khalid, G. M. Dunn, R. F. Macpherson, S. Thoms, D. Macintyre, C. Li, M. J. Steer, V. Papageorgiou, I. G. Thayne, M. Kuball, and et al., "Terahertz oscillations in an $In_{0.53}Ga_{0.47}As$ submicron planar Gunn diode," *Journal of Applied Physics*, vol. 115, no. 11, p. 114502, 2014.

[27] U. Mishra, P. Parikh, and Y.-F. Wu, "AlGaN/GaN HEMTs-an overview of device operation and applications," *Proceedings of IEEE*, vol. 115, no. 90, 6, pp. 1022 – 1031, 2002.

[28] M. Büttiker and R. Landauer, "Traversal time for tunneling," *Physical Review Letters*, vol. 49, no. 23, p. 1739–1742, 1982.

[29] R. Landauer, "Barrier traversal time," *Nature*, vol. 341, no. 6243, p. 567–568, 1989.

[30] R. Tsu and L. Esaki, "Tunneling in a finite superlattice," *Applied Physics Letters*, vol. 22, no. 11, p. 562–564, 1973.

[31] L. L. Chang, L. Esaki, and R. Tsu, "Resonant tunneling in semiconductor double barriers," *Applied Physics Letters*, vol. 24, no. 12, p. 593–595, 1974.

[32] M. Feiginov, C. Sydlo, O. Cojocari, and P. Meissner, "Operation of resonant-tunnelling oscillators beyond tunnel lifetime limit," *EPL (Europhysics Letters)*, vol. 94, no. 4, p. 48007, 2011.

[33] S. Luryi, "Frequency limit of double-barrier resonant-tunneling oscillators," *Applied Physics Letters*, vol. 47, no. 5, p. 490–492, 1985.

[34] H. Morkoç, J. Chen, U. K. Reddy, T. Henderson, and S. Luryi, "Observation of a negative differential resistance due to tunneling through a single barrier into a Quantum Well," *Applied Physics Letters*, vol. 49, no. 2, p. 70–72, 1986.

[35] T. Weil and B. Vinter, "Equivalence between resonant tunneling and sequential tunneling in double-barrier diodes," *Applied Physics Letters*, vol. 50, no. 18, p. 1281–1283, 1987.

[36] T. Nakagawa, H. Imamoto, T. Kojima, and K. Ohta, "Observation of resonant tunneling in AlGaAs/GaAs triple barrier diodes," *Applied Physics Letters*, vol. 49, no. 2, p. 73–75, 1986.

[37] M. Nakamura, S. Takahagi, M. Saito, and M. Suhara, "Analysis of a monolithic integrated rectenna by using an InGaAs/InAlAs triple-barrier resonant tunneling diode for zero bias detection of submilimeter-waves," *Physica Status Solidi C*, vol. 9, no. 2, p. 377–380, 2011.

[38] M. Feiginov, "Frequency limitations of resonant-tunnelling diodes in sub-THz and THz oscillators and detectors," *Journal of Infrared, Millimeter, and Terahertz Waves*, vol. 40, no. 4, p. 365–394, 2019.

[39] M. Asada, S. Suzuki, and N. Kishimoto, "Resonant tunneling diodes for sub-terahertz and terahertz oscillators," *Japanese Journal of Applied Physics*, vol. 47, no. 6, p. 4375–4384, 2008.

[40] E. R. Brown, J. R. Söderström, C. D. Parker, L. J. Mahoney, K. M. Molvar, and T. C. Mcgill, "Oscillations up to 712 GHz in InAs/AlSb resonant-tunneling diodes," *Applied Physics Letters*, vol. 58, no. 20, p. 2291–2293, 1991.

[41] E. R. Brown, T. C. L. G. Sollner, C. D. Parker, W. D. Goodhue, and C. L. Chen, "Oscillations up to 420 GHz in GaAs/AlAs resonant tunneling diodes," *Applied Physics Letters*, vol. 55, no. 17, pp. 1777–1779, 1989.

[42] S. Suzuki, M. Asada, A. Teranishi, H. Sugiyama, and H. Yokoyama, "Fundamental oscillation of resonant tunneling diodes above 1 THz at room temperature," *Applied Physics Letters*, vol. 97, no. 24, p. 242102, 2010.

[43] M. Zhang, S. Clochiatti, A. Rennings, K. Arzi, W. Prost, N. Weimann, and D. Erni, "Antenna design for Subharmonic Injection-Locked Triple Barrier RTD oscillator in the 300 GHz band," *2019 Second International Workshop on Mobile Terahertz Systems (IWMTS)*, pp. 1–4, 2019.

[44] J. Wang, K. Alharbi, A. Ofiare, H. Zhou, A. Khalid, D. Cumming, and E. Wasige, "High performance resonant tunneling diode oscillators for THz applications," *2015 IEEE Compound Semiconductor Integrated Circuit Symposium (CSICS)*, pp. 1–4, 2015.

[45] R. Montecillo, R. E. S. Otadoy, M. L. A. D. Lee, F. A. Buot, and M. D. Nacar, "The dependence of the characteristics of THz current oscillations on the quantum-well width in resonant tunneling diode," *AIP Conference Proceedings*, vol. 1871, no. 1, p. 030002, 2017.

[46] P. Zhao, D. L. Woolard, and H. L. Cui, "Multisubband theory for the origination of intrinsic oscillations within double-barrier quantum well systems," *Physical Review B*, vol. 67, no. 8, p. 085312, 2003.

[47] O. Jonasson and I. Knezevic, "Coulomb-driven terahertz-frequency intrinsic current oscillations in a double-barrier tunneling structure," *Physical Review B*, vol. 90, no. 16, p. 165415, 2014.

[48] P. Wójcik, B. J. Spisak, M. Wołoszyn, and J. Adamowski, "Intrinsic current oscillations in an asymmetric triple-barrier resonant tunnelling diode," *Semiconductor Science and Technology*, vol. 25, no. 12, p. 125012, 2010.

[49] A. Buot, "Quantum Algorithm," *Nonequilibrium Quantum Transport Physics in Nanosystems*, p. 687–710, 2009.

[50] M. Villani, G. Albareda, C. Destefani, X. Cartoixà, and X. Oriols, "Scattering in terms of Bohmian conditional wave functions for scenarios with non-commuting energy and momentum operators," *Entropy*, vol. 23, no. 4, p. 408, 2021.

[51] Z. Zhan, E. Colomés, and X. Oriols, "Unphysical features in the application of the Boltzmann collision operator in the time-dependent modeling of Quantum Transport," *Journal of Computational Electronics*, vol. 15, no. 4, p. 1206–1218, 2016.

[52] M. Suhara, S. Takahagi, K. Asakawa, T. Okazaki, M. Nakamura, S. Yamashita, Y. Itagaki, M. Saito, A. Tchegho, G. Keller, and et al., "Analysis of terahertz zero bias detectors by using a triple-barrier resonant tunneling diode integrated with a self-complementary bow-tie antenna," *70th Device Research Conference*, pp. 77–78, 2012.

[53] S. Clochiatti, E. Mutlu, C. Preuss, R. Kress, W. Prost, and N. Weimann, "Broadband THz detection using InP Triple-barrier resonant tunneling diode with integrated antenna," *2021 Fourth International Workshop on Mobile Terahertz Systems (IWMTS)*, pp. 1–5, 2021.

[54] Q. Liu, A. Seabaugh, P. Chahal, and F. Morris, "Unified ac model for the resonant tunneling diode," *IEEE Transactions on Electron Devices*, vol. 51, no. 5, p. 653–657, 2004.

[55] R. Lake and J. Yang, "A physics based model for the rtd quantum capacitance," *IEEE Transactions on Electron Devices*, vol. 50, no. 3, p. 785–789, 2003.

[56] E. R. Brown, C. D. Parker, and T. C. Sollner, "Effect of quasibound-state lifetime on the oscillation power of resonant tunneling diodes," *Applied Physics Letters*, vol. 54, no. 10, p. 934–936, 1989.

[57] E. R. Brown, W. D. Goodhue, and T. C. Sollner, "Fundamental oscillations up to 200 ghz in resonant tunneling diodes and new estimates of their maximum oscillation frequency from stationary-state tunneling theory," *Journal of Applied Physics*, vol. 64, no. 3, p. 1519–1529, 1988.

[58] N. Orihashi, S. Hattori, S. Suzuki, and M. Asada, "Experimental and theoretical characteristics of sub-terahertz and terahertz oscillations of resonant tunneling diodes integrated with slot antennas," *Japanese Journal of Applied Physics*, vol. 44, no. 11, p. 7809–7815, 2005.

[59] M. N. Feiginov, "Does the quasibound-state lifetime restrict the high-frequency operation of resonant-tunnelling diodes?," *Nanotechnology*, vol. 11, no. 4, p. 359–364, 2000.

[60] J. V. Neumann, *Mathematical Foundations of Quantum Mechanics*. Princeton University, 2018.

[61] B. S. DeWitt and N. Graham, *The many worlds interpretation of quantum mechanics*. Princeton University Press, 2015.

[62] L. D. Broglie, "La mécanique ondulatoire et la structure atomique de la matière et du rayonnement," *Journal de Physique et le Radium*, vol. 8, no. 5, p. 225–241, 1927.

[63] D. Bohm, "A Suggested Interpretation of the Quantum Theory in Terms of "Hidden" Variables. I," *Physical Review*, vol. 85, no. 2, p. 166–179, 1952.

[64] D. Bohm, "A Suggested Interpretation of the Quantum Theory in Terms of "Hidden" Variables. II," *Physical Review*, vol. 85, no. 2, p. 180–193, 1952.

[65] J. S. Bell, "On The Einstein Podolsky Rosen Paradox," *Physics Physique Fizika*, vol. 1, no. 3, p. 195—200, 1964.

[66] K. Svozil, "Shut up and calculate," *Physical (A)Causality*, p. 47–49, 2018.

[67] K. Camilleri, "Constructing the Myth of the Copenhagen Interpretation," *Perspectives on Science*, vol. 17, no. 1, p. 26–57, 2009.

[68] X. Oriols and D. K. Ferry, "Why engineers are right to avoid the quantum reality offered by the orthodox theory? [point of view]," *Proceedings of the IEEE*, vol. 109, no. 6, p. 955–961, 2021.

[69] X. Oriols and J. Mompart, "Overview of Bohmian Mechanics," *Applied Bohmian Mechanics*, p. 19–166, 2019.

[70] D. Durr and S. Teufel, *Bohmian Mechanics: The Physics and Mathematics of Quantum Theory*. Springer Berlin Heidelberg, 2009.

[71] D. Dürr, S. Goldstein, and N. Zanghì, "Bohmian Mechanics and Quantum Field Theory," *Quantum Physics Without Quantum Philosophy*, p. 239–246, 2012.

[72] E. Colomés, G. Albareda, Z. Zhan, D. Pandey, A. Alarcón, F. Traversa, and X. Oriols, "Nanoelectronics: Quantum Electron Transport," *Applied Bohmian Mechanics*, p. 400–462, 2019.

[73] A. Benseny, G. Albareda, n. S. Sanz, J. Mompart, and X. Oriols, "Applied Bohmian mechanics," *The European Physical Journal D*, vol. 68, no. 10, p. 286, 2014.

[74] H.-P. Breuer and F. Petruccione, "The Theory of Open Quantum Systems," pp. 5–23, 2007.

[75] A. Rivas, S. F. Huelga, and M. B. Plenio, "Quantum non-Markovianity: Characterization, quantification and detection," *Reports on Progress in Physics*, vol. 77, no. 9, p. 094001, 2014.

[76] G. Lindblad, "On the generators of quantum dynamical semigroups," *Communications in Mathematical Physics*, vol. 48, no. 2, p. 119–130, 1976.

[77] F. Rossi, *The Density-Matrix Approach, Theory of Semiconductor Quantum Devices NanoScience and Technology*. Berlin, Heidelberg, 2010.

[78] R. C. Iotti, E. Ciancio, and F. Rossi, "Quantum transport theory for semiconductor nanostructures: A density-matrix formulation," *Physical Review B*, vol. 72, no. 12, 2005.

[79] J. Weinbub and D. K. Ferry, "Recent advances in Wigner function approaches," *Applied Physics Reviews*, vol. 5, no. 4, p. 041104, 2018.

[80] W. R. Frensley, "Wigner-function model of a resonant-tunneling semiconductor device," *Physical Review B*, vol. 36, no. 3, p. 1570–1580, 1987.

[81] E. Wigner, "On the quantum correction for thermodynamic equilibrium," *Physical Review*, vol. 40, no. 5, p. 749–759, 1932.

[82] R. P. Zaccaria and F. Rossi, "Generalized Weyl–Wigner formalism for the simulation of open quantum devices: a Density-Matrix approach," *Semiconductor Science and Technology*, vol. 19, no. 4, p. 146603, 2004.

[83] P. Pearle, "Combining stochastic dynamical state-vector reduction with spontaneous localization," *Physical Review A*, vol. 39, no. 5, p. 2277–2289, 1989.

[84] H. Carmichael, "An open systems approach to Quantum Optics," *Lecture Notes in Physics Monographs*, 1993.

[85] D. Gatarek and N. Gisin, "Continuous quantum jumps and infinite-dimensional stochastic equations," *Journal of Mathematical Physics*, vol. 32, no. 8, p. 2152–2157, 1991.

[86] N. G. Van Kampen, *Stochastic processes in physics and Chemistry*. Elsevier, 2010.

[87] P. Goetsch and R. Graham, "Linear stochastic wave equations for continuously measured quantum systems," *Physical Review A*, vol. 50, no. 6, p. 5242–5255, 1994.

[88] D. Pandey, E. Colomés, G. Albareda, and X. Oriols, "Stochastic Schrödinger equations and conditional states: A general non-Markovian quantum electron transport simulator for THz Electronics," *Entropy*, vol. 21, no. 12, p. 1148, 2019.

[89] R. Lake, G. Klimeck, R. C. Bowen, and D. Jovanovic, "Single and multiband modeling of quantum electron transport through layered semiconductor devices," *Journal of Applied Physics*, vol. 81, no. 12, p. 7845–7869, 1997.

[90] G. Klimeck, S. Ahmed, H. Bae, N. Kharche, S. Clark, B. Haley, S. Lee, M. Naumov, H. Ryu, F. Saied, and et al., "Atomistic Simulation of Realistically Sized Nanodevices Using NEMO 3-D—Part I: Models and Benchmarks," *IEEE Transactions on Electron Devices*, vol. 54, no. 9, p. 2079–2089, 2007.

[91] A. G. M. Schmidt, B. K. Cheng, and M. G. E. D. Luz, "Green function approach for general quantum graphs," *Journal of Physics A: Mathematical and General*, vol. 36, no. 42 L545, 2003.

[92] K. Sabirov, U. Aminov, K. Saparov, M. Karimov, and K. Abdikarimov, "The Green function for simplest quantum graphs," *Nanosystems: Physics, Chemistry, Mathematics*, p. 762–766, 2015.

[93] R. Kubo, "Statistical-mechanical theory of irreversible processes. I. General theory and simple applications to magnetic and conduction problems," *Journal of the Physical Society of Japan*, vol. 12, no. 6, pp. 570–586, 1957.

[94] R. Kubo, "Statistical-mechanical theory of irreversible processes. II. Response to thermal disturbance," *Journal of the Physical Society of Japan*, vol. 12, no. 11, pp. 1203–1211, 1957.

[95] K. Chadova and H. Ebert, *Electronic transport within the Kubo-Bastin formalism*. PhD thesis.

[96] Z. Fan, J. H. Garcia, A. W. Cummings, J. E. Barrios-Vargas, M. Panhans, A. Harju, F. Ortmann, and S. Roche, "Linear scaling quantum transport methodologies," *Physics Reports*, vol. 903, p. 1–69, 2021.

[97] M. V. Fischetti, "Theory of electron transport in small semiconductor devices using the Pauli master equation," *Journal of Applied Physics*, vol. 83, no. 1, p. 270–291, 1998.

[98] A. Y. Klimenko, "Symmetric and antisymmetric forms of the Pauli master equation," *Scientific Reports*, vol. 6, no. 1, pp. 1–11, 2016.

[99] T. Gurov, M. Nedjalkov, P. Whitlock, H. Kosina, and S. Selberherr, "Femtosecond relaxation of hot electrons by phonon emission in presence of electric field," *Physica B: Condensed Matter*, vol. 314, no. 1-4, p. 301–304, 2002.

[100] D. Querlioz, P. Dollfus, and M. Mouis, "Theoretical framework of quantum transport in semiconductors and devices," *The Wigner Monte Carlo Method for Nanoelectronic Devices*, p. 1–56, 2013.

[101] M. Nedjalkov, D. Vasileska, D. K. Ferry, C. Jacoboni, C. Ringhofer, I. Dimov, and V. Palankovski, "Wigner transport models of the electron-phonon kinetics in quantum wires," *Physical Review B*, vol. 74, no. 3, p. 035311, 2006.

[102] T. Kramer, C. Kreisbeck, and V. Krueckl, "Wave packet approach to transport in mesoscopic systems," *Physica Scripta*, vol. 82, no. 3, p. 038101, 2010.

[103] C. Bracher, J. B. Delos, V. Kanellopoulos, M. Kleber, and T. Kramer, "The photoelectric effect in external fields," *Physics Letters A*, vol. 347, no. 1-3, p. 62–66, 2005.

[104] J. Gambetta and H. M. Wiseman, "Non-Markovian stochastic Schrödinger equations: Generalization to real-valued noise using quantum-measurement theory," *Physical Review A*, vol. 66, no. 1, p. 012108, 2002.

[105] J. Gambetta and H. M. Wiseman, "Interpretation of non-Markovian stochastic Schrödinger equations as a hidden-variable theory," *Physical Review A*, vol. 68, no. 6, p. 062104, 2003.

[106] E. Colomés, Z. Zhan, D. Marian, and X. Oriols, "Quantum dissipation with conditional wave functions: Application to the realistic simulation of Nanoscale Electron Devices," *Physical Review B*, vol. 96, no. 7, p. 075135, 2017.

[107] D. Dürr, S. Goldstein, and N. Zanghì, "Quantum equilibrium and the origin of absolute uncertainty," *Quantum Physics Without Quantum Philosophy*, p. 23–77, 2012.

[108] D. Dürr, S. Goldstein, and N. Zanghì, "Quantum equilibrium and the role of operators as observables in quantum theory," *Journal of Statistical Physics*, vol. 116, no. 1-4, p. 959–1055, 2004.

[109] X. Oriols, "Quantum-Trajectory Approach to Time-Dependent Transport in Mesoscopic Systems with Electron-Electron Interactions," *Physical Review Letters*, vol. 98, no. 6, p. 066803, 2007.

[110] "The BITLLES simulator." http://europe.uab.es/xoriols/The_BITLLES_simulator.html.

[111] R. C. Iotti, F. Dolcini, and F. Rossi, "Wigner-function formalism applied to semiconductor quantum devices: Need for nonlocal scattering models," *Physical Review B*, vol. 96, no. 11, p. 115420, 2017.

[112] O. Jonasson and I. Knezevic, "Dissipative transport in superlattices within the Wigner function formalism," *Journal of Computational Electronics*, vol. 14, no. 4, p. 879–887, 2015.

[113] M. Villani and X. Oriols, "Can Wigner distribution functions with collisions satisfy complete positivity and energy conservation?," *Journal of Computational Electronics*, vol. 20, no. 6, p. 2232–2244, 2021.

[114] I. de Vega, "Non-Markovian stochastic Schrödinger description of transport in Quantum Networks," *Journal of Physics B: Atomic, Molecular and Optical Physics*, vol. 44, no. 24, p. 245501, 2011.

[115] G. Albareda, F. L. Traversa, A. Benali, and X. Oriols, "Computation of quantum electrical currents through the ramo–shockley–pellegrini theorem with trajectories," *Fluctuation and Noise Letters*, vol. 11, no. 03, p. 1242008, 2012.

[116] J. D. Jackson, *Classical Electrodynamics*. J. Wiley, 1975.

[117] M. Javid and P. M. Brown, *Field Analysis and Electromagnetics*. Dover Publications, Inc., 1963.

[118] S. Ramo, "Currents Induced by Electron Motion," *Proceedings of the IRE*, vol. 27, no. 9, p. 584–585, 1939.

[119] W. Shockley, "Currents to Conductors Induced by a Moving Point Charge," *Journal of Applied Physics*, vol. 9, no. 10, p. 635–636, 1938.

[120] B. Pellegrini, "Electric charge motion, induced current, energy balance, and noise," *Physical Review B*, vol. 34, no. 8, p. 5921–5924, 1986.

[121] B. Pellegrini, "Extension of the electrokinematics theorem to the electromagnetic field and quantum mechanics," *Il Nuovo Cimento D*, vol. 15, no. 6, p. 855–879, 1993.

[122] B. Pellegrini, "Elementary applications of quantum-electrokinematics theorem," *Il Nuovo Cimento D*, vol. 15, no. 6, p. 881–896, 1993.

[123] P. D. Yoder, K. Gärtner, and W. Fichtner, "A generalized Ramo–Shockley theorem for classical to quantum transport at arbitrary frequencies," *Journal of Applied Physics*, vol. 79, no. 4, p. 1951–1954, 1996.

[124] M. O. Scully and M. S. Zubairy, *Quantum Optics*. Cambridge University Press, 2008.

[125] G. Grynberg, A. Aspect, C. Fabre, and C. Cohen-Tannoudji, "Quantization of free radiation," *Introduction to Quantum Optics*, pp. 310–318.

[126] M. Ashcroft, *Solid state physics: Revised edition*. Cengage Learning, 2016.

[127] R. Landauer and T. Martin, "Barrier interaction time in tunneling," *Reviews of Modern Physics*, vol. 66, no. 1, p. 217–228, 1994.

[128] A. S. Landsman and U. Keller, "Attosecond science and the tunnelling time problem," *Physics Reports*, vol. 547, p. 1–24, 2015.

[129] E. H. Hauge and J. A. Støvneng, "Tunneling Times: A critical review," *Reviews of Modern Physics*, vol. 61, no. 4, p. 917–936, 1989.

[130] D. Sokolovski and E. Akhmatskaya, "Wigner's friends, Tunnelling Times and Feynman's "Only mystery of quantum mechanics"," *Europhysics Letters*, vol. 136, no. 2, p. 20001, 2021.

[131] D. Pandey, M. Villani, E. Colomés, Z. Zhan, and X. Oriols, "Implications of the Klein tunneling times on high frequency graphene devices using Bohmian trajectories," *Semiconductor Science and Technology*, vol. 34, no. 3, p. 034002, 2019.

[132] M. Villani, D. Pandey, E. Colomes, X. Oriols, and Z. Zhan, "Tunneling Times in graphene FET: From fundamental physics to Practical Engineering," *2018 Spanish Conference on Electron Devices (CDE)*, pp. 1–4, 2018.

[133] D. Pandey and X. P. Oriols, *Quantum Transport in Solid State Devices for Terahertz Frequency Applications*. PhD thesis, Universitat Autónoma de Barcelona, 2020.

[134] E. Colomés and X. Oriols, *Quantum Transport with Bohmian Mechanics: Application to Graphene Devices*. PhD thesis, Universitat Autónoma de Barcelona, 2018.

[135] Z. Zhan and X. Oriols, *On the Displacement Current in THz Quantum Nanodevices: Application to the Simulation of Graphene Transistors*. PhD thesis, Universitat Autónoma de Barcelona, 2017.

[136] M. Villani, S. Clochiatti, W. Prost, N. Weimann, and X. Oriols, "There is Plenty of Room for THz Tunneling Electron Devices Beyond the Transit Time Limit," *IEEE Electron Device Letters*, vol. 42, no. 2, p. 224–227, 2021.

[137] M. Villani, X. Oriols, S. Clochiatti, N. Weimann, and W. Prost, "The accurate predictions of THz quantum currents requires a new displacement current coefficient instead of the traditional transmission one," *2020 Third International Workshop on Mobile Terahertz Systems (IWMTS)*, pp. 1–5, 2020.

[138] S. Laux, "Techniques for small-signal analysis of semiconductor devices," *IEEE Transactions on Electron Devices*, vol. 32, no. 10, p. 2028–2037, 1985.

[139] E. Fernandez-Diaz, A. Alarcon, and X. Oriols, "Modeling Quantum Transport Under AC Conditions: Application to Intrinsic High-Frequency Limits for Nanoscale Double-Gate Si MOSFETs," *IEEE Transactions On Nanotechnology*, vol. 4, no. 5, p. 563–569, 2005.

[140] X. Oriols, A. Alarcón, and E. Fernàndez-Díaz, "Time-dependent quantum current for independent electrons driven under nonperiodic conditions," *Physical Review B*, vol. 71, no. 24, p. 245322, 2005.